AD-A054 637 NAVAL RESEARCH LAB WASHINGTON D C F/G 11/4
HIGH PERFORMANCE COMPOSITES AND ADHESIVES FOR V/STOL AIRCRAFT.(U)
FEB 78 W D BASCOM, L B LOCKHART
UNCLASSIFIED NRL-MR-3721 SBIE-AD-E000 155 NL

1 OF 2
AD A054637

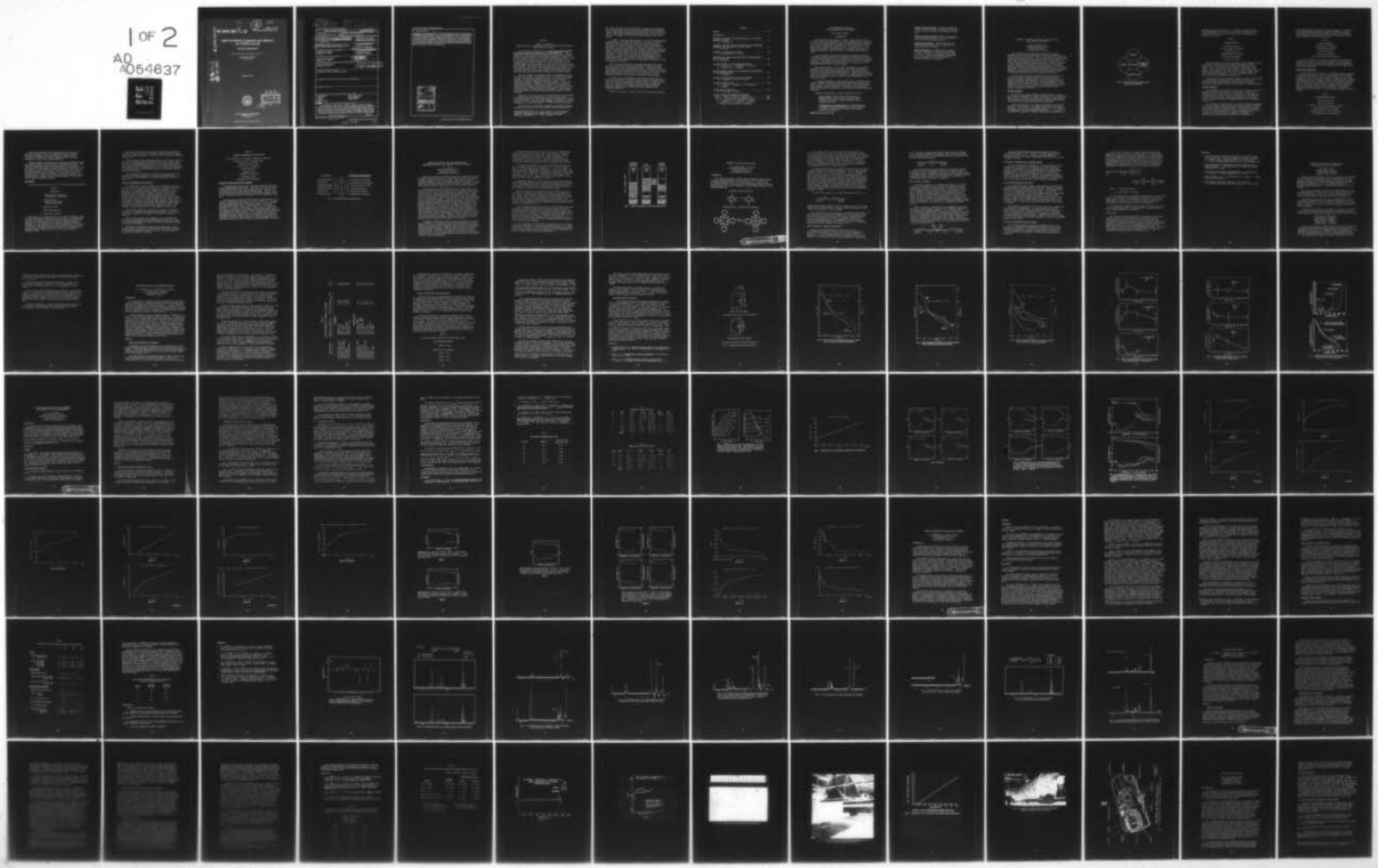

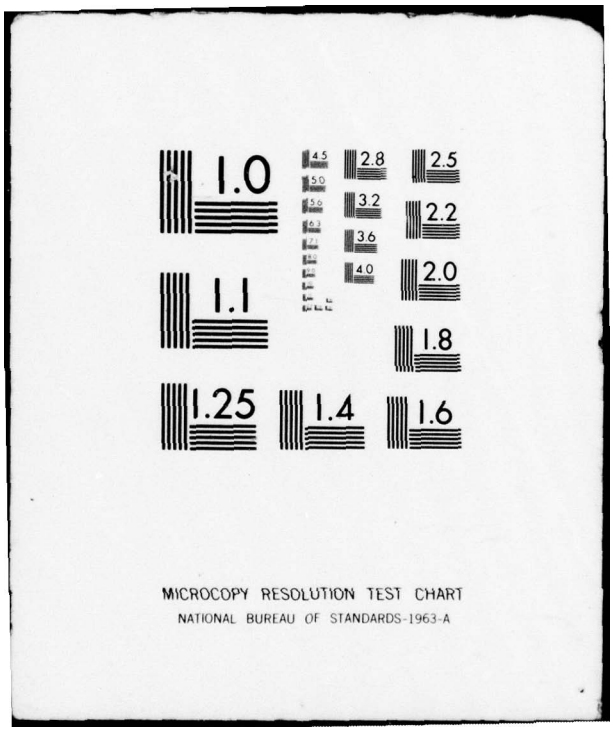
1.0
1.1
1.25
1.4
1.6
1.8
2.0
2.2
2.5
2.8
3.2
3.6
4.0
4.5
5.0
5.6
6.3
MICROCOPY RESOLUTION TEST CHART
NATIONAL BUREAU OF STANDARDS-1963-A

NRL Memorandum Report 3721

High Performance Composites and Adhesives for V/STOL Aircraft

Second Annual Report

WILLARD D. BASCOM AND LUTHER B. LOCKHART, JR.

Polymeric Materials Branch
Chemistry Division

February 1978

NAVAL RESEARCH LABORATORY
Washington, D.C.

(18) SBIE

(19) AD-E000 155

(9) Annual rept. no. 2, 1 Sep 76-31 Aug 77,

SECURITY CLASSIFICATION OF THIS PAGE *(When Data Entered)*

REPORT DOCUMENTATION PAGE

READ INSTRUCTIONS BEFORE COMPLETING FORM

1. REPORT NUMBER
NRL Memorandum Report 3721

2. GOVT ACCESSION NO. (14) NRL-MR-3721

3. RECIPIENT'S CATALOG NUMBER

(6) 4. TITLE *(and Subtitle)*
HIGH PERFORMANCE COMPOSITES AND ADHESIVES FOR V/STOL AIRCRAFT. ~~SECOND ANNUAL REPORT~~

AD-A022331

5. TYPE OF REPORT & PERIOD COVERED
Progress report for the period 1 Sept. 1976 — 31 Aug. 1977.

6. PERFORMING ORG. REPORT NUMBER

(10) 7. AUTHOR(s)
Willard D. Bascom and Luther B. Lockhart, Jr. Editors

8. CONTRACT OR GRANT NUMBER(s)
(16) F54593

(17) WF54593201

9. PERFORMING ORGANIZATION NAME AND ADDRESS
Naval Research Laboratory
Washington, D.C. 20375

10. PROGRAM ELEMENT, PROJECT, TASK AREA & WORK UNIT NUMBERS
NRL Problem C04-10
PE 62761 N; F 54593201

11. CONTROLLING OFFICE NAME AND ADDRESS
Naval Air Systems Command
Washington, D.C. 20361

(11) 12. REPORT DATE
Feb[redacted]978

13. NUMBER OF PAGES
153

14. MONITORING AGENCY NAME & ADDRESS *(if different from Controlling Office)*
Naval Air Development Center
Warminster, PA 18974

15. SECURITY CLASS. *(of this report)*
UNCLASSIFIED

(12) 154 p.

15a. DECLASSIFICATION/DOWNGRADING SCHEDULE

16. DISTRIBUTION STATEMENT *(of this Report)*
Approved for public release; distribution unlimited.

17. DISTRIBUTION STATEMENT *(of the abstract entered in Block 20, if different from Report)*

18. SUPPLEMENTARY NOTES

19. KEY WORDS *(Continue on reverse side if necessary and identify by block number)*

V/STOL aircraft
Composites
Adhesives
Polymer synthesis
Fracture
Polymer characterization
Design optimization
Radiation curing

20. ABSTRACT *(Continue on reverse side if necessary and identify by block number)*

An interdisciplinary program has been undertaken to address the composite and adhesive materials requirements of V/STOL aircraft. The primary tasks are to develop and characterize high modulus, high toughness resins with use temperatures of 350°F to 450°F or higher, to develop fabrication technology for newly developed resin matrices for graphite-fiber reinforced composites, to develop composite failure criteria for design optimization and to establish appropriate quality control parameters. This report is the second annual review of the program, covering the period

(Continues)

next page

DD FORM 1 JAN 73 1473 EDITION OF 1 NOV 65 IS OBSOLETE
S/N 0102-014-6601

SECURITY CLASSIFICATION OF THIS PAGE *(When Data Entered)*

251 950

20. Abstract (Continued)

1 September 1976 to 31 August 1977. The principle accomplishments during the reporting period have been (a) to obtain commercial sources for the C_{10} phthalocyanine resin and composite prepreg of this resin with graphite fiber, (b) to define the fracture behavior of a variety of commercial and in-house high performance resins, (c) to establish quality control methods for the phthalocyanine resins based on nmr spectroscopy, (d) to formulate a polyimide-based resin curable by ionizing radiation and demonstrate that graphite-fiber composites can be fabricated using ionizing radiation, and (e) to show that failure criteria for composites determined with small scale test coupons accurately predict failure of flaws in a box-beam substructure.

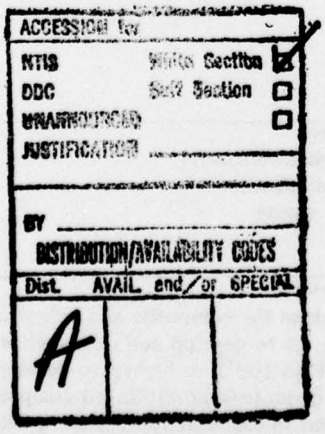

PREFACE*

Albert I. Schindler
Associate Director of Research for Materials and General Sciences
Naval Research Laboratory

I would like to welcome you to the Second Annual Review on High Performance Composites and Adhesives for V/STOL Aircraft. I was pleased to be invited to make these opening remarks since I strongly believe that this composites and adhesives program has served as an excellent model for many of the materials programs that we have at NRL. As you know the Naval Research Laboratory has traditionally had a strong materials research program that is characterized by its outstanding breadth as well as depth. As such, we have been able to gather together workers from different disciplines to attack important Navy problems. This V/STOL materials program is a good example of such a multidisciplinary effort. Drs. Lockhart and Bascom in their overviews will more fully elaborate on how they have orchestrated this effort and how much of our research feeds into the V/STOL Program.

NRL's involvement in materials research and development in the Navy has also included the development of a 6.2 materials investment strategy. The materials strategy, as some of you may know, was put together by a team of people who represented nearly all Navy Laboratories, Systems Commands and the Marine Corps. As such, the strategy represented a consensus on how the Navy's 6.2 materials money should be spent in the next five years. I am sure that this community will be happy to know that one of the major thrusts of the strategy was that of V/STOL materials development - which includes both light-weight structural materials and high-temperature turbine materials.

Funding for this major thrust of V/STOL materials was recommended to average close to the $3M/YR level for the five-year period, representing nearly 14% of the total materials technology 6.2 program. So you can see that the Navy and R&D managers have indicated a strong commitment to the continued support of V/STOL materials development.

The driving force behind this composites and adhesives program continues to be the need for light-weight structural composites for

*Opening Remarks at the Second Annual Review on High Performance Composites and Adhesives for V/STOL Aircraft, Naval Research Laboratory, Washington, D. C. 20375, September 8, 1977.

the V/STOL aircraft which the Navy hopes to develop by the Mid-80's. While design changes have been made that apparently have reduced the service temperatures originally projected for such aircraft, there are numerous areas where high-temperature performance is still required, such as, for example, for hot gas ducts and in areas close to the engines.

A number of promising resin systems - including the NRL-developed phthalocyanines - are under consideration as the resin matrix for graphite-reinforced composites. Final selection will be based ultimately on a number of critical factors including fabricability, performance, cost and availability. Today you will hear of the important resin properties that could influence composites performance - fracture toughness, thermal and moisture resistance, fire resistance, rheology, etc. The necessity to have adequate quality control procedures to assure that results can be replicated will also be emphasized. Indeed, the most significant accomplishments of this program promise to be the ability to predict the resistance of composites to flaw propagation and the development of failure criteria for composite structures.

One of the many advances in the program during the past year involves the successful technology transfer to industry for large scale production of the phthalocyanine resins. This NRL-industry involvement will be increased with the letting of contracts to prepare graphite-fiber phthalocyanine-resin prepreg which will provide us with needed materials for fabrication and test, and which will also familiarize industry with this new, potentially useful material.

I mentioned in the beginning of these remarks how we like to consider this program as a model for other materials programs at NRL. After listening to the talks and discussion today, I am sure you will agree that this multidisciplinary effort represents a significant model for carrying out a successful materials program, from the fundamental research level through the stage of demonstrating production capability.

Thank you very much. I hope you have a very productive meeting.

CONTENTS

PREFACE iii

INTRODUCTION 1

OVERVIEW OF RESEARCH ON POLYMERIC MATERIALS AT THE NAVAL RESEARCH LABORATORY 3
L. B. Lockhart, Jr.

TECHNICAL OVERVIEW OF THE NRL PROGRAM ON HIGH PERFORMANCE COMPOSITES AND ADHESIVES FOR V/STOL AIRCRAFT 11
W. D. Bascom

SYNTHESIS OF PHTHALOCYANINE RESINS 15
J. R. Griffith and J. G. O'Rear

PROJECTION FOR LARGE SCALE PRODUCTION OF PHTHALOCYANINE RESIN INTERMEDIATES 21
W. C. Lyman

FRACTURE BEHAVIOR OF HIGH TEMPERATURE RESINS 23
W. D. Bascom, R. L. Cottington, J. L. Bitner, D. L. Hunston and J. Oroshnik

TORSION PENDULUM ANALYSIS OF THE FORMATION AND PROPERTIES OF A POLYPHTHALOCYANINE 37
J. K. Gillham

CHEMICAL CHARACTERIZATION FOR QUALITY CONTROL 61
C. F. Poranski, Jr. and W. B. Moniz

RADIATION CURABLE RESINS 79
F. J. Campbell, W. Brenner, L. M. Johnson and M. E. White

FABRICATION OF COMPOSITES 93
R. Y. Ting and H. C. Nash

FAILURE CRITERIA FOR COMPOSITE STRUCTURES
Part I. Failure Criteria for Composites 103
Part II. Failure Criteria for Adhesive Joints 133
L. A. Beaubien, M. F. Clifford, P. W. Mast, D. R. Mulville, S. A. Sutton, R. W. Thomas, J. Tirosh, I. Wolock and D. L. Hunston

HIGH PERFORMANCE COMPOSITES AND ADHESIVES FOR V/STOL AIRCRAFT

Second Annual Report

INTRODUCTION

This Nation's limited capacity to deploy large aircraft carriers and their increasing vulnerability to enemy countermeasures (sea/sea and air/sea ballistic missiles and torpedoes) suggests that the future Navy must rely on a larger fleet of smaller, less costly carriers or other ships capable of deploying combat aircraft. The ability to do this effectively depends on the development of V/STOL aircraft having the combat effectiveness, range and payload of conventional carrier aircraft.

Today's military and civilian aircraft are making use of fiber-reinforced composite materials as a substitute for metals both because of the weight savings and the cost effectiveness of these new structural materials. This weight savings is even more critical to the successful development and deployment of V/STOL aircraft to compensate for the larger and heavier turbine engine required.

The program described in this report is designed to provide the performance and design data on graphite fiber-reinforced composite materials and on improved adhesives needed for their optimum use as structural materials for Navy V/STOL aircraft. Basically, the requirements are for materials that will operate in a higher temperature regime than state-of-the-art composites and will resist degradation by the marine environment.

An integrated approach is used in this program to bring into play the key elements of materials properties, fabricability and processability, quality control and design optimization. Interaction between these elements provides feedback for resin modifications leading to improved materials for adhesives and as the matrix for fiber-reinforced composites.

The major program tasks and their responsibilities are:

Resin Synthesis - Make chemical modifications to phthalocyanine resins to provide optimum thermomechanical properties; develop commercial source of promising materials.

Thermomechanical Characterization - Evaluate behavior of commercial and experimental resins under mechanical and thermal stress; provide feedback on structure/property relationships.

Manuscript submitted February 8, 1978.

Chemical Characterization - Develop techniques for analysis of resin systems for purposes of identification and quality control, and evaluation of cure state.

Radiation Curing of Resins - Evaluate potential of electron-beam curing of selected resin systems to provide strain-free adhesive joints.

Composites Fabrication - Develop procedures for obtaining reproducible, low-void composites for design optimization studies.

Design Optimization - Develop failure criteria for crack propagation in composites; demonstrate validity of criteria in predicting defect growth in a typical structural subcomponent; incorporate data in an automated closed loop system for optimized design of the component.

OVERVIEW OF RESEARCH ON POLYMERIC MATERIALS AT THE NAVAL RESEARCH LABORATORY

Luther B. Lockhart, Jr.
Polymeric Materials Branch
Chemistry Division
Naval Research Laboratory

As an introduction to this review of the Naval Research Laboratory program on High Performance Composites and Adhesives for V/STOL Aircraft, I would like to give a brief overview of current NRL research on polymeric materials. This overview will acquaint you with some of NRL's interests and capabilities rather than describe our formal research program in polymeric materials. Though a large part of this program is located organizationally within the Chemistry Division, significant portions are the responsibility of the Ocean Technology, Radiation Technology and Engineering Materials Divisions. Fortunately, the Laboratory management encourages a multidisciplinary approach to problem solving and the scientists themselves freely and informally interact across the interdivisional barriers.

Figure 1 shows a matrix of interacting areas which cover the field of research in polymeric materials: synthesis, polymer properties, chemical characterization, curing and fabrication, and finally performance and reliability. NRL has significant efforts underway in each of these broad areas of polymer research. A third dimension would be required to depict the interfaces between these facets and the current and potential uses and applications of polymeric materials in the Navy.

POLYMER SYNTHESIS

The aim of our polymer synthesis program has been to develop new classes of polymers whose properties will satisfy recognized Navy needs. We do not attempt to compete with industry, whose resources far outdistance ours, but select specialty areas and apply research ideas that are not being vigorously pursued elsewhere.

This approach has led to a number of promising new materials (Figure 2). Two of these - the phthalocyanine resins and fluoroacrylates - are covered in the program review to follow. Technology for synthesis of the fluorourethanes and fluoroepoxides has been successfully transferred to industry (DuPont) and the materials are

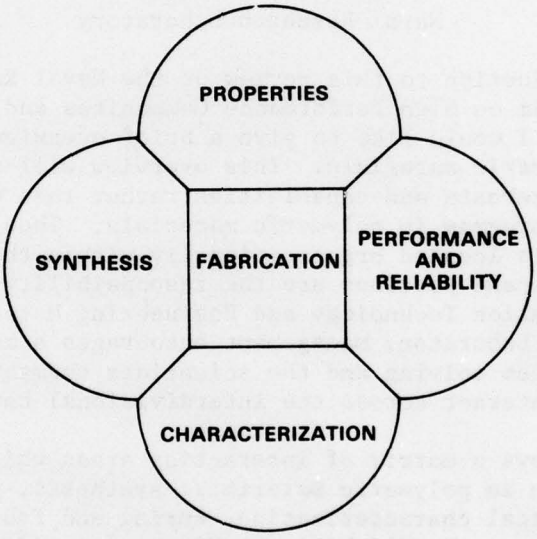

Fig. 1 — Research on polymeric materials at the Naval Research Laboratory

undergoing in-service evaluation. For example, one entire bilge of the USS FORRESTAL (CV 59) was coated with Teflon-pigmented fluorourethane paint during its recent overhaul and is now undergoing operational evaluation.

Figure 2

POLYMER SYNTHESIS

Polyphthalocyanines

Fluorourethanes and Epoxies

Fluoroacrylates

"Command-Destruct" Polymers

Electroactive Polymers

Inorganic Polymers

Current synthetic work is being directed toward "command-destruct" polymers which have built-in weak links that facilitate their destruction on challenging with an appropriate reagent or thermal stress. Use of such material would simplify paint removal, for example, without necessity for sand blasting. Other work is directed toward the development of thermally stable inorganic polymers and toward electroactive polymers, i.e. those that exhibit semi- and photoconductivity, piezoelectric behavior, etc.

In conjunction with the synthesis approach, we are also interested in the mechanisms and kinetics of the chemical reactions and in developing a basic understanding of the influence of molecular structure on the mechanical and electrical behavior of these materials.

POLYMER PROPERTIES

The determination of relevant properties is a necessary prelude to finding appropriate applications for new polymers. However, our interests are more basic than that - we would like to know why the polymer behaves as it does. With this information we should be able to both predict performance and provide guidance to our synthetic efforts to produce polymers with properties optimized for a specific application.

Our ultimate and long-term aim is to develop sufficient knowledge of structure property relationships so that we can molecularly design new polymeric materials with predictable, useful properties. Some areas of involvement are shown in Fig. 3. In addition to measurement of the usual strength properties - tensile, modulus, shear, etc. - emphasis is placed on the fracture behavior of polymers. In particular we are interested in identifying the molecular or

morphological factors that impart fracture toughness. Our studies on the time-dependent behavior of polymers are directed toward identifying and enhancing those molecular features that provide an energy dissipating mechanism which will blunt crack growth during cyclic loading or inhibit impact failure.

Figure 3

POLYMER PROPERTIES

Thermomechanical Properties

Time-Dependent Behavior

Fracture Mechanics

Electrical Properties

Structure/Property Relationships

Our recent foray into the field of electroactive polymers has required us to develop facilities for evaluating their electrical properties as a guide to our synthetic effort. At the appropriate time we will turn to our physicist colleagues for more sophisticated electrical measurements.

POLYMER CHARACTERIZATION

We feel that characterization is an extremely important component of any materials program. We need to know details of the chemical composition, molecular structure and impurity levels in a material on which we expect to spend many man-hours of research time. Detailed knowledge of the initial chemical state is necessary also for studies which address the subtle changes in structure or composition which occur on stressing or aging. Finally, quality assurance procedures based on both material properties and composition are needed to insure that subsequent batches of a material will replicate the behavior of the test specimen. Topics of general interest are listed in Fig. 4.

Figure 4

POLYMER CHARACTERIZATION

Chemical Composition

Molecular structure

Impurity Identification/Quality Control

Polymer Degradation mechanisms

Mechanochemistry of Polymer Fracture

Structure/Property Relationships

NRL has an impressive array of analytical toals that can be employed: infrared, ultraviolet, NMR/EPR spectroscopy and mass spectroscopy; ESCA and Auger spectroscopy; scanning electron microscopy; differential scanning calorimetry (DSC) and allied techniques; GPC and liquid chromatography; etc.

Magnetic resonance techniques are assuming an increasingly larger role in the analysis of bulk materials - both liquid and solid. One interesting new study involves the mechanochemistry of polymer fracture; fast EPR techniques are being applied to identify and follow the reactions of free radicals formed in polymers as the result of mechanical stress or chain rupture. CIDNP is being used to identify the radical species formed on chemical or photolytic scission of polymer chains. Finally, pulsed carbon-13 NMR techniques are under development which promise to give resolvable spectra of rigid solids such as highly crosslinked polymers.

FABRICATION

Fabrication, as indicated in Fig. 5, involves more than processing

Figure 5

FABRICATION

Fiber-Reinforced Composites
  Polymer-Fiber Interactions

Adhesive Bonds
  Adhesive Joint Design
  Surface Preparation

Radiation Curing

Tank Lining Materials

Protective Coatings

a raw material into a finished product; it requires developing a means for identifying and controlling the critical steps in the fabrication process. For example, our research interests address polymer-fiber interactions, the fabrication of accurately registered angle-ply laminates, and the minimization of voids in composites, as well as the effects of bond geometry and polymer-adherend surface interactions in adhesives. Continued application is made of the extensive background in surface chemistry and surface analytical techniques available at NRL.

NRL's past experience in the effects of radiation on materials is being called on to develop and evaluate radiation-curable adhesive systems for V/STOL application. This work will be covered in subsequent presentations.

One particularly cogent problem involves the fabrication of lining systems for reconditioning and upgrading of Navy fuel storage tanks. The energy crisis requiring full usage of all available fuel storage facilities, including old World War II concrete tanks, the change to a lower viscosity fuel, EPA requirements for a pollution-free environment, and OSHA bans on use of certain key materials have combined to make this a thorny problem.

Paint formulation falls into the fabrication category also, and has been a necessary prerequisite to getting the NRL-developed fluorourethane coatings system into the operating Navy for test and evaluation.

MATERIALS PERFORMANCE AND RELIABILITY

The final proof of any new system is how it behaves in service. One of our aims is to shorten this process by developing criteria that will enable us to predict the performance and lifetime of a new material. To do this we attempt to identify and evaluate critical parameters that might effect strength or failure rates: polymer properties such as toughness, moisture absorption; fabrication variables such as cure state, flaw frequency and flaw size; loading rates, stress levels, etc. Design optimization will result from the integration of the above factors with design variables such as ply orientation in composites and adhesive joint geometry. Major emphasis is currently on fracture criteria and flaw growth in composites and adhesives under in-plane and multiaxial loading conditions. This research is covered more fully in a later section of this review.

As indicated in Figure 6, other areas of interest include the performance of composite armor materials and studies on metal-matrix composites, particularly the effects of electrolysis and stress corrosion.

NRL also has a strong effort underway on the development and application of non-destructive evaluation methods which are the key to successful depolyment of polymeric materials as structural elements in critical Navy systems.

Though NRL has considerable expertise and experience in metal fatigue, there is presently no on-going effort in studies of fatigue in composites and adhesive systems. We hope in the near future to correct our deficiency in this area.

Figure 6

MATERIALS PERFORMANCE AND RELIABILITY

Failure Criteria for Polymers, Adhesives, Composites

Stress Corrosion of Adhesive Bonds

Failure Analysis (SEM)

Flaw Growth in Composites

Design Optimization

Composite Armor

Metal-Matrix Composites

Fatigue Behavior

Non-Destructive Evaluation

COUPLING OF BASIC AND APPLIED RESEARCH

I mentioned earlier that work on polymeric materials is spread across organizational lines at NRL. This does not imply that there is no interaction between the various research groups - there is much interaction on both a formal and an informal basis. Moreover, each of the groups is involved in both basic and applied research and has on call colleagues with other specialties which can supplement their own.

The program which we are reviewing today takes advantage of this wealth of expertise and experience, as shown in Figure 7. The basic research programs have been on-going for a number of years and each has contributed significantly to the advancement of scientific knowledge in its field. What we have tried to do is to coordinate and direct the resources and talents of these research groups into the critical task areas of this program on High Performance Composites and Adhesives for V/STOL Aircraft. We are finding that the pattern of progression does not always proceed, as indicated, from research to development; problems encountered in the development area often have provided new research leads to explore or indicated deficiencies in knowledge that must be overcome before orderly development can proceed.

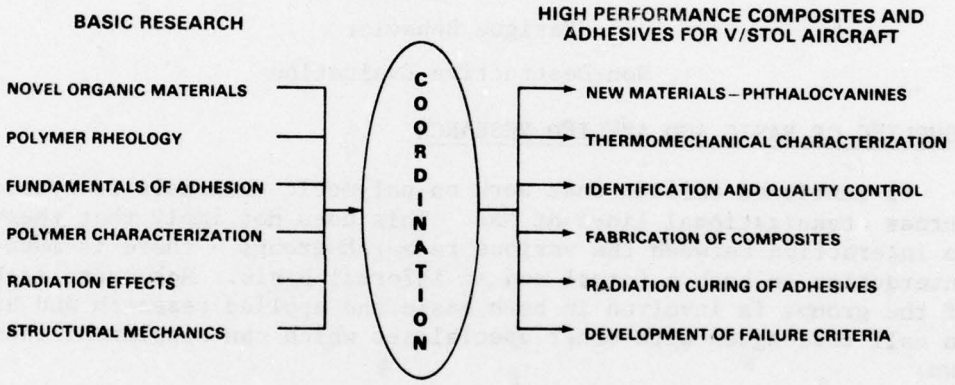

Fig. 7 — Coupling of basic and applied research

TECHNICAL OVERVIEW OF THE NRL PROGRAM ON HIGH PERFORMANCE COMPOSITES AND ADHESIVES FOR V/STOL AIRCRAFT

W. D. Bascom
Polymeric Materials Branch
Chemistry Division
Naval Research Laboratory

Present day military and civilian aircraft are making use of fiber-reinforced composite materials as a substitute for metals both because of weight savings and cost effectiveness. This weight savings is especially important to the successful development of vertical and short take-off and landing (V/STOL) aircraft in order to compensate for the large and heavy turbine engine required for vertical lift (Figure 1).

There are certain problem areas that must be solved before composites and adhesives can be effectively used in high performance aircraft structures. Resins are needed with use temperature up to 350°F and higher but, although there are materials rated for these temperatures, it remains to be demonstrated that these claims are realistic. The low fracture energy (low strain-to-failure) of many high performance resins is recognized; however, it has not yet been shown how this property translates into composite mechanical properties. The high performance adhesives generally lack peel strength which severely limits bonding to wide area structures and/or requires the inclusion of mechanical fasteners in the bond line. The chemical composition of the high performance resins is largely unknown, yet this information is essential for quality control. The intractable nature of some of the high performance resins presents serious problems in composite fabrication, so there is a need for development of more processable resins or alternative fabrication methods. Finally, the successful use of composites and adhesives in airframe structures requires more meaningful design criteria, especially with respect to flaw growth.

A program was undertaken at NRL to provide performance and design data on graphite fiber-reinforced composites and adhesives for V/STOL aircraft. This is a multi-disciplinary, interdivisional program which combines NRL capabilities in polymer synthesis, chemical and mechanical characterization of polymers, composite fabrication, electron-beam radiation curing of polymers, and composites and adhesives failure characterization. Also, private industry is involved in the production of NRL-invented resins and graphite-fiber tapes impregnated with these resins for test and evaluation.

Commercial high performance resins as well as the NRL-developed phthalocyanines have been characterized with respect to chemical composition and mechanical properties. Nuclear magnetic resonance spectroscopy (NMR) has been especially useful for chemical characterization of these resins. This type of modern analytical capability is essential for quality control of the complex resins and adhesives used in critical structural components of all aircraft.

The mechanical property of the candidate polymers that is being most thoroughly studied in this program is their fracture energy ($\mathcal{G}_{I_c}$), i.e. their resistance to flaw growth. It has been found that the thermosetting (crosslinked) polymers are rather brittle ($\mathcal{G}_{I_c}$ ~ 100 J/m^2) whereas the thermoplastic (uncrosslinked) polymers are especially tough ($\mathcal{G}_{I_c}$ = 500 to 5000 J/m^2). Furthermore, thermal aging of the thermosets near their use temperature increases the density of cross-links and reduce their toughness even further.

A promising, radiation curable resin has been developed based on dissolving bismaleimide resins in a radiation-reactive monomer such as N-vinyl pyrollidone and using the solution as a laminating lacquer or as an adhesive. Electron beam curing minimizes thermal stresses and can be more cost effective than conventional heat cures.

Failure criteria for the growth of a flaw or defect have been determined for composites and bonded joints under a broad range of in-plane loads. Data obtained by testing under these multi-axial conditions can be used to predict conditions for the initiation of failure under loadings similar to those observed in actual service. The validity of this approach has been demonstrated by predicting to within 10% the failure initiation load for a graphite/epoxy box-beam structure containing a controlled flaw.

There is strong interaction between the various program task areas. For example, mechanical property data is used to guide the polymer synthesis work and the formulation of radiation curable resins. The storage stability of prepreg is being monitored by both chemical analysis of the resin and evaluation of mechanical properties when the prepreg is fabricated into composites. Having found significant differences in the fracture toughness of the various matrix resins, an effort is underway to determine if this toughness affects the mechanical properties of the composite.

At the termination of this program recommendations will be forthcoming as to the choice of composite and adhesive materials for V/STOL applications, assessments of their advantages and limitations, fabrication procedures, quality control parameters and proven methodology for failure characterization and design optimization.

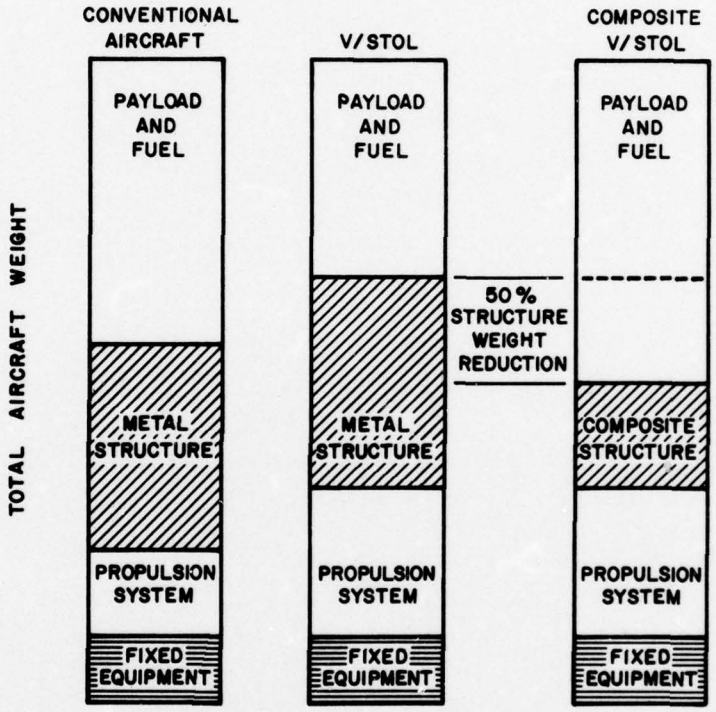

Fig. 1 — Effect of composites on V/STOL payload and fuel

SYNTHESIS OF PHTHALOCYANINE RESINS

J. R. Griffith and J. G. O'Rear
Polymeric Materials Branch
Chemistry Division
Naval Research Laboratory

INTRODUCTION

The reaction by which a phthalonitrile-terminated molecule reacts to form a polyphthalocyanine is quite similar to the reaction of an acetylene-terminated moiety that produces benzene. In either case, an aromatic structure is produced from multiply-bonded simple functional groups although the overall complexity of the process is greater in the phthalocyanine case.

Acetylene → Benzene Reaction

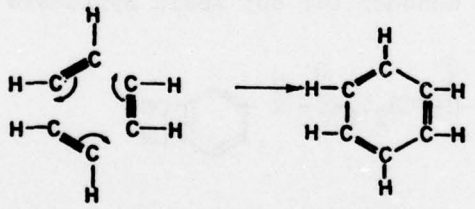

Phthalonitrile → Phthalocyanine Reaction

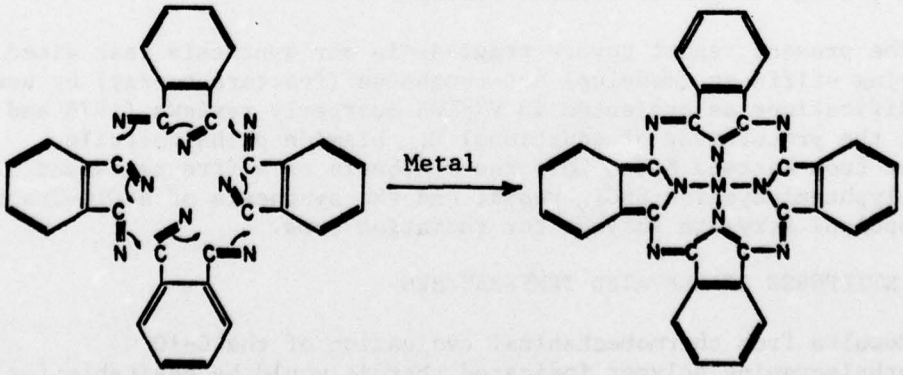

In both cases, there is a coupling of molecules without the concurrent elimination of some small molecule or molecular fragment which would result in foaming of a plastic being formed by the reaction, and the products are resonance-stabilized structures which are capable of withstanding relatively high temperatures without decomposition. A major advantage of the phthalocyanine reaction is that it can be induced to proceed to high yield, and, consequently, to mechanically strong products under less severe thermal and catalytic conditions than those required for the acetylene reaction.

The phthalocyanine resins are among the contenders for application as matrix materials in composites intended for use on V/STOL aircraft because of a number favorable characteristics. They are probably the nearest analogs to epoxy resins in general properties, including processing characteristics, of the available high temperature resins. Also, they are NRL in-house, Navy-owned materials which offers special advantages with respect to definite quality control and composition but which results in some problems of technology transfer and industrial production. During the last year, since the first annual report (1), we have sought to optimize the polyphthalocyanines with respect to processing and performance parameters and to pave the way for smooth technology transfer and large-scale production if these materials are selected for V/STOL.

The basic resin monomer for our Resin Synthesis Task (2,3,4) is

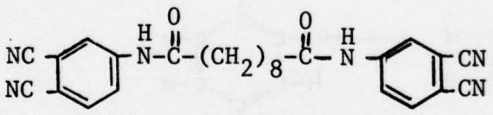

This C_{10} Diamide phthalonitrile monomer is polymerized via a "B" stage (200°C) and a postcure (240°C) to develop stable phthalocyanine nuclei linked through aliphatic diamide linkages.

The present report covers progress in our synthesis task aimed at improving stiffness (modulus) and toughness (fracture energy) by use of modifications as projected in V/STOL quarterly reviews (1976 and 1977); the procurement of additional C_{10} Diamide phthalonitrile monomer from Eastman Kodak Co.; the synthesis of a fire resistant C_{10} polyphthalocyanine-$SnCl_2$ resin; and the synthesis of a Cis-Trans Fluoropolyol Acrylate Polymer for radiation cure.

RESIN STIFFNESS AT ELEVATED TEMPERATURES

Results from thermomechanical evaluation of the C-10 polyphthalocyanine polymer indicated that it would be desirable for the material to have greater stiffness at the higher ranges of temperature. Since the aliphatic chain of this resin is inherently flexible, it was obviously indicated that replacement of some portion

of the C-10 with a stiffer molecular unit should effect the desired result. The prime candidate for stiffer resin is called the Dianil for convenience, and it is the condensation product of terephthalaldehyde and 4-aminophthalonitrile:

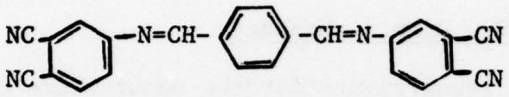

This very rigid molecule was prepared in substantial quantity during the last year and combined in 25:75 mole % mixture with the C_{10} Diamide monomer. Preliminary experiments show that polymers from this mixture improve stiffness but give some loss in fracture toughness. A compromise between stiffness and toughness by this approach is indicated and work in this area is continuing.

RESIN FRACTURE TOUGHNESS

It has been regarded as of paramount importance to the V/STOL program that the composite matrix resins be as resistant to crack propagation as possible in the belief that structural reliability will be dependent upon this resin property. Consequently, a great deal of thought and effort has gone into attempts to obtain the greatest fracture toughness possible in the polyphthalocyanines without sacrifice of other essential properties. Not all of these efforts have been successful in enhancing fracture toughness, but perhaps the most successful entailed synthesis of a long-chain, C-22 resin. Unfortunately, the C-22 resin is an expensive material because the diacid from which it is made is not a commercially available product.

Another approach for improving fracture toughness involves the synthesis of the C_{36} Diamide monomer from the EMPOL 1010 dimer acid sold commercially by Emery Industries, Inc. The dimer acid is produced by the polymerization of unsaturated C_{18} acids (e.g. linoleic acid) via the Diels-Alder Reaction. Essentially the dimer acid is a long chain dicarboxylic with two alkyl side chains. These features assure the lengthening of the diamide moiety, known to improve toughness, and introduce pendant alkyl chains capable of entanglement in the cured phthalocyanine polymer. The C_{36} Diamide monomer can be represented schemtically as

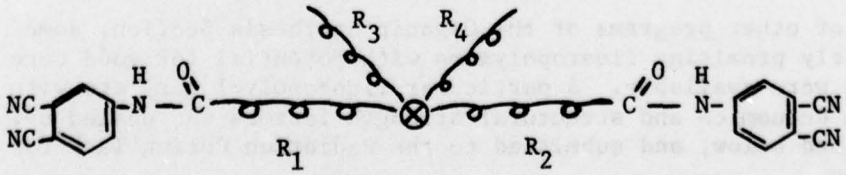

The C_{36}-polyphthalocyanine polymers derived from the above C_{36} Diamide continue to be of interest due to their potential high fracture energy and low cost. Several C_{36} Diamide samples of appropriate size for the compact tension test have been cast and cured at 220°C for 16 hrs.

Procurement of Additional C_{10} Diamide Monomer

To meet the projected requirements for the manufacture of T-300 graphite fiber prepreg and to provide the substantial quantities required for fabrication of test specimens during the coming year, contracts for 66 lbs of the C_{10} Diamide monomer have been awarded to Eastman Kodak Co. The first delivery (44 lbs) was received in September 1977 and approved for acceptance by our quality assurance tests. The remaining 22 lbs of monomer is scheduled for delivery in late December 1977. The 66 lbs of monomer will provide the necessary quantity of material to carry the DLF to completion as planned.

C_{10} Polyphthalocyanine-$SnCl_2$ Resin

C_{10} Polyphthalocyanine polymers coordinated with stoichiometric amounts of $SnCl_2$ have been of interest ever since exploratory studies demonstrated their high flammability resistance. This polymerization requires a "B" stage reaction and a post cure. The "B" stage reaction is accomplished by stirring an intimate mixture of C_{10}-Diamide (2 moles) and $SnCl_2 \cdot 2H_2O$ (1 mole) at 175-180°C. With good heat transfer, the reaction eliminates water quantitatively in 15 to 20 minutes leaving a brittle, amber resin melting at about 150°C. Post curing the amber resin at 190°C leads to a solid dark green resin in 20 minutes and to a fully cured C_{10} Polyphthalocyanine · $SnCl_2$ resin in 16 hours.

The flammability resistance of the above resin can be demonstrated qualitatively in a simple test. If held in a Bunsen flame, the polymer smokes and chars slowly but extinguishes itself immediately if the flame is removed. Two panels (6" x 6" x 1/8") of the resin have been submitted to National Bureau of Standards for evaluation of thermostability and fire resistance. Samples of both the "B" staged and fully cured resin have also been submitted for study in the Chemical Characterization Task.

Cis-Trans Fluoropolyol Acrylate Polymer

Out of other programs of the Organic Synthesis Section, some particularly promising fluoropolymers with potential for good cure by radiation were available. A particular fluoropolyol acrylate with favorable economics and structural strength factors was scaled up, as described below, and submitted to the Radiation Curing Task for evaluation.

The cis-trans fluoropolyol acrylate resin is synthesized in three steps. The first step is a modification of the NRL-devised method for preparing a fluoropolyol prepolymer (5). In the present case the cis-trans diols (1.00 mole), derived from hexafluoroacetone and propene, and the fluoroaromatic diols, i.e., 1,3- and 1,4-bis (2-hydroxyhexafluoro-2-proply) benzene (1.00 mole) are reacted with epichlorohydrin (2.00 moles) using a 10% excess of aqueous sodium hydroxide in refluxing acetone. This step leads to a fluoropolyol prepolymer as a light amber solid of the following structures.

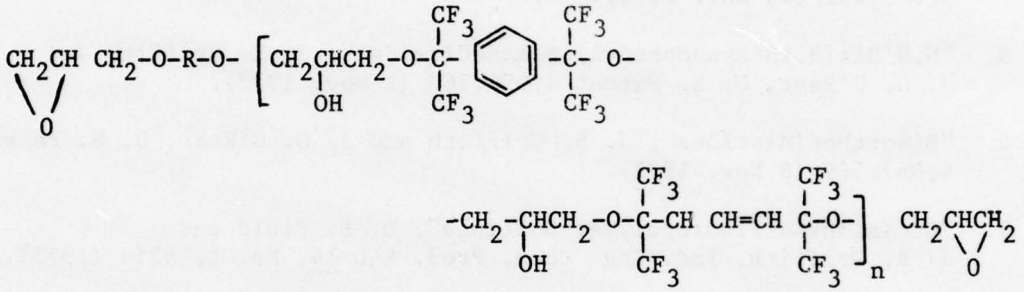

where R = $-C(CF_3)_2C_6H_4C(CF_3)_2-$

or $-C(CF_3)_2CH_2CH = CH(CF_3)_2C -$

In the second step, the fluoropolyol prepolymer is esterified with acrylic acid anhydride, using appropriate solvents and a catalyst. Solvent removal leaves the fluoropolyol acrylate as a viscous light amber liquid. An optically clear ester is readily prepared by percolating its ether solution through neutral alumina.

The third step crosslinks the fluoropolyol acrylate ester into a stable thermosetting polymer. Polymerization is promoted either by free radical catalysts or by radiation.

FUTURE PLANS

Due to the limited remaining time for synthesis in the present program, attempts to develop intrinsically new resins will not be undertaken. Our major efforts will be directed toward the synthesis of additional quantities of known or modified Diamide-based phthalonitrile monomers and their thermosetting resins as required. Additional amounts of the C_{10} Polyphthalocyanine-$SnCl_2$ will be synthesized if justified by the NBS thermostability tests. The 22 lbs of C_{10} Diamide due for delivery in December will be examined for acceptance by appropriate quality assurance tests.

REFERENCES

1. " High Performance Composites and Adhesives for V/STOL Aircraft, First Annual Report", (Willard D. Bascom and Luther B. Lockhart, Jr., Editors), Task A. Resin Synthesis, J. R. Griffith and J. G. O'Rear, NRL Memorandum Report 3433, pp. 7-13 (December 1976).

2. "Polyphthalocyanines Prepared from N,N'Bis(3,4-Dicyanophenyl) alkane Diamides", J. R. Griffith and J. G. O'Rear, U. S. Patent 3,993,631 (23 Nov. 1976).

3. "N,N'Bis(3,4Dicyanophenyl) Alkanediamides", J. R. Griffith and J. G. O'Rear, U. S. Patent 4,056,560 (1 Nov. 1977).

4. "Bisorthodinitriles", J. R. Griffith and J. G. O'Rear, U. S. Patent 4,057,569 (8 Nov. 1977).

5. "Crosslinked Fluoropolymer Coatings", D. E. Field and J. R. Griffith, Ind. Eng. Chem. Prod. R&D 14, No. 1, 5254 (1975).

PROJECTION FOR LARGE SCALE PRODUCTION OF PHTHALOCYANINE RESIN INTERMEDIATES

William C. Lyman
Eastman Organic Chemicals
Eastman Kodak Company
Rochester, New York 14650

Highly stable phthalocyanine resins can be prepared by polymerization of resin monomers synthesized from 4-aminophthalonitrile and aliphatic diacids. Eastman Kodak Company, through Eastman Organic Chemicals, has supplied to the Naval Research Laboratory the diamide prepared from sebacyl chloride. This compound (N,N-bis(3,4-dicyanophenyl)decanediamide) is colloquially referred to as the C_{10} diamide.

We prepare 4-aminophthalonitrile from 4-nitrophthalimide by the procedure developed by Walton, Griffith, and O'Rear, except for the last (reduction) step. Here we use a catalytic hydrogenation with alcohol and platinum oxide instead of aqueous sodium dithionite.

The preparative procedure for the C_{10} diamide supplied by the Naval Research Laboratory had to be modified extensively to allow for large scale production. We do not propose to describe this process in detail. Suffice it to say that it took us a long time to deliver our first large order.

That development activity is now behind us, and we are confident of our ability to supply larger quantities of high-quality product. Product having the following characteristics is being supplied readily:

Melting Point: 186°-189°C.
Infrared matches standard
Carbon Assay: $69.01 \pm 0.3\%$
Hydrogen Assay: $5.35 \pm 0.3\%$
Nitrogen Assay: $18.57 \pm 0.3\%$

Studies now underway at the Naval Research Laboratory will provide information about the effectiveness of this product in meeting the requirements, particularly its adaptability in the preparation of fiber reinforced composites and the stability of these composites when exposed to high temperatures. If they are highly effective, demand for these products will increase, but only if the polymer cost is

reasonable. Small quantities have been relatively expensive; therefore, it is useful to project what might happen to the prices of demand were to increase.

Based on our present manufacturing procedure, we expect to be able to supply 100,000-lb. quantities of 4-aminophthalonitrile for about $35/lb. and equivalent amounts of the C_{10} diamide for about $50/lb.

We are not aware of any patents which describe the 4-aminophthalonitrile or the N,N-bis(3,4-dicyanopheny)decanediamide. However, the polymer is described in U. S. Patent 3,993,631 dated November 23, 1976, "Polyphthalocyanines Prepared from N,N-Bis(3,4-dicyanophenyl) alkanediamide," by inventors James Griffith and Jacques O'Rear, assignee The United States of America as represented by the Secretary of the Navy.

The future utilization of these interesting compounds remains to be determined. Eastman Kodak Company looks forward to continued participation in the development of these materials.

FRACTURE BEHAVIOR OF HIGH TEMPERATURE RESINS

W. D. Bascom, R. L. Cottington, J. L. Bitner,
D. L. Hunston and J. Oroshnik
Polymeric Materials Branch
Chemistry Division

INTRODUCTION

The most important mechanical property requirements of the matrix resins of composites for advanced V/STOL aircraft are stiffness (high modulus) and toughness (high fracture energy). It is the purpose of this task to determine the effect of temperature, moisture, and thermal aging on these properties for a variety of candidate resins. One basis for resin selection is that the candidate be a potential matrix resin with use temperature in excess of 204°C (400°F).

Joining composite structural elements, either to themselves or to metals, is most effectively done by adhesive bonding. At present there are no high peel strength (high fracture energy) structural adhesives available for use above 120°C (250°F). There are also design problems associated with the adhesive bonding of composites in that there is a need to develop failure criteria both for normal load-bearing applications and for stress corrosion conditions. Work is underway in this Task on increasing the toughness of high temperature, thermosetting resins by incorporating a dispersed elastomeric (rubber) phase to give acceptable peel strengths. This effort is informally coordinated with similar work underway at other DoD and industrial laboratories. The mechanisms involved in obtaining a dispersed elastomeric phase are so complex that an empirical approach must be taken.

PROGRESS

Matrix Resin Modulus and Toughness

The modulus and fracture energy have been determined for various commercial high performance polymers and for the C_{10}-phthalocyanine polymer. The modulus measurements were made using the torsion pendulum which gives the shear modulus (G) and also the log decrement damping factor (loss tangent, tan δ).

The resin toughness is determined using the compact tension (CT) fracture specimens (2,3) illustrated in Figure 1. For this measurement neat resin plates are prepared by compression molding and

cut into approximately 2.5-cm squares. Alternatively, 5-cm diameter, moldings are made and tested as round compact tension specimens. In Figure 1, W is about 2.5-cm for the rectangular CT specimen and about 3.8 cm in. for the round CT specimen. The specimen widths (b) range from 3 mm to 6 mm. The fracture energy ($\mathcal{G}_{I_c}$) is obtained from the failure load, P_c, the tensile modulus E, the specimen dimensions and the geometry factors, Y, given in Figure 1 in terms of W and a, the crack length. The latter is measured from the center of the loading holes to the end of the notch dovetail.

Precracks were made in the dovetail by tapping with a knife blade or by making a razor cut. To obtain minimum root diameter precracks in the more brittle thermosetting polymers, it was necessary that the impact of the knife blade induce a running crack which is usually arrested by the increasing cross section of the dovetail. In the case of the much tougher thermoplastic polymers a cut made by a sharp razor blade gave a sufficiently sharp precrack.

Torsion pendulum shear modulus curves are given in Figures 2, 3 and 4 for various of the candidate resins. The tetra-functional epoxy, NARMCO 5208, has been taken as a "standard" for comparison purposes since engineering experience indicates its modulus is sufficiently high for use in advanced composites. The results in Figs. 2-4 suggest that over much of the operational temperature range the stiffness of all the resins, save for the polysulfone (PS), is quite comparable to that of the NARMCO 5208.

The various polymers do, of course, begin to differ significantly in the upper temperature region near their glass transition temperatures, T_g, where the modulus declines very rapidly with increasing temperature. The T_g values of the polymers are given in Table I and were determined from the shear modulus and tan δ plots. The actual upper service temperature will be much lower than T_g for various reasons: (a) tendency for the polymers to creep near T_g, (b) the onset of thermal decomposition, and (c) plasticization by absorbed water.

The "neat" polymer fracture energies, $\mathcal{G}_{I_c}$, are also given in Table I. This parameter characterizes the material's resistance to flaw growth under sustained, rising loads. It usually parallels crack growth resistance under fatigue or impact loads but the relationships are complicated by the rate dependence of polymer mechanical properties.

Polymer toughness should be reflected in the resin-dominated properties of composites, e.g. interlaminar shear strength, transverse strength and impact damage. It is problematical to what extent the resin toughness translates into comparable composite properties, although there is evidence both in the literature and in practice that increased resin toughness does improve certain composite properties. The effect of resin toughness on composite mechanical properties is being addressed in this program.

TABLE I

FRACTURE ENERGIES OF COMMERCIAL POLYMERS

Chemical Type	Commercial Designation	Fracture Energy, $\mathcal{G}_{I_c}$ kJ/m^2	Tg, ^{o}C
	THERMOSETS		
tetrafunctional epoxy	NARMCO 5208	0.082	260
polyimide (addition)	Hexcel F-178	0.104	360
polyimide (acetylenic)	Gulf T-600	0.175	330
polytriazine	Ciba-Geigy NCNS	0.085	250
polyphthalocyanine	NRL/Eastman, C_{10}	0.110	360
	THERMOPLASTICS		
polyarylsulfone (PAS)	Carborundum ASTREL	2.3	350
polyarylsulfone	Union Carbide, RADEL	1.3	220
polysulfone (PS)	Union Carbide, UDEL	~5.0	174
polyethersulfone (PES)	ICI, P300	0.51	230
polyimide (PI)	Upjohn 2080	0.92	326
polyimide	DuPont NR150 B2	2.3	360
polyamide-imide	Amoco 4000T	3.9	274

Considered from a molecular point-of-view, the higher toughness of the thermoplastics compared to the thermosets, evident in Table I, is not unexpected. Polymer toughness can be attributed to energy dissipation by the slippage and untangling of long polymer molecules in the region of high stress concentration at a crack tip. The uncrosslinked thermoplastics have considerable capability for such irreversible deformation. On the other hand, the high density of crosslinks between polymer chains, which characterizes the molecular structure of the thermosets, inhibits molecular flow and limits the fracture energy of thermosetting polymers.

Effect of Heat Soak on Resin Toughness

In earlier work (1) the C_{10}-phthalocyanine and Hexcel F-178 polyimide resins were heat soaked at 288°C (550°F) and then the shear modulus and damping factor evaluated using the torsion pendulum. Heating times up to 480 hours caused a gradual increase in modulus and T_g, which suggested that the cure state of polymers was being advanced, i.e., increased crosslinking was taking place. The torsion pendulum data did not suggest any significant polymer degradation. However, the polymers showed qualitative evidence of becoming increasingly brittle with the length of the heat soak in that the specimen became more fragile and difficult to handle.

A study was undertaken to determine the extent of this loss in toughness by subjecting compact tension fracture specimens to thermal soaks at 220°C (428°F), 240°C (464°) and 260°C (500°F) for various times up to 240 hrs. The results are given in Figure 5 for the C_{10}-phthalocyanine and Figure 6 for the Hexcel F-178 polyimide. The initial cure schedule for these resin is given in Table II. Note that the initial cure schedule for the Hexcel F-178 was devised to minimize heat buildup from the reaction exotherm. Unfortunately, this produced very uncured specimens which were too fragile to test and so no values are plotted for zero soak times in Figure 6.

TABLE II

Curing Procedures Selected for Thermal Aging Study

C_{10}-polyphthalocyanine

200°C - 24 hrs.

Hexcel F-178, polyimide

135°C - 1 hr.

177°C - 1 hr.

246°C - 3 hrs.

The data in Figures 5 and 6 indicate that neither resin suffers a significant loss in room temperature toughness after aging at 220°C or 240°C and, in fact, after 24 to 48 hours there is some slight increase in $\mathcal{G}_{I_c}$. At 260°C, however, there is a factor of 10 decline in $\mathcal{G}_{I_c}$ for the C_{10}-polyphthalocyanine between 24 and 48 hours and a less abrupt but none-the-less distinct decrease in $\mathcal{G}_{I_c}$ for the F-178 polyimide. After 460 hours at 260°C the polyimide had about the same $\mathcal{G}_{I_c}$ value as after 240 hrs (~50 J/m^2) which suggests the loss in toughness had begun to level off.

The C_{10}-polyphthalocyanine could not be tested after 240 hours exposure at 260°C because the specimens developed large internal blisters and had puffed-up into the shape of pillows. Evidently a vapor is evolved at this temperature which cannot escape from the interior where it forces open an internal pocket. This same volatile material - presumably a thermal decomposition product - must also have been generated during the 120-hr 260°C heat soak of the C_{10}-polyphthalocyanine. Its action as a plasticizer could explain the curious rise in $\mathcal{G}_{I_c}$ (Figure 5) from the very low value after 48 hours at 260°C. Differential scanning calorimetry (DSC) of the C_{10}-polyphthalocyanine that had been heat aged at 220°C for 48 hours (after initial cure) also gave evidence of the evolution of a low molecular weight, volatile material during the heat scan between 250-350°C. The DSC also revealed an exotherm attributable to additional curing of the polymer, as discussed in the next paragraph.

Torsion pendulum tests were run on the C_{10}-polyphthalocyanine polymer after heat soaking for various times and the shear modulus and damping factor data are presented in Figure 7. These results clearly show that the thermal treatment is increasing the crosslink density as evidenced by the progressive increase in modulus above 100°C and in the T_g. The low temperature transitions, $T_{(CH_2)_n}$ and T_{H_2O}, are discussed in detail in the next chapter.

The loss in toughness with heat aging, shown here for the C_{10}-polyphthalocyanine and the F-178 polyimide, is not surprising although it does not appear to have been documented quantitatively before. The principle factor contributing to this embrittlement is the increase in crosslink density which reduces what little capacity for plastic deformation the polymer network may have had initially. The result is that when the polymer is fully cured, $\mathcal{G}_{I_c}$ is reduced to a value more characteristic of a ceramic or silicate glass (10-20 J/m^2) than an organic polymer. The effect was more serious for the phthalocyanine resin than for the polyimide.

The results of this thermal aging study point up the fact that the upper use temperature of a thermosetting resin is significantly less than the T_g to which it can be ultimately cured. Indeed, post curing to maximize T_g can be expected to reduce the resin toughness to unacceptably low levels. In the case of the polyphthalocyanine and the polyimide, the upper limit is 240°C compared to their ultimate T_g of ~350°C.

The embrittlement effect of thermal aging is, of course, not limited to the two resins studied here but can be expected for any thermosetting polymers. It is not possible to predict the degree of loss in toughness or the temperature or rate at which it will occur because of the complexity of the processes involved.

Conclusions and Future Work

The various candidate matrix resins examined here are essentially indistinguishable so far as stiffness is concerned at least up to temperatures near their T_g. Even among those polymers usually considered for use at 450°F (232°C), the T_g values fall in a relatively narrow range of about 300-350°C. As for resin toughness, the two general classes of polymers - thermosetting and thermoplastic - differ considerably, with the thermoplastics having fracture energies 10 to 40 times greater than those of the thermosets. It was shown for two thermosetting resins that thermal aging advances the state of cure and reduces their fracture energy still further.

Future work will be on the thermal aging of other resins including some of the thermoplastics listed in Table I. An effort is underway to formulate high temperature, high toughness adhesives and these, along with some commercial materials, will be tested for adhesive $\mathcal{G}_{I_c}$. Work is underway on the rate of water sorption by the C_{10}-polyphthalocyanine and the F-178 polyimide as a function of post-cure temperature. Water pickup by certain of the thermoplastic polymers will also be determined. A study has been initiated on the reduction in T_g by absorbed water. This lowering in T_g has generally been observed as a decrease in modulus at temperatures near T_g which are high enough to promote thermal decomposition (possibly assisted by water). The work here is aimed at differentiating the two effects.

References

1. NRL Memo Report 3433, "High Performance Composites and Adhesives for V/STOL Aircraft", Dec. 1976, W. D. Bascom and L. B. Lockhart, Jr., p. 15.

2. Knott, J. F., "Fundamentals of Fracture Mechanics", Butterworths, London, 1973, p. 130.

3. Schutz, W., in "Fracture Mechanics of Aircraft Structures", H. Liebowitz, Ed., AGARD., AG-176, NTIS, Springfield, VA, p. 371.

$$\mathcal{G}_{I_c} = Y^2 \frac{P_c^2}{E W^2 b^2}$$

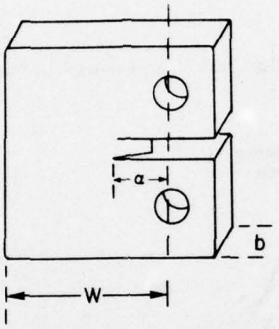

COMPACT TENSION SPECIMEN

$$Y = 29.6 - 186\ a/W + 656\ (a/W)^2 - 1017\ (a/W)^3 + 639\ (a/W)^4$$

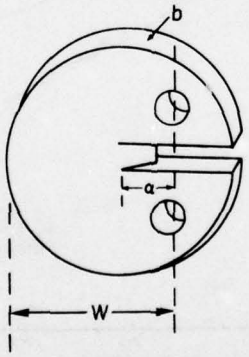

ROUND COMPACT TENSION SPECIMEN

$$Y = 30.0 - 162\ a/W + 493\ (a/W)^2 - 664\ (a/W)^3 + 405\ (a/W)^4$$

Fig. 1 — Compact tension fracture test specimens

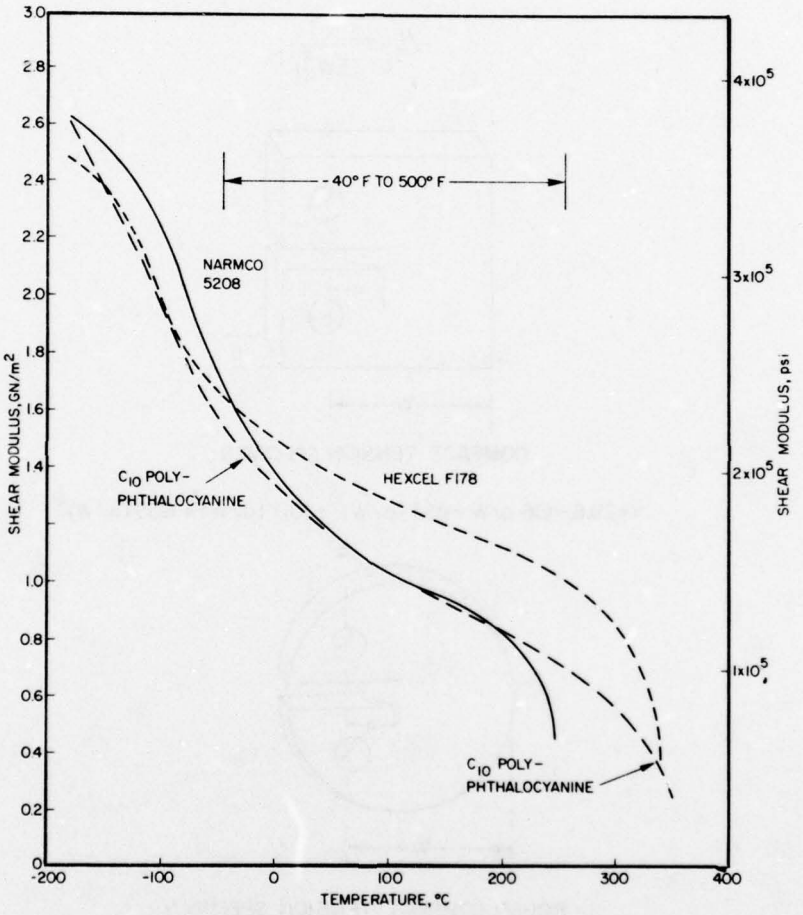

Fig. 2 — Shear modulus vs temperature from torsion pendulum tests. See Table I for polymer identification.

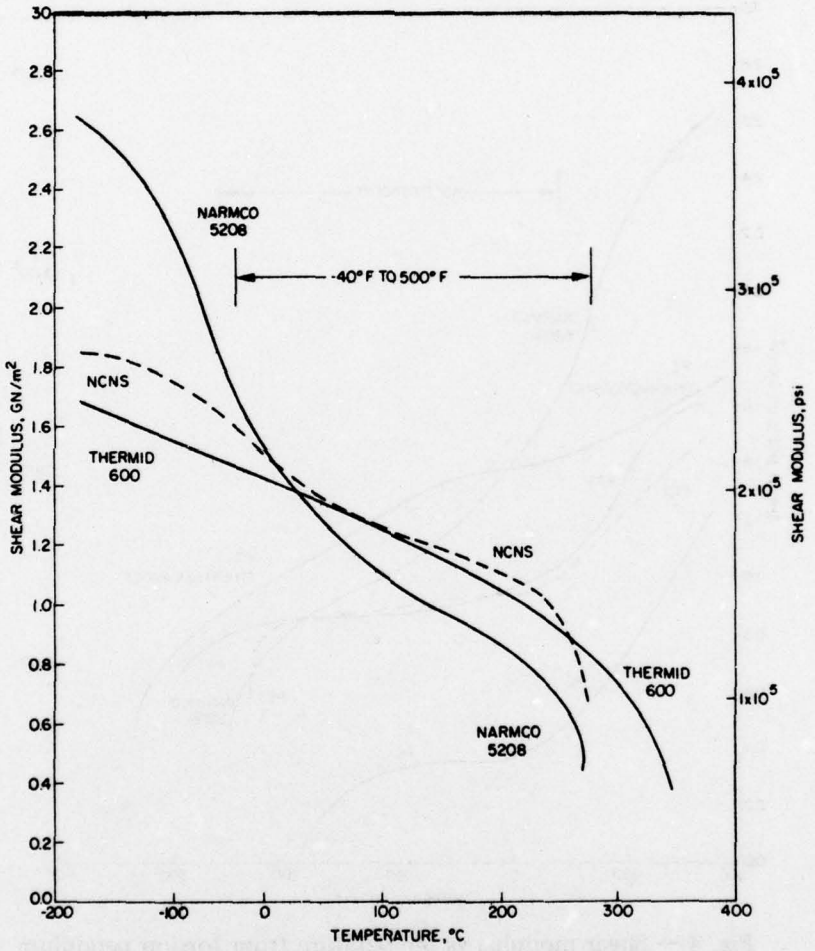

Fig. 3 — Shear modulus vs temperature from torsion pendulum tests. See Table I for polymer identification.

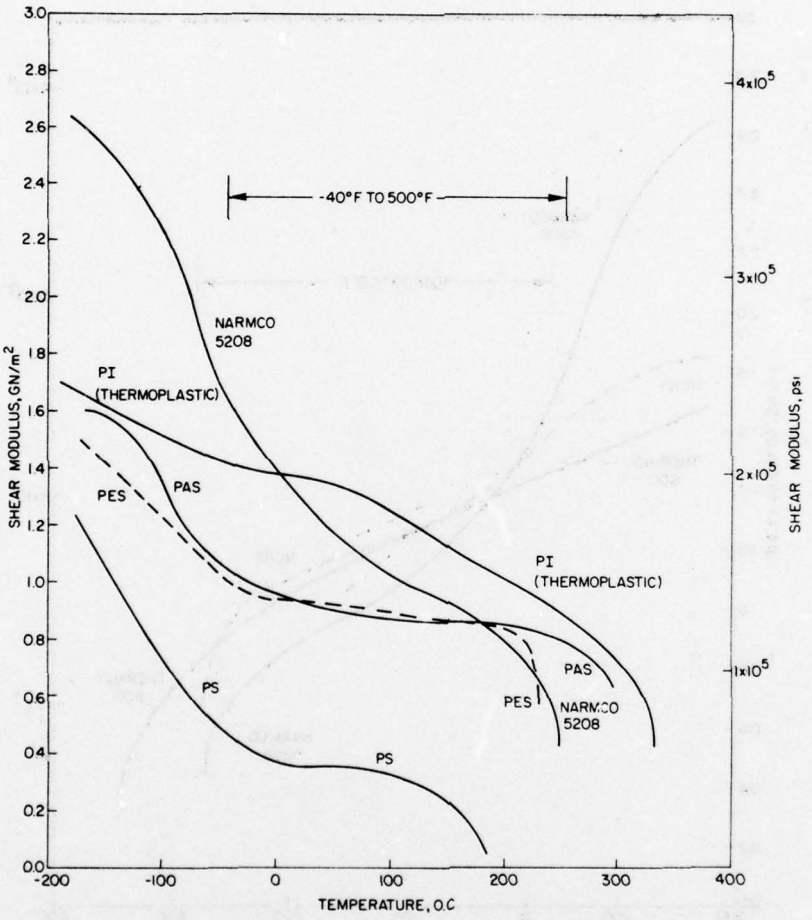

Fig. 4 — Shear modulus vs temperature from torsion pendulum tests. See Table I for polymer identification.

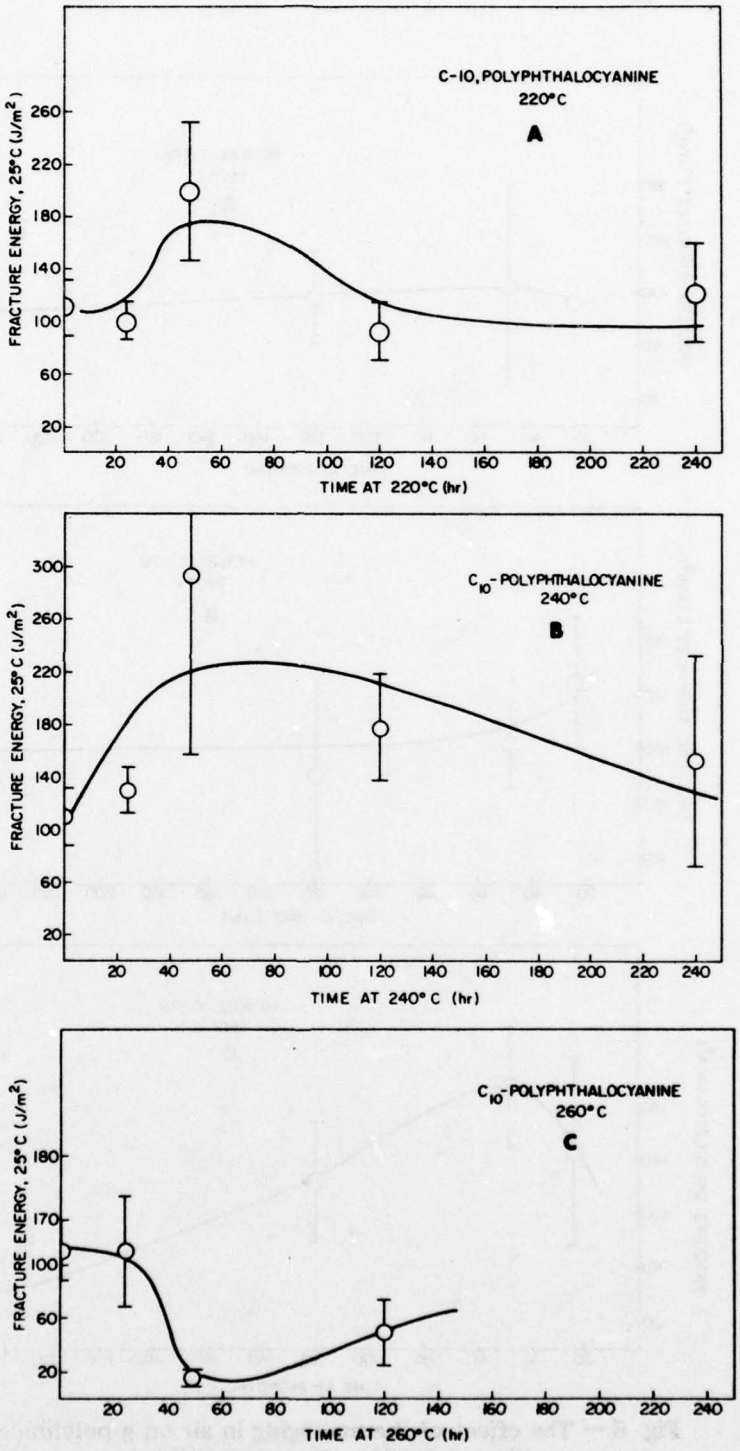

Fig. 5 — Effect of thermal aging in air on the fracture energy of C_{10}-polyphthalocyanine. Tested at 25°C.

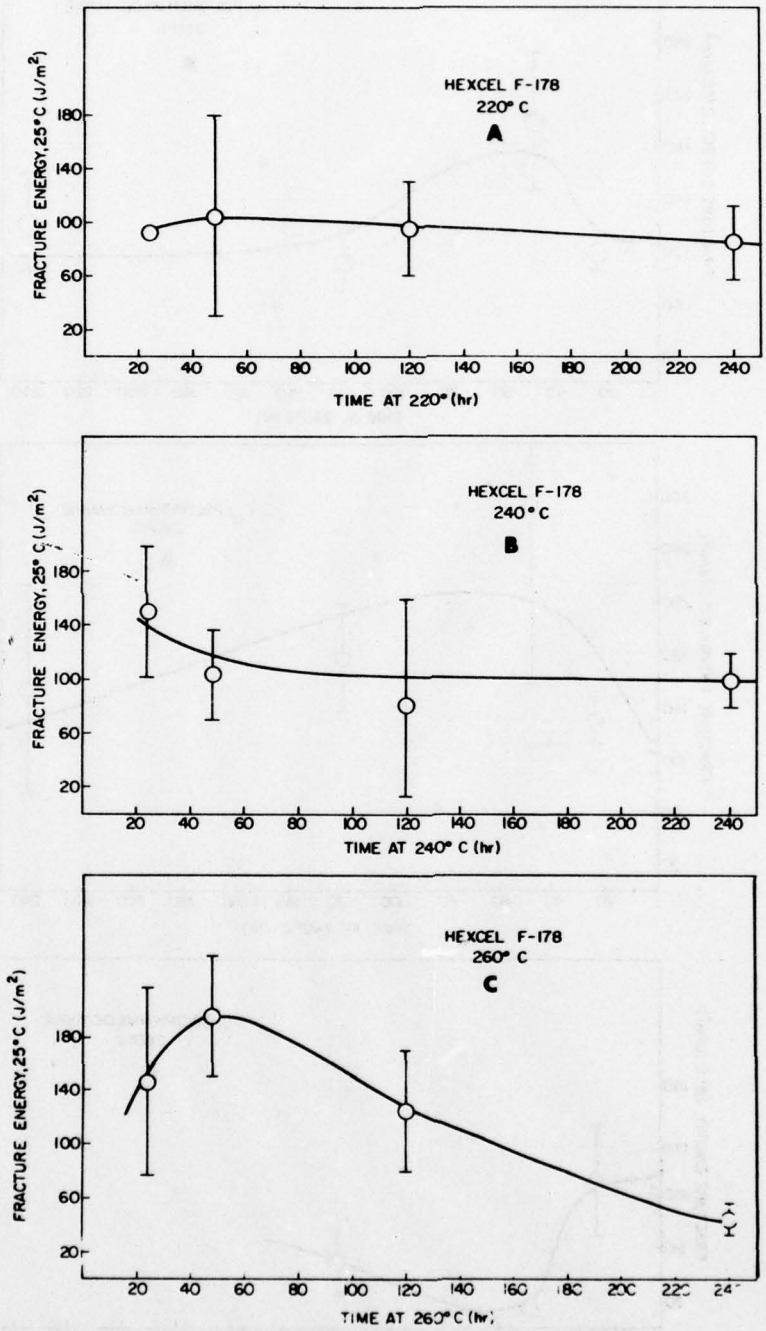

Fig. 6 — The effect of thermal aging in air on a polyimide (Hexcel F-178). Tested at 25°C.

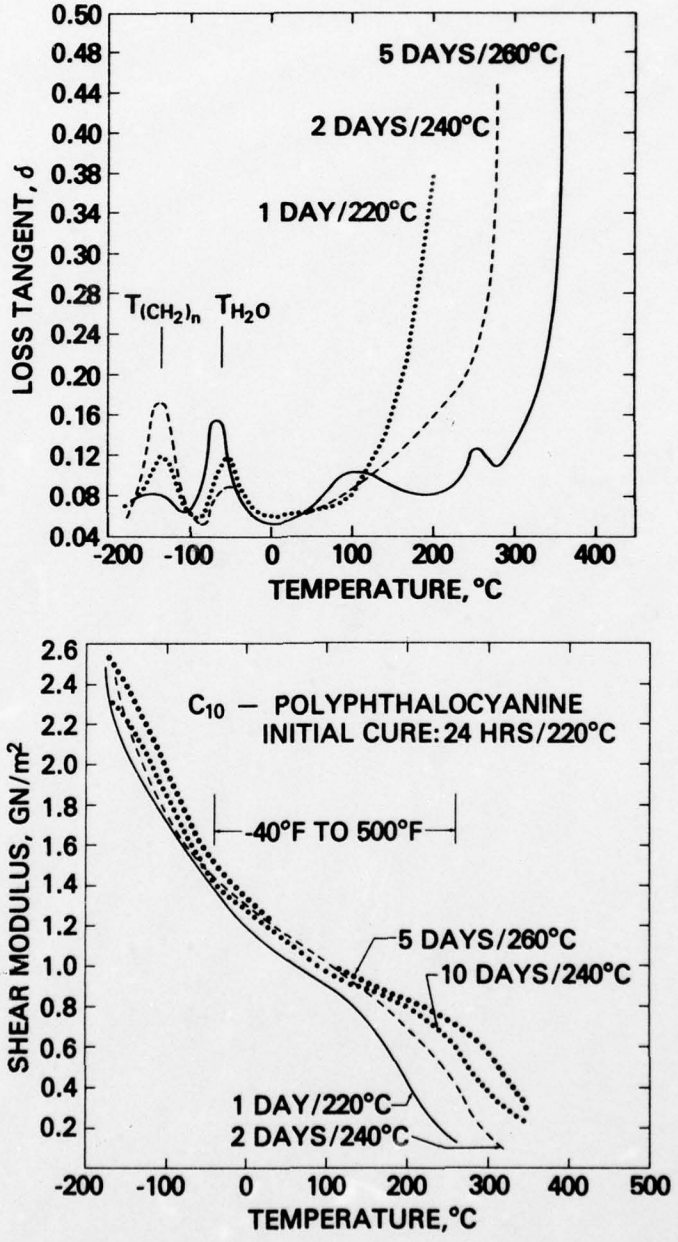

Fig. 7 — Effect of thermal aging on the shear modulus and loss tangent of C_{10}-polyphthalocyanine

TORSION PENDULUM ANALYSIS OF THE FORMATION AND PROPERTIES OF A POLYPHTHALOCYANINE

J. K. Gillham
Polymer Materials Program
Department of Chemical Engineering
Princeton University
Princeton, New Jersey 08540

INTRODUCTION

An automated torsion pendulum has been used to investigate the transformation (cure) of the C_{10} diamide phthalocyanine resin monomer to thermoset polymer using supported specimens (torsional braid analysis). Cure was examined directly from isothermal plots and from transitions versus time of isothermal cure, which were obtained from thermomechanical plots of intermittently cooled specimens. Also investigated was the influence of the level of water vapor ($ppm_v H_2O$ in He) on a water-induced low temperature transition ["T_{H_2O}" = ~-75°C(<1 Hz)] and on a low temperature transition ["T_{sec}" = ~-150°C(<1 Hz)] inherent in the cured polyphthalocyanine resin.

EXPERIMENTAL

Monomer

"C_{10} monomer" was obtained from the Naval Research Laboratory, Washington, D. C. The sample, coded 14939EK Lot A7, had been prepared by the Eastman Kodak Company. The white crystals had a melting point of 185-189°C: the melting point of analytically pure monomer, recrystallized several times from acetonitrile, has been reported to be 192-194°C (1). The monomer was melted to form a prepolymer (with a glass transition temperature of about 60°C) which reacted above 200°C to form polymer as described below.

Torsion Pendulum Procedure

An automated torsion pendulum (2) was used for all of the experiments.

Specimens were formed by dipping a glass braid into a slurry of the C_{10} diamide monomer in ethyl alcohol [weight monomer (g)/volume alcohol (ml) ≃ 1/3]. After evaporation of the ethanol, the dispersed

reactions leading to gelation, each specimen (after mounting) was inserted into the cool upper zone of the apparatus to remove air before being lowered into the hot zone which had been preset at a particular isothermal temperature. For the experiments in which a specimen was to be intermittently cooled from an isothermal temperature, the specimen was inserted in the apparatus at RT and the temperature raised to its isothermal value (at 5^{o}C/min to 240^{o}C; at 1.5^{o}C/min to 215^{o}C). All experiments were performed at a heating and cooling rate of 1.5^{o}C/minute in an atmosphere of slowly flowing helium, unless stated to the contrary.

During an experiment, a mounted specimen is intermittently set into torsional oscillation to generate a series of freely damped waves. The frequency of oscillation is about 1 Hz. The character of these waves provides a monitor of the chemical and physical changes that occur. Two mechanical functions, rigidity and damping, are obtained from the frequency and decay constants which characterize each wave. The experiment provides plots of relative rigidity ($1/P^2$, where P is the period in seconds) and logarithmic decrement ($\Delta = \ln A_i/A_{i+1}$, where A_i is the amplitude of the i^{th} oscillation) vs. temperature (mV from an iron-constantan thermocouple) or time. The relative rigidity is directly proportional to the in-phase shear modulus (G'); the logarithmic decrement is directly proportional to the ratio of the out-of-phase shear modulus (G") to G'. G' and G" are material parameters of the specimen which characterize the storage and loss of mechanical energy on cyclic deformation.

Specimens were exposed to various levels of water vapor (ppm_v, parts per million by volume, measured continuously by an electronic hygrometer) in a flowing stream of helium formed by mixing dry and saturated streams of helium in various proportions (3). After conditioning at a definite temperature for a measured period of time, thermomechanical data were obtained in the conditioning atmosphere on cooling to -195^{o}C and on subsequent heating.

RESULTS

I. Gelation time versus temperature of cure.

Isothermal curves of rigidity and mechanical loss at a series of temperatures from 201^{o}C to 252.5^{o}C are shown in Figure 1. (For clarity, the curves are displaced vertically by arbitrary amounts.) Consistent and sometimes subtle trends are especially apparent in the loss curves with change of temperature.

The loss peak accompanying the initial increase in rigidity in each isothermal experiment is associated with gelation. This follows

since a loss peak (Tg) occurred with a corresponding increase in rigidity below the temperature of isothermal cure on cooling each specimen at the end of the isothermal cure. Vitrification had not therefore occurred during the isothermal cures. The time to gelation was taken as the time interval between the beginning of an isothermal experiment and the occurrence of the maximum of the loss peak. Since the chemical conversion at the point of gelation for a thermosetting system is considered to be independent of temperature, a plot (Figure 2) of the time to gelation versus 1/temperature (^{o}K) provided an activation energy for the reactions leading to gelation. A tabulation of the times to gelation versus isothermal cure temperature appears in Table 1. The value 23.70 kca/mole is in line with activation energies for the cure of some epoxy resins.

II. Transitions versus extent of cure.

The influence of time of isothermal cure on thermomechanical transitions was investigated by curing isothermally and interrupting the cure intermittently to obtain the thermomechanical behavior. Two temperatures for isothermal cure were employed. At 215^{o}C thermomechanical plots (Figure 3) were obtained after lapsed times from 0.1 to 55.05 hours. At 240^{o}C thermomechanical plots (Figure 4) were obtained after lapsed times from 0.05 to 40.85 hours. The plots can be integrated (see Figure 5 and Figure 6) on the basis of the change of the main transitions which are designated T' > Tg, T > Tg, Tg, T'$_{sec}$ and T$_{sec}$ with time of cure. Tabulations of the transitions versus time of cure appear in Tables 2 and 3. Tg, T > Tg and T' > Tg increase in their temperature assignments and decrease in intensities with extent of reaction.

T' > Tg. This relaxation moves from ~130^{o}C (T_{cure} 215^{o}C/time 0.1 hr) to above 240^{o}C (T_{cure} 240^{o}C/time 0.8 hr). The transition corresponds presumably to the T > Tg transition of amorphous linear polymers in separating two types of fluid behavior (4). Processing will be facilitated by operating above this and the T' > Tg relaxation. The T' > Tg and T > Tg relaxations move more rapidly to higher temperatures with extent of reaction than does Tg.

Tg. This transition moves from 65^{o}C (T_{cure} 215^{o}C/time 0.1 hr) to 208^{o}C (T_{cure} 240^{o}C/time 40.85 hr). However, its increase with time of cure after 9.75 hours is slow at 240^{o}C.

T'$_{sec}$ (~0-15^{o}C). This low temperature transition appears in all stages of cure. It presumably is connected with motions of the flexible methylene chain segment of the structure. The influence of water on it (see below) suggests that the segment includes the polar amide linkages.

At the end of the isothermal cures at 215^{o}C/55.05 hours and at 240^{o}C/40.85 hours, thermomechanical spectra were obtained to -195^{o}C

(to complete the series for Figures 3 and 4) and then from -195°C to 300°C to -195°C (Figure 7 and Figure 8) in order to measure the influence of further heating to 300°C.

It is noted (Figure 3 and Figure 4) that the extent of thermohysteresis (T > Tg) decreases as the cure progresses. Thermohysteresis arises from crazing and subsequent heating of the brittle low molecular weight material; closing of the hysteresis loop is evidence for the thermoplastic nature of the material in the early states of cure.

It is further noted that a subtle relaxation develops at about -85°C with extended cure (Figures 3, 4, 7 and 8) and that there are changes in the character of the region above Tg with extent of cure.

III. Influence of Water

Experiments on the influence of the level of water vapor ($ppm_v H_2O$) in the atmosphere (He) were performed on cured polymer (cured 240°C/12 hr/100 $ppm_v H_2O$). The specimen was conditioned at a particular level of water vapor at 35°C for 17 hours after which the thermomechanical behavior was obtained on cooling from 35°C to -195°C without changing the moisture level of the input atmosphere. A plot was then also obtained on heating from -195°C to 170°C with the same input atmosphere (plots not shown). The same specimen was cooled to 35°C in a dry atmosphere and then reconditioned at another level of water vapor.

The maximum temperature of 170°C in the cycling experiments was considered to be high enough to eliminate water and yet low in comparison with the cure temperature (240°C) to minimize further chemical cure reactions on temperature cycling.

It has been shown (3) that the kinetics of water sorption and desorption for epoxies is slow below 35°C in the time scale of the experiment so that thermomechanical spectra at low temperatures are independent of the water content of the testing atmosphere. The thermomechanical spectra for the polyphthalocyanine under investigation were also independent of the moisture level in the measuring, as distinct from the conditioning, atmosphere below ~0°C (data not shown).

The dry cured (240°C/12 hr/100 $ppm_v H_2O$) polymer (Figure 9) displayed the following transitions: T_{sec} [-146°C (2.1 Hz)], T_{H_2O} (weak) [-73.5°C (1.9 Hz)], T'_{sec} [~0°C] and Tg [200°C (1.1 Hz)].

Representative thermomechanical plots taken from conditioning in various levels of water vapor appear in Figure 10; in particular they show the induced water transition ("T_{H_2O}") and the secondary polyphthalocyanine relaxation (T_{sec}). The influence of water on the T_{H_2O} and T_{sec} transitions are summarized in Figure 11 both for increases and

(after a maximum level of exposure) for incremental decreases of water vapor.

The apparent temperature of the T_{H_2O} transition decreases and the intensity increases, both to asymptotic levels. Concurrently, the apparent temperature of the T_{sec} transition decreases and its intensity decreases, again both to asymptotic levels. This suggests that both transitions are coupled and that there are a limited number of sites for interaction with water. The decrease in temperature assignments for both relaxations with increasing water is to be noted. The processes are reversible, removal of water resulting in the restoration of the thermomechanical behavior of the dry starting material.

CONCLUSIONS

An automated torsion pendulum has been used to study the cure of C_{10} diamine polyphthalocyanine by the torsional braid method. Isothermal runs at temperatures between 201°C and 252°C were made to determine an activation energy of 23.7 kcal/mole for the reactions leading to gelation. Various transitions in the log decrement vs temperature plot developed as the resin cured and were observed to shift to higher temperatures as the cure progressed. Two transitions were found above T_g in the early stages of cure. The recommendation is made that curing of B-staged resin be performed at temperatures above these transitions. A maximum T_g could not be found for this polymer because the transition shifted toward the limiting temperature (300°C) of the experiments with extended cure. The loss peak and change in rigidity for this transition became very weak as the cure progressed.

Two distinct transitions were observed below T_g, which are attributed to motion of the alkyl chain (T_{sec}) and to absorbed water (T_{H_2O}), respectively. Observations of the effect of changing the amount of absorbed water on T_{sec} and T_{H_2O} leads to the conclusions (a) that the molecular segments responsible for T_{sec} include the amide linkages as well as the alkyl chain between them and (b) that water hydrogen bonds to polar groups and that there is a saturation limit to this hydration.

ACKNOWLEDGMENTS

Appreciation is expressed to Drs. W. D. Bascom and J. R. Griffith of the Naval Research Laboratory who provided the samples of C_{10} diamide monomer and discussed earlier torsion pendulum data (5) and the chemistry and properties of polyphthalocyanines with the author.

REFERENCES

1. J. R. Griffith and J. G. O'Rear, in High Performance Composites and Adhesives for V/STOL Aircraft, NRL Memorandum Report 3433, pp. 7-

14, (Ed. W. B. Bascom and L. B. Lockhart, Jr.), Naval Research Laboratory, Washington, D. C., December 1976.

2. J. K. Gillham, A.I.Ch.E. J., 20 (6), 1066 (1974).

3. J. K. Gillham, C. A. Glandt and C. A. McPherson, in Chemistry and Properties of Crosslinked Polymers, (Ed. S. S. Labana), Academic Press, New York, pp. 491-520 (1977).

4. J. K. Gillham, J. A. Benci and R. F. Boyer, Polymer Engineering and Science, Vol. 16, No. 5, 357 (1976).

5. W. D. Bascom, R. L. Cottington, J. L. Bitner and J. Oroshnik, in High Performance Composites and Adhesives for V/STOL Aircraft, NRL Memorandum Report 3433, pp. 15-34, (Ed. W. D. Bascom and L. B. Lockhart, Jr.), Naval Research Laboratory, Washington, D. C., December 1976.

Table 1

Gel Time Vs Temperature of Cure

Plot No.	Temp. ^{o}C	Gelation Time Log_{10} time (sec)
6A	201	4.521
5A	212	4.170
4A	221.5	4.065
3A	232	3.878
2A	242.5	3.621
1A	252.5	3.435

Table II

TRANSITIONS VS. TIME OF CURE AT 215°C

Plot	Time (Hr)	T' > Tg °C	T > Tg °C (Hz)	Tg °C (Hz)	T_{sec}' °C (Hz)	T_{sec} °C (Hz)
1	0.1	∿130	93 (0.29)	65 (0.61)	hysteresis	-153 (1.8)
2	0.2	∿144	102 (0.28)	68.5 (0.68)	"	-153 (1.8)
3	0.7	∿168	121.5 (0.28)	74.5 (0.72)	"	-155 (1.8)
4	2.2	>215 (?)	∿154	83 (0.79)	"	-152 (1.9)
5	5.1	>215 (?)	∿213	104 (0.96)	"	-150 (2.1)
6	14.6	>215 (?)	>215 (?)	132 (1.01)	∿0	-149 (2.2)
7	30.25	>215 (?)	>215 (?)	166.5 (1.05)	∿10	-147 (2.2)
8	55.05	>215 (?)	>215 (?)	187.5 (1.10)	∿5	-145 (2.2)
9	Heated to 300°C	>300 (?)	>300 (?)	221 (1.20)	7	-144.5 (2.2)

Table III

TRANSITIONS VS. TIME OF CURE AT 240°C

Plot (Cycle)	Time (Hr)	T' > Tg °C	T > Tg °C (Hz)	Tg °C (Hz)	T_{sec}' °C (Hz)	T_{sec} °C (Hz)
1 (1)	0.05	∿137	98.5 (0.27)	69 (1.24)	hysteresis	-153 (1.8)
1 (2)	0.25	∿186 (?)	142 (0.25)	78 (0.78)	"	-153 (1.9)
1 (3)	0.80	>240 (?)	186(?)(0.36)	97 (0.90)	"	-152 (2.1)
2 (1)	3.3	>240 (?)	>240 (?)	154 (1.05)	∿10	-147 (2.3)
2 (2)	9.75	>240 (?)	>240 (?)	197 (1.18)	9	-145 (2.3)
2 (3)	40.85	>240 (?)	>240 (?)	208 (1.39)	15	-145 (2.3)
3	Heated to 300°C	>240 (?)	>240 (?)	230 (1.30)	15.5	-145 (2.3)

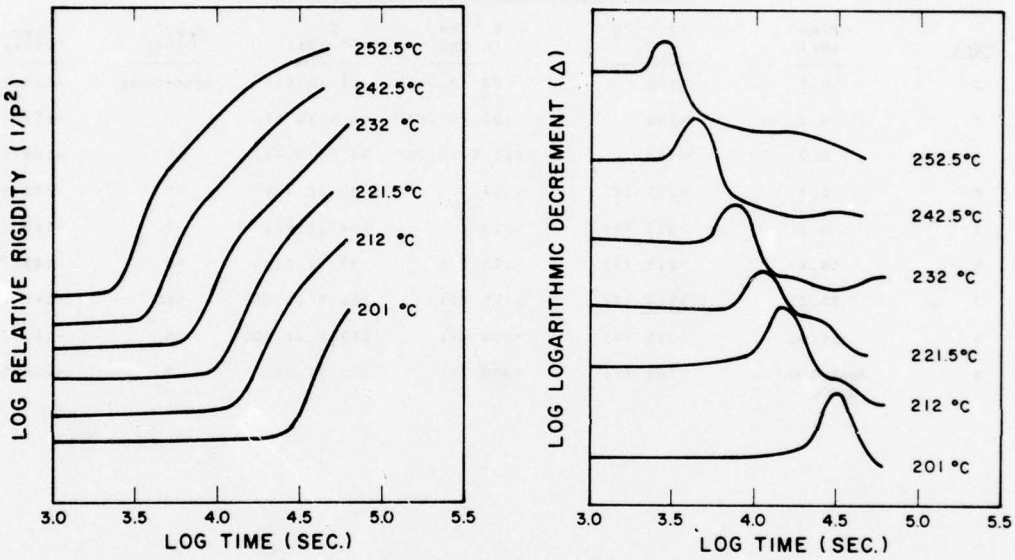

Fig. 1 — Isothermal cures at a series of temperatures. Left: relative rigidity versus $\log_{10}$ time (seconds). Right: logarithmic decrement versus $\log_{10}$ time (seconds). (Note: for clarity the isothermal curves have been displaced vertically by arbitrary amounts.) These plots yield time to gelation versus temperature of cure.

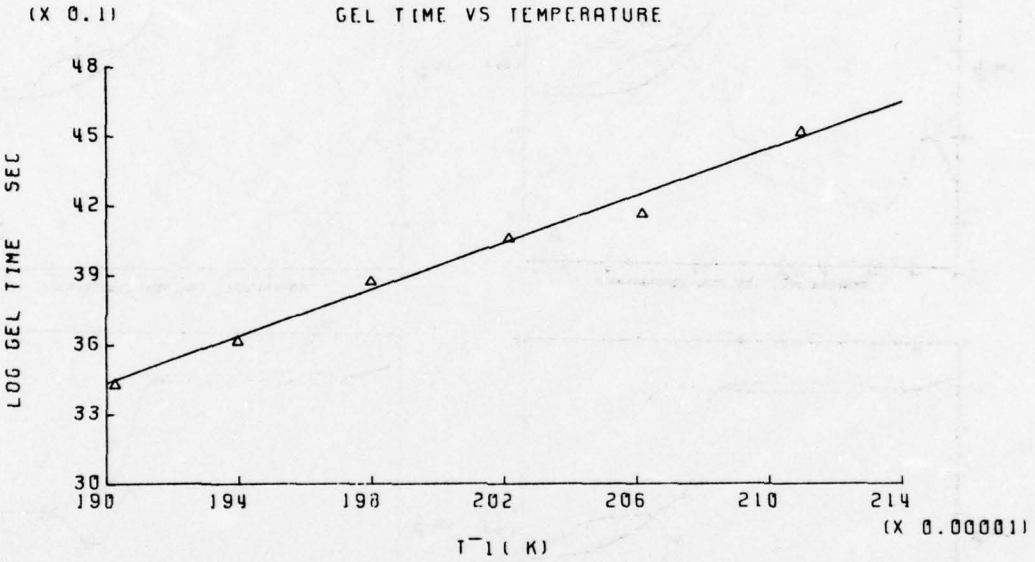

Fig. 2 — Arrhenius plot: time to gelation vs isothermal cure temperature

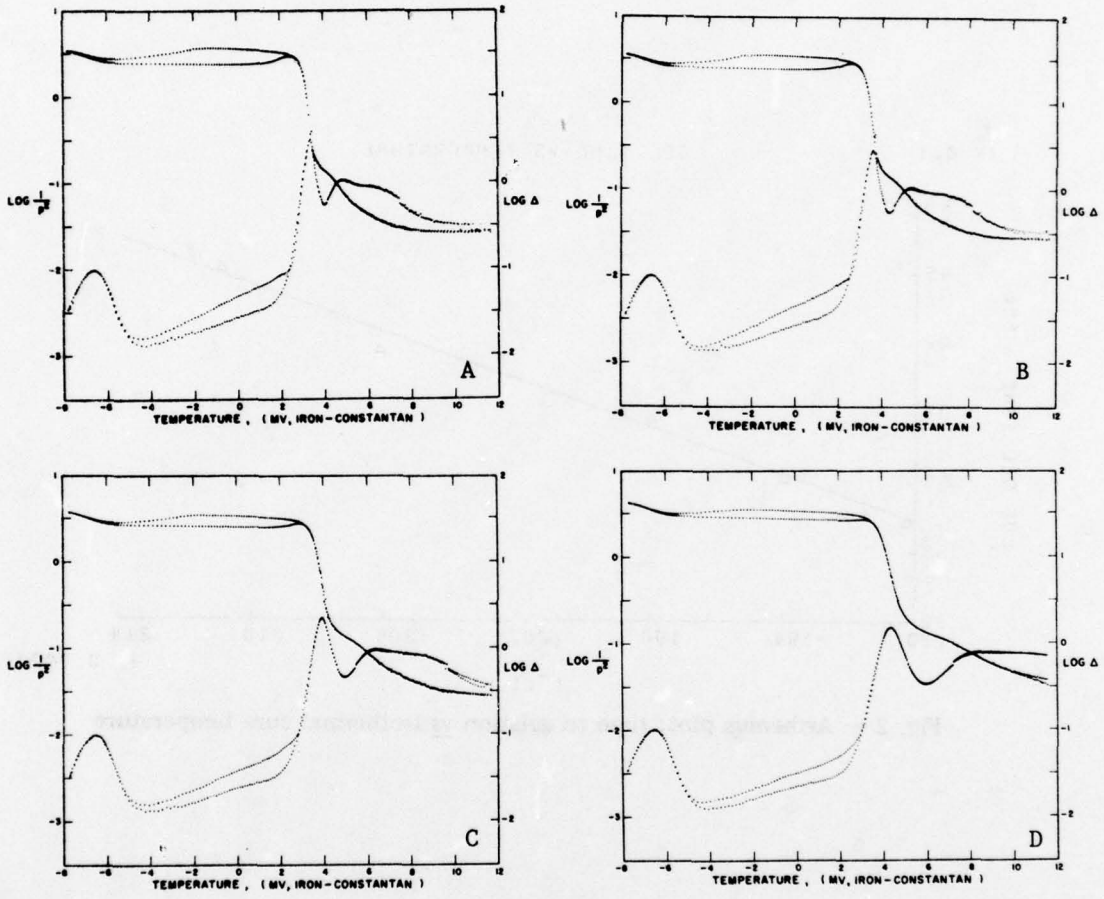

Fig. 3 (Continues)

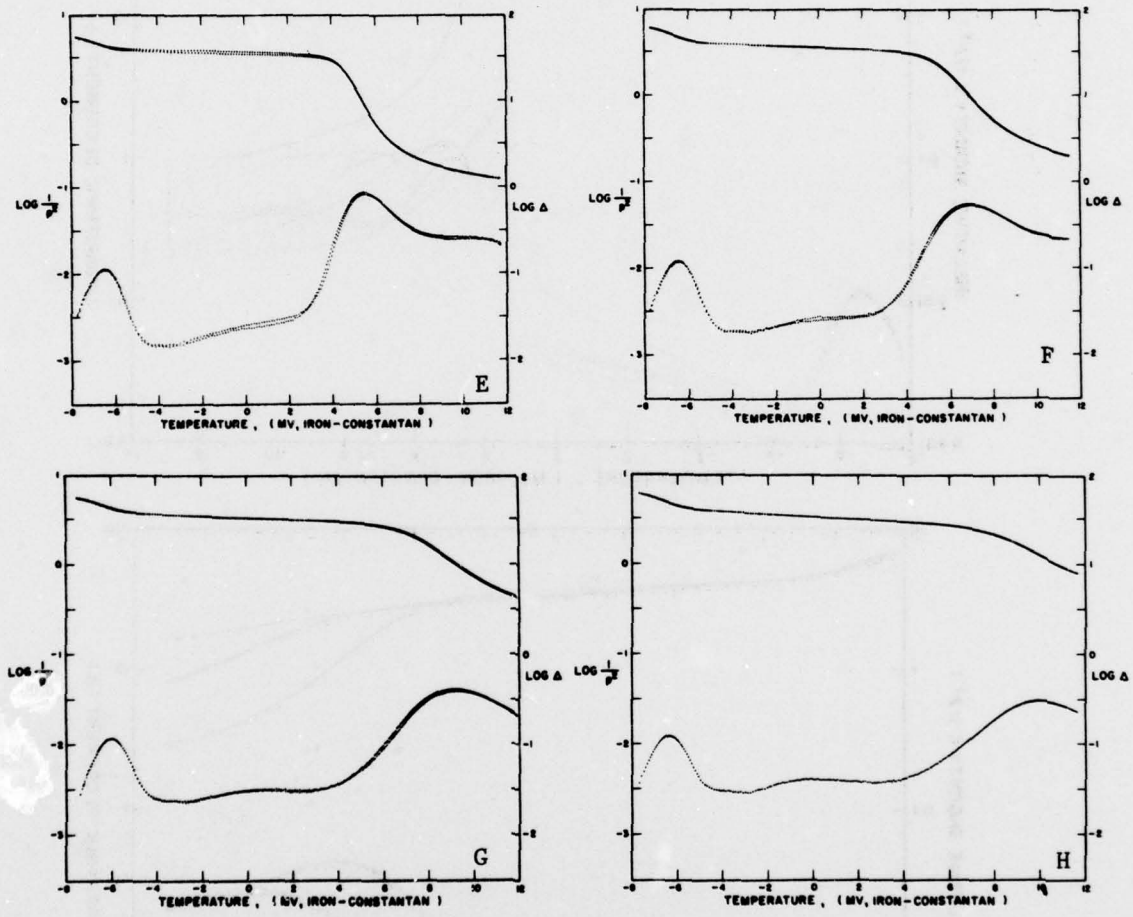

Fig. 3 — Isothermal (215°C) cure. Thermomechanical spectra (215°C → −195°C → 215°C)* of intermittently cooled specimen after: (A) 215°C/0.1 hr., (B) 215°C/0.2 hr., (C) 215°C/0.7 hr., (D) 215°C/2.2 hr., (E) 215°C/7.3 hr., (F) 215°C/14.6 hr., (G) 215°C/30.25 hr., (H) 215°C/55.05 hr., (215°C → −195°C)*.

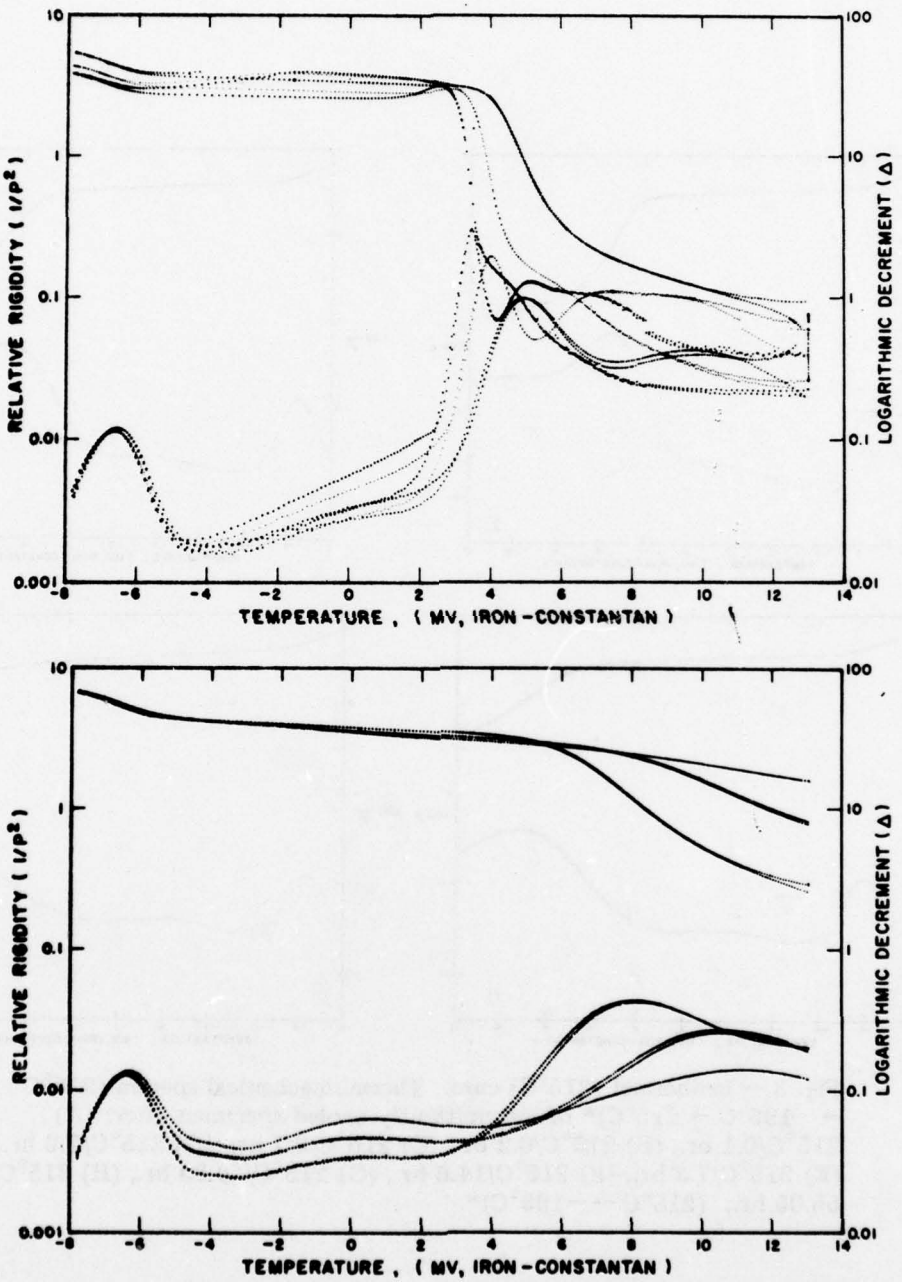

Fig. 4 — Isothermal (240°C) cure. Thermomechanical spectra (240°C → −195°C → 240°C) of intermittently cooled specimen after: top (A) 240°C/0.05 hr., (B) 240°C/0.25 hr., (C) 240°C/0.80 hr., bottom, (D) 240°C/3.3 hr., (E) 240°C/9.75 hr., and (F) 240°C/40.85 hr., (240° → −195°C).

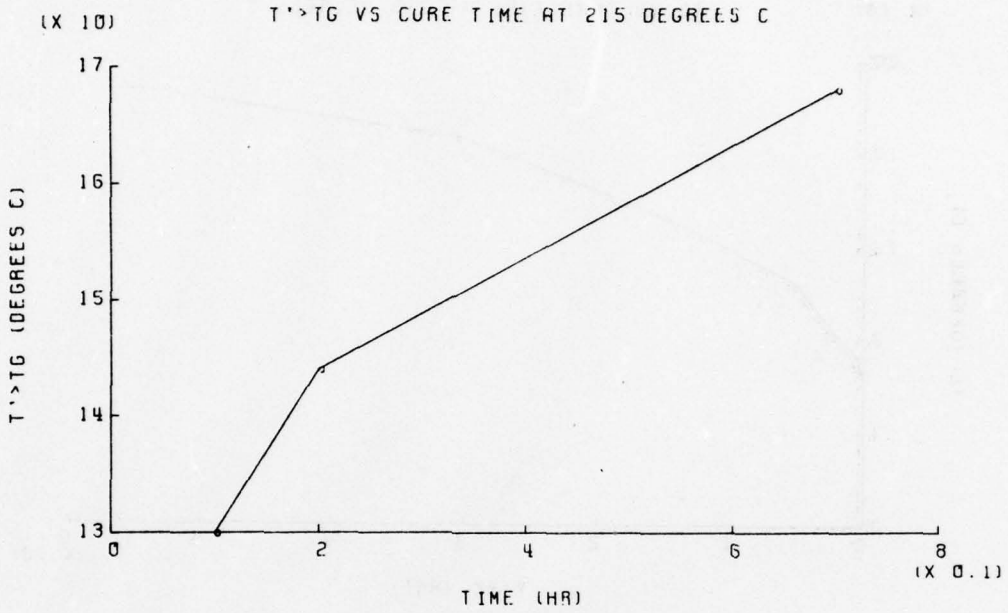

Figure 5a

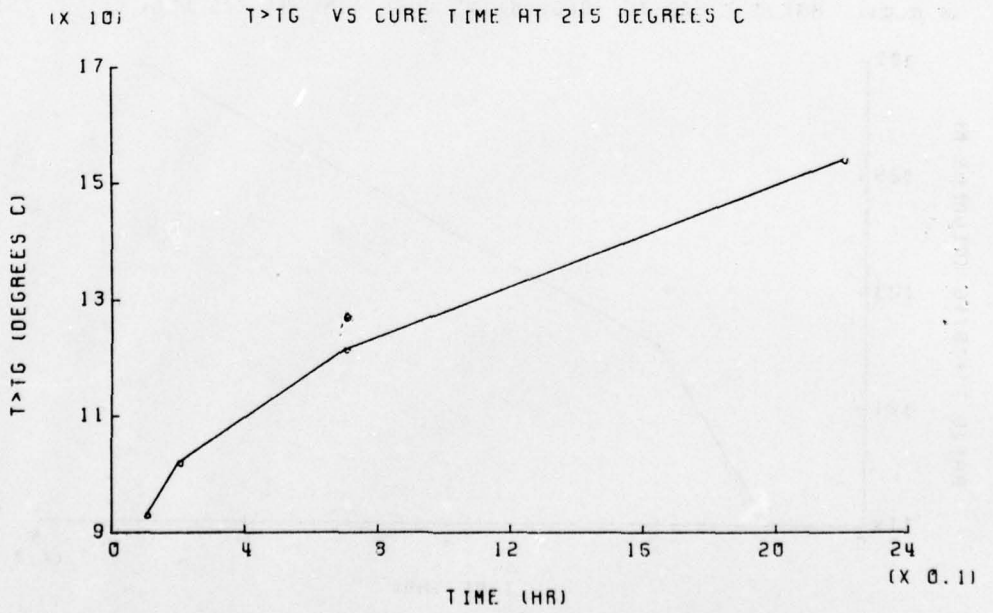

Figure 5b

(Continues)

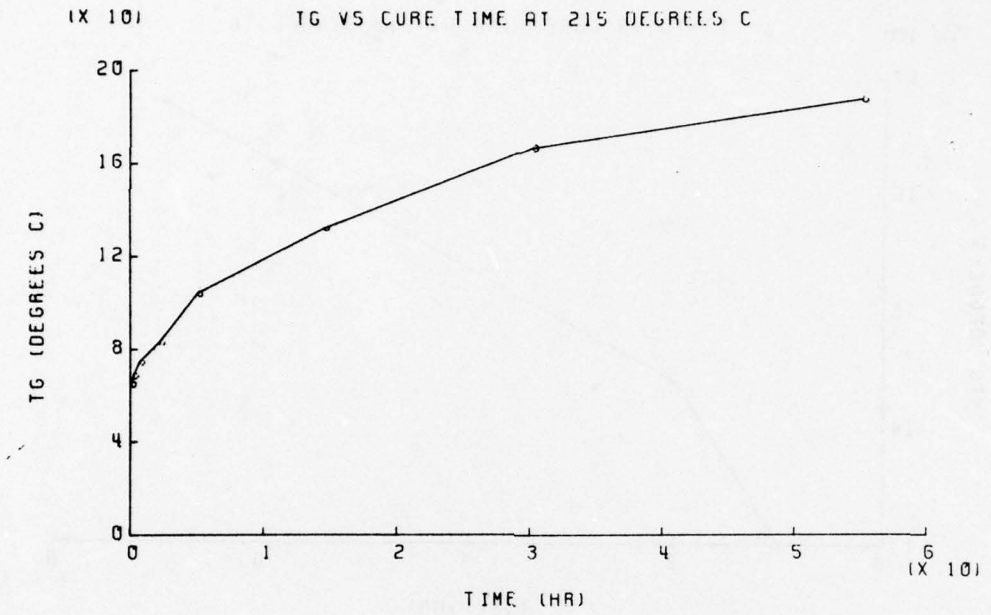

Figure 5c

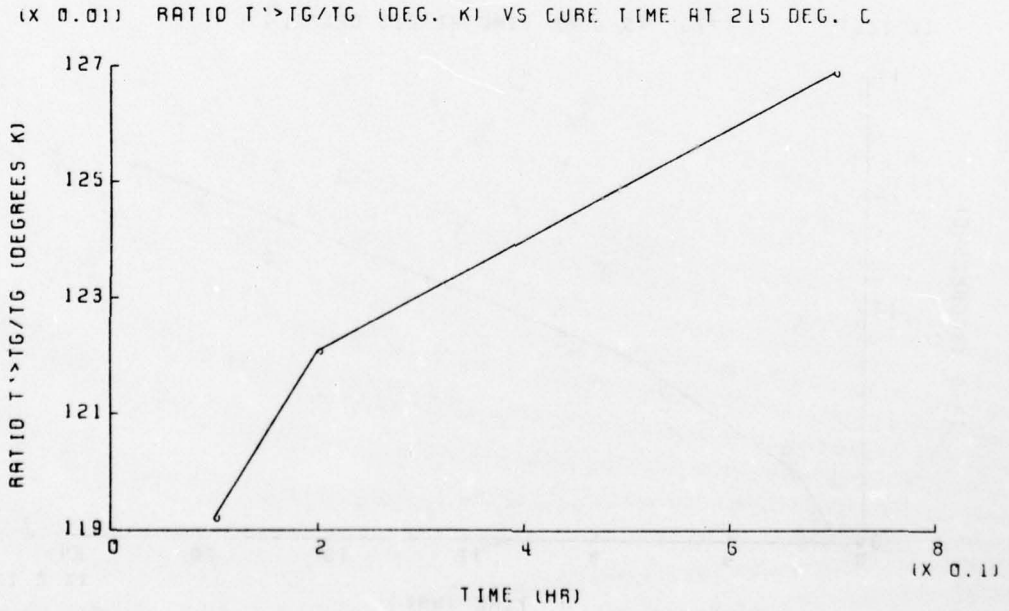

Figure 5d

(Continues)

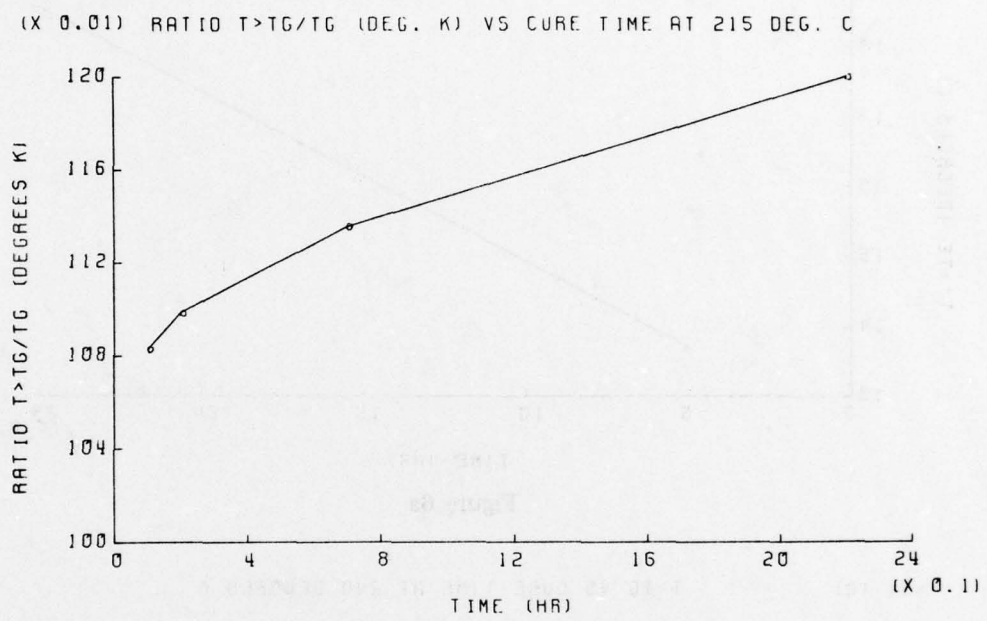

Figure 5e (Concluded)

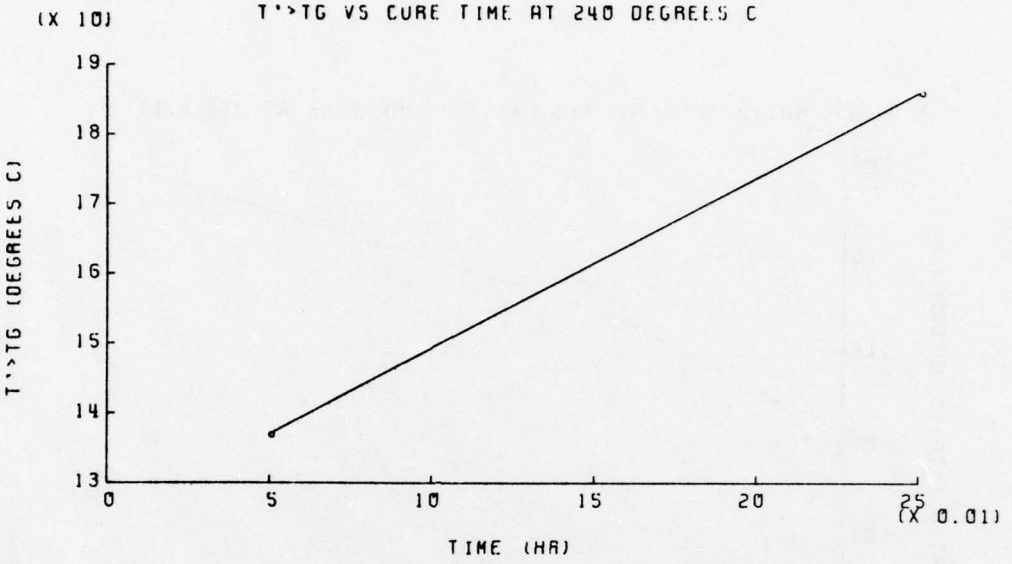

Figure 6a

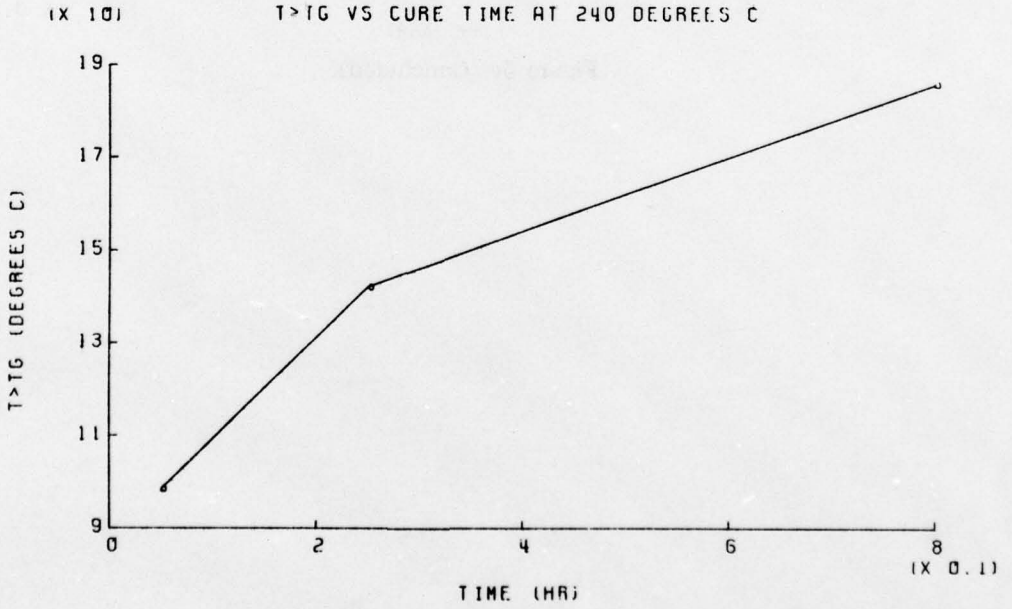

Figure 6b

(Continues)

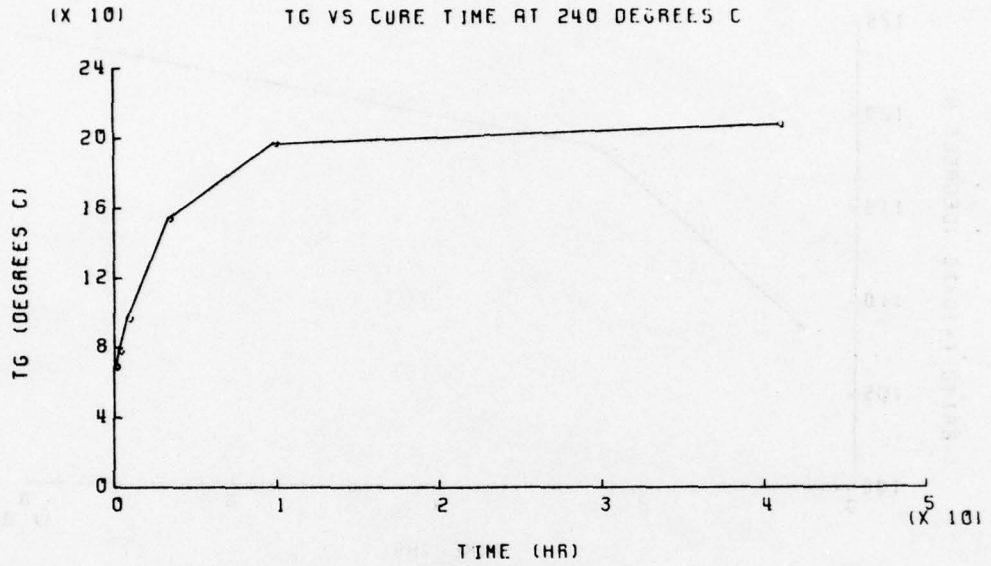

Figure 6c

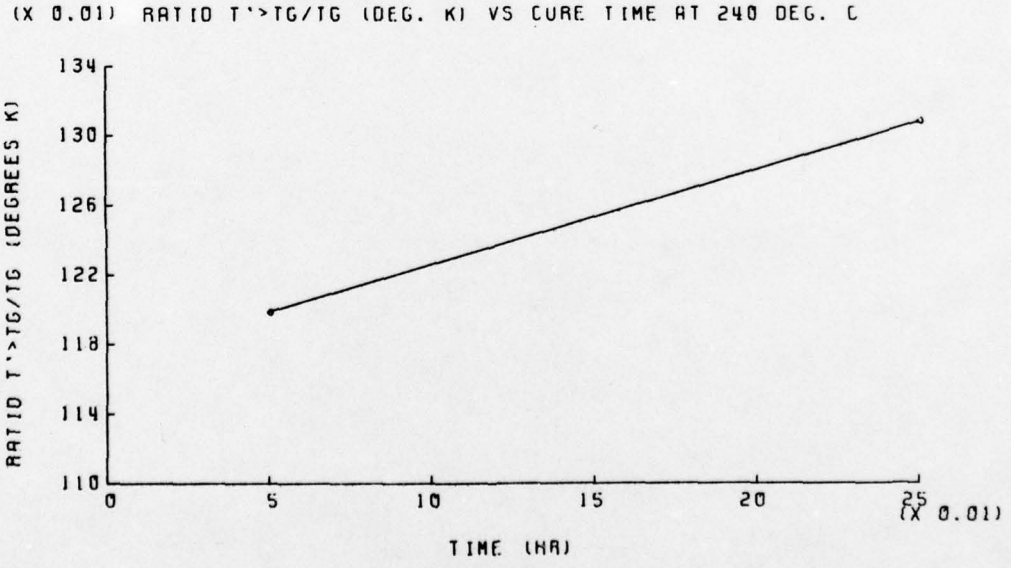

Figure 6d

(Continues)

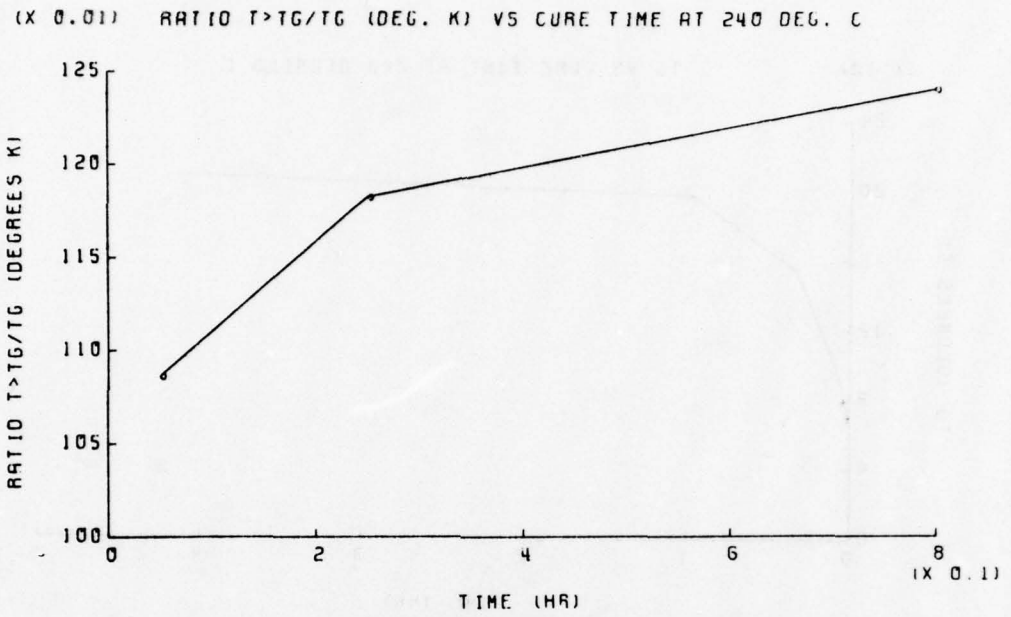

Figure 6e (Concluded)

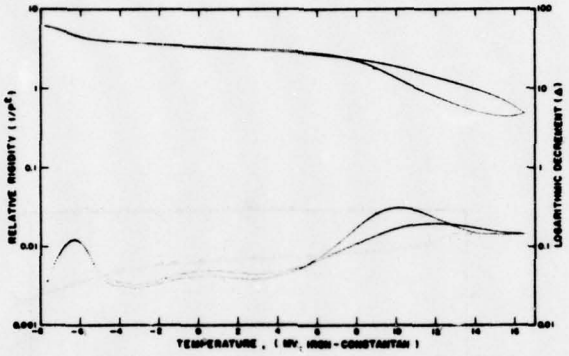

Thermomechanical spectra (-195°C → 300°C → -195°C) after 215°C/55.05 hr cure (same specimen as for Figure 3). This plot shows the influence of post-cure to 300°C on material cured at 215°C.

Figure 7

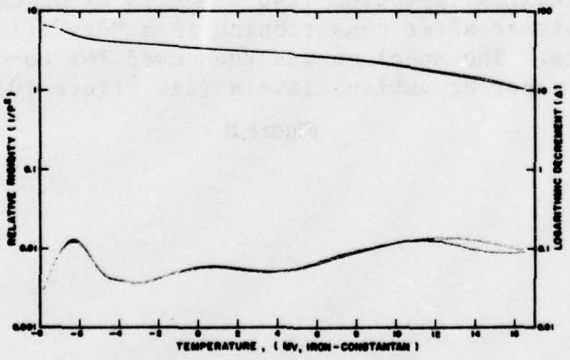

Thermomechanical spectra (-195°C T 300°C → -195°C) after 240°C/40.85 hr cure (same specimen as for Figure 4). This plot shows the influence of post-cure to 300°C on material cured at 240°C.

Figure 8

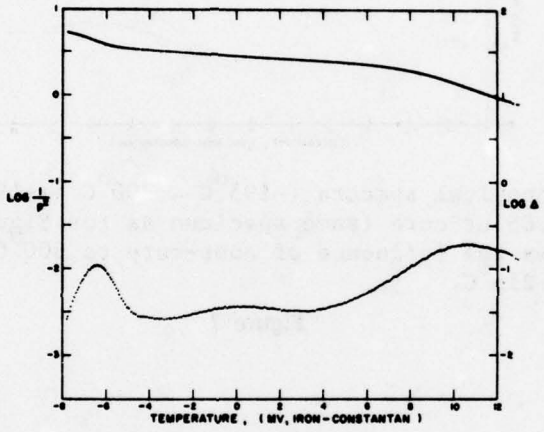

Thermomechanical spectrum (240°C → -195°C) of cured (240°C/12 hr) polymer after conditioning in a "dry" (130 $ppm_v H_2O$) atmosphere. The specimen was then used for conditioning in water vapor at various levels (see Figure 10).

Figure 9

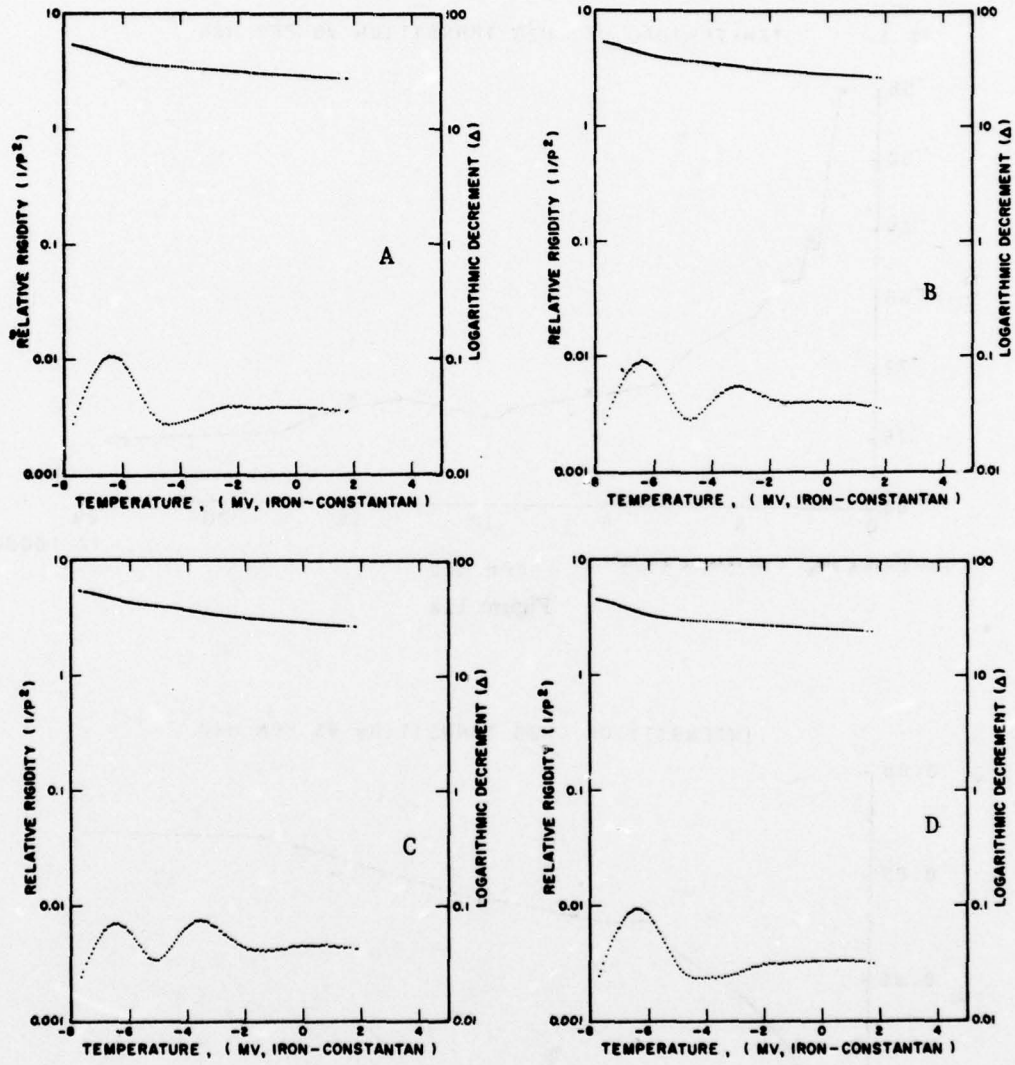

Thermomechanical spectra (35°C → -195°C) of cured polymer after conditioning at 35°C for 17 hours in (A) 460 $ppm_v H_2O$, (B) 2400 $ppm_v H_2O$, (C) 23000 $ppm_v H_2O$ and in (D) 300 $ppm_v H_2O$ after drying at end of moisture conditioning experiments. Note: compare (D) with (A) for test of reversibility of influence of water vapor.

Figure 10

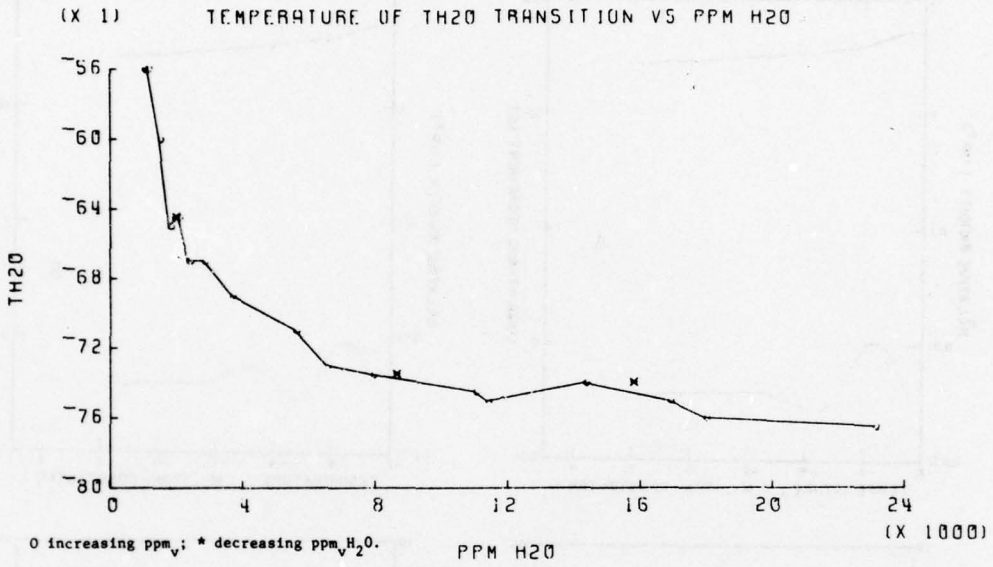

Figure 11a

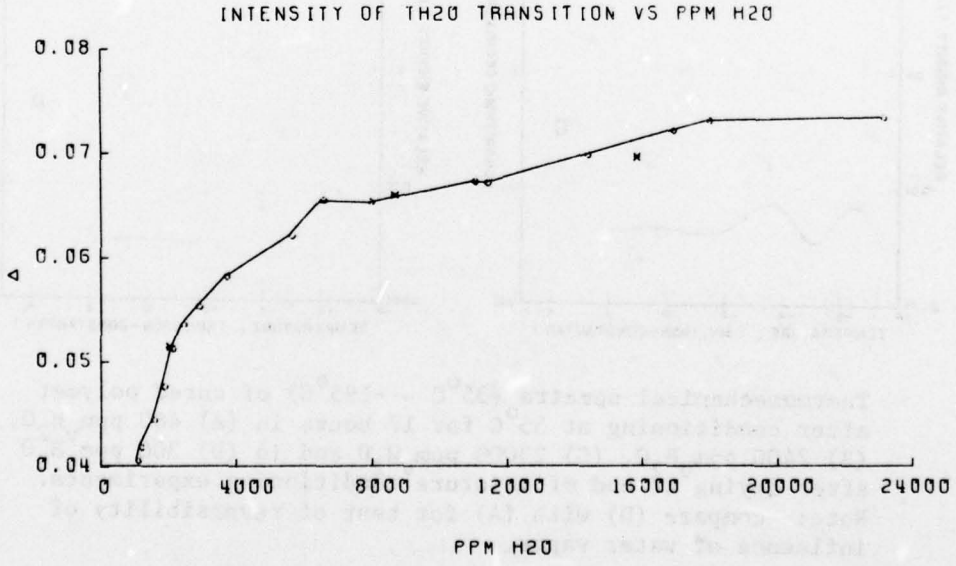

Figure 11b

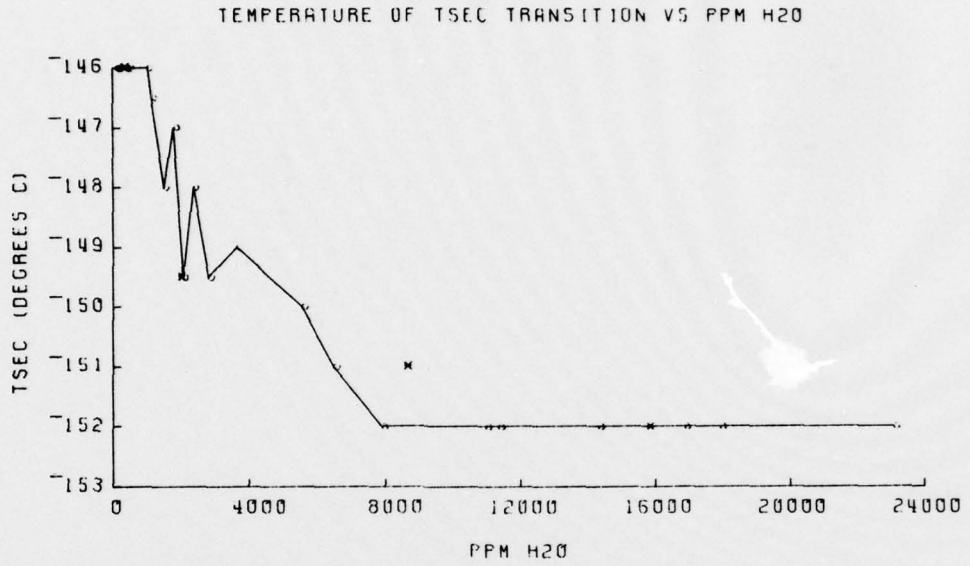

Figure 11c

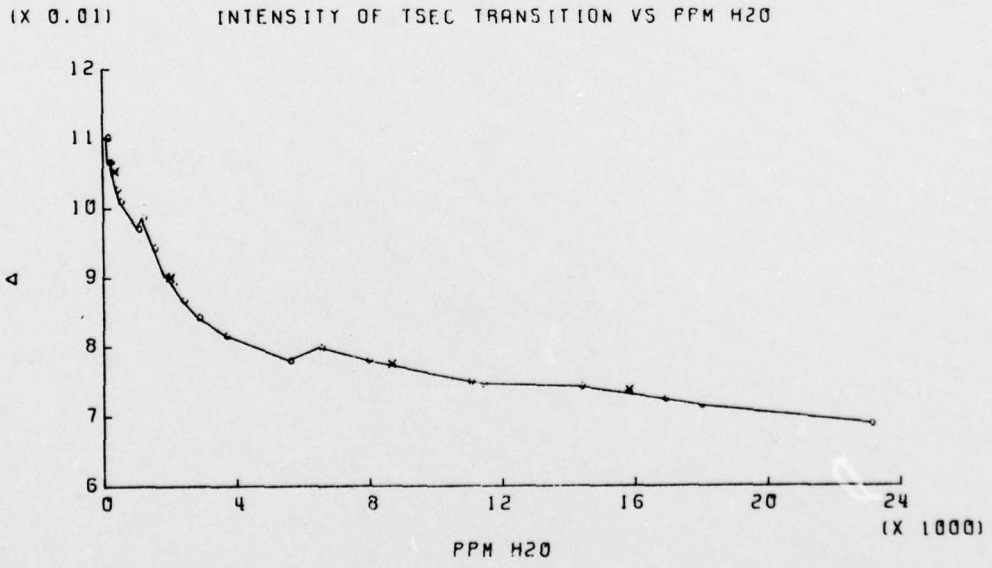

Figure 11d

CHEMICAL CHARACTERIZATION FOR QUALITY CONTROL

C. F. Poranski, Jr., and W. B. Moniz
Chemical Diagnostics Branch
Chemistry Division
Naval Research Laboratory

INTRODUCTION

Present design allowables for structural adhesives and fiber-reinforced organic-matrix composites incorporate large knockdown factors for batch-to-batch variability in engineering properties. To the extent that stringent quality assurance procedures can improve engineering reliability, the high strength-to-weight ratio of structural composites and adhesives can be more fully exploited.

The Chemical Characterization Task has a central role in this Program's effort to produce a reliable, reproducible, and serviceable resin system for V/STOL applications. The Task determines the identity, purity, and quantity of ingredients of candidate resin systems in the NRL V/STOL Program. Screening, usually by carbon-13 and proton nuclear magnetic resonance spectroscopy (C-13 or proton NMR) (1), confirms or establishes the chemical nature of the material. Resin systems selected for extensive evaluation are studied by a battery of analytical procedures.

The Chemical Characterization Task also develops methodology to monitor composition so that adverse effects upon engineering properties due to variability in raw materials may be minimized. The chemical results, correlated with physical and thermomechanical results obtained in other Tasks, generate meaningful quality control parameters. The final goal is a quality assurance scheme based on composition for the resin system which meets the performance goals of the NRL V/STOL Program..

The objectives for FY77 were (a) development of analytical techniques for C_{10} Diamide and other precursors to phthalocyanine resins; (b) production and distribution of Volume 1 of the NMR Spectra Catalog; (c) investigation of compositional changes occurring during aging of prepreg materials; (d) general characterization of commercial resin systems of interest to the NRL V/STOL program; and (e) evaluation of quality control parameters for selected resin systems.

PROGRESS

Highlights

Carbon-13 and proton NMR spectra were obtained for all available batches of C_{10} Diamide as well as for a number of reactive modifiers for the C_{10} system.

One batch of C_{10} Diamide with an anomalously low melting point was shown to be contaminated with 4-aminophthalonitrile and sebacic acid. Little effect upon melting point is noted for the commonly detected solvent residues of ethanol, acetone, water, or dimethylformamide.

Preliminary analysis of a room temperature aging study on Hexcel F-178 polyimide prepreg (done in cooperation with the Composites Fabrication Task) showed no significant changes in proton NMR or IR spectra after 21 days.

Volume 1 of the NMR Spectral Catalog has been published and distributed (2). An article on C-13 NMR characterization of epoxy resins was written for the Journal of Coatings Technology (3).

General characterization was completed for several commercial imide, polysulfone and epoxy systems.

C_{10} Diamide

As the precursor of one of the more promising polyphthalocyanine resins, C_{10} Diamide is receiving considerable attention in the NRL V/STOL program.

The Chemical Characterization Task has analyzed all available batches of C_{10} Diamide. Starting materials, modifiers of the C_{10} system, and residues extracted from lower quality batches of C_{10} Diamide have also been examined. Details of these studies are given below.

Thin-layer Chromatography: A study of the application of thin layer chromatography (TLC) to the analysis of C_{10} Diamide resins (from NRL and Eastman) was begun using standard adsorption TLC and reverse-phase TLC. In standard adsorption TLC, the developing solvent system of acetonitrile and toluene (2:5 vol. ratio) used with a hard-coated silica gel plate offered the best resolution. In the reverse-phase TLC method, a solvent system of acetonitrile: water:methanol (equal parts by volume) separated a solution of C_{10} Diamide and 4-aminophthalonitrile into two spots. The system showed only one spot for a pure C_{10} Diamide solution. The sensitivity of the method for 4-aminophthalonitrile and other possible impurities must be determined before a judgment can be made on the value of TLC as a quality control procedure for C_{10} Diamide.

Melting point of C_{10} Diamide: Since it is a single component system, C_{10} Diamide can be characterized by its melting point. After extensive purification C_{10} Diamide has a melting point of 192-194°. Such extensive purification is uneconomical for commercial production. Some compromise in purity must be made with a concomitant lowering of the melting point. Figure 1 shows the ranges of melting points obtained by the Organic Synthesis Task for the batches of C_{10} Diamide also characterized by C-13 and proton NMR. Most of the samples melt between 185 and 190°. These samples also cured under standard conditions to satisfactory polyphthalocyanine. Current procurement specifications call for a 3° range in melting point with melting starting at 185° or higher. The melting point is judged to be a good candidate for a quality control parameter.

Carbon-13 and Proton NMR: C-13 and proton NMR spectra have been obtained on 11 batches of NRL-synthesized C_{10} Diamide and 5 batches supplied by Eastman.

Figure 2 shows typical C-13 NMR spectra for two samples. The C-13 NMR spectra of all samples were similar, showing no significant differences in number of resonance lines, their positions, or their relative intensities.

Figure 3 shows proton NMR spectra of C_{10} Diamide in two solvents, perdeutero-dimethylsulfoxide (DMSO-d_6) and perdeutero-dimethyl formamide (DMF-d_7). DMF-d_7 has a number of advantages over DMSO-d_6 as an NMR solvent for C_{10} Diamide. First, C_{10} Diamide is considerably more soluble in DMF-d_7 (~160 mg/ml) than in DMSO-d_6 (~9 mg/ml). Second, the peaks due to the residual protons in the solvent occur at 2.7 and 2.9 ppm in DMF-d_7, and do not obscure the triplet at 2.4 ppm due to the methylene protons alpha to the amide group of C_{10} Diamide. In DMSO-d_6 only two of the three peaks are observed because of overlap by the solvent peak. Although the appearance of the aromatic protons of C_{10} Diamide (centered around 8 ppm) is different in DMF-d_7, this creates no problem for qualitative analysis. This different appearance probably indicates solvent/solute interaction which is responsible for the greater solubility. The disadvantage of DMF-d_7 is that it is much more expensive than DMSO-d_6 ($12.00 vs $1.00 per NMR sample).

The proton NMR spectra of the various batches of C_{10} Diamide generally were similar. However, in a few cases there were notable differences. For example, in DMSO-d_6 solutions the spectrum of Eastman batch B-7 (Figure 4) showed two extra lines (2.6 and 2.9 ppm) which were found to be due to dimethyl formamide (DMF). In DMF-d_7, the spectra of NRL batch 2 and Eastman batch 20* contained peaks assignable to ethanol. The amounts of these solvents, estimated to be 1-2% DMF and 0.5-1% ethanol, do not seriously affect the melting

*This batch number was assigned by the Chemical Characterization Task to the first batch of C_{10} Diamide received from Eastman.

point of the sample. The Eastman batch which contained ethanol had an anomalously low melting point, but other impurities were found to be responsible (see below).

Acetone was often observed in the proton spectra of C_{10} Diamide samples.** Acetone and ethanol are low boiling and should be driven off during the curing cycle of C_{10} Diamide. DMF, which boils at 154°, may associate strongly with the C_{10} Diamide and remain in the material above the melting point, or even react with it. These possibilities need to be checked carefully. Thermomechanical testing of all batches of C_{10} Diamide is not yet complete.

Water is another possible contaminant whose origin is difficult to pinpoint. It may be used as a wash solvent during synthesis. The NMR solvents DMSO and DMF are very hygroscopic and water can contaminate a prepared solution by leaking in through the cap of the sample tube. Water may also adsorb on the walls of the NMR tube and be washed in when the sample solution is added. A number of precautions are taken to reduce the chances of water contamination. The sample tubes and vials used for preparing solutions are kept in a drying oven until needed. The DMSO-d_6 and DMF-d_7 are in sealed glass ampoules containing just enough solvent for one sample solution. If the spectra are run within an hour of sample preparation, the amount of water diffusing into the tube is negligible.

Batch 20 of Eastman C_{10} Diamide had a low melting point (174-177°). Proton NMR spectra of batch 20 showed no sign of impurities other than trace amounts of ethanol. Other samples with trace amounts of ethanol had acceptable melting points, so this was not felt to be the problem. A portion of batch 20 was extracted with ethanol and the dried extract was examined by proton NMR (Figure 5). In addition to peaks of C_{10} Diamide, the spectrum contains a number of other lines which can be assigned to 4-aminophthalonitrile and sebacic acid (see Figures 6 and 7). Thus it appears that the low melting point of this particular batch is due to the presence of unreacted starting material, probably as a result of insufficient washing of the reaction product.

Reactive Modifiers for C_{10} Diamide: The properties of the C_{10} Diamide resin system may be altered by the addition of reactive modifiers, several of which have been characterized in this program.

The compound, N-(3,4-dicyanophenyl)hexadecylamide, or C_{16} Monoamide, has a C-13 NMR spectrum (Figure 8) which contains all of the resonance lines observed in the spectrum of C_{10} Diamide, as well as three extra lines at 14.4, 23.2 and 32.5 ppm due to the terminal

**In a few cases, the acetone was due to insufficient care in preparing the NMR sample. Acetone is a common rinse solvent in organic laboratories and is frequently detected when glassware is not dried properly.

CH_3-CH_2-CH_2 carbons respectively. Ideally, C_{16} Monoamide should cure to a monophthalocyanine compound containing four C_{16} Monoamide molecules, thus serving as a model for the cured C_{10} Diamide system. Work on characterizing cured C_{16} Monoamide has been hampered by its low solubility. Further attempts will be made to find a suitable solvent.

The compound N,N'-(1,4-phenylenedimethylidene) bis-(3,4-dicyanoaniline), referred to as p-Dianil, is another reactive modifier for C_{10} Diamide systems. Proton NMR showed that p-Dianil exists in the trans, trans form in solution in hexamethylphosphoric triamide. It has been shown that most imines exist as trans isomers because the cis form provides steric interference with the coplanarity required for maximum stability (4).

Aging of Hexcel F-178/T300 Prepreg

The Chemical Characterization and Composite Fabrication Tasks cooperated in a short term aging study of Hexcel F-178/T300 polyimide. Processing parameters of the prepreg and mechanical properties of the cured composite were determined as a function of prepreg out-time at room temperature at various relative humidities. Concurrently, infrared and proton NMR spectra of extracts of the aging prepreg were obtained. As the spectroscopic data have not been fully analyzed, only preliminary results are presented here.

Precut, packaged kits of fresh prepreg were stored at room temperature in relative humidities of 16%, 45% and 95%. Each kit contained enough prepreg to prepare one 6" x 6", 16-ply cured panel and provide samples for chemical analysis. At specified times, the kits were removed from storage, the panels laid up and cured, and chemical tests made. The panels were cut to provide samples for measuring interlaminar shear strength and flexural strength. (See report on Fabrication of Composites for preliminary results of these tests).

The most obvious change during the aging period was a steady loss of tackiness until, at the end of three weeks, the prepreg was quite dry. The material also became brittle; it was very difficult to cut cleanly with a knife blade.

Figure 9 gives proton NMR spectra of the control sample and of the sample aged for 21 days at 16% RH. There is no significant change in relative intensities of the peaks after 21 days. For example, the ratio of the peak at 6.9 ppm to that at 4.08 ppm is 1.9 in the control spectrum, and 1.7 in the 21 day spectrum. The infrared spectra showed the same general result; i.e. no changes in relative intensities.

Commercial Resin Systems

Table 1 lists the commercial resin systems screened by the Chemical Characterization Task during FY77 and the NMR techniques used

Table 1

NMR Spectra Run on Commercial Materials During FY77

	^{13}C	^{1}H	^{19}F
IMIDES			
Rhodia Nolimid 605	X		
" Kerimid 353	X	X	
DuPont NR-150A2	X	X	X
" NR-150B2	X	X	X
" NR-150A2G	X	X	X
" NR-150B2G	X	X	X
POLYSULFONES			
Carborundum Astrel	X	X	
Union Carbide Udel P-1700	X		
" " Radel R-5010	X		
ICI United States Inc. "Grade 100P"	X	X	
EPOXY RELATED MATERIALS			
American Cyanamid FM 100	X		
3 M Co. PR-313	X	X	
" AF-143	X		
B. F. Goodrich PL 729	X		
Ozark-Mahoning Resicure-2	X		X
J. T. Baker BF_3 MEA	X		X
Ciba-Geigy CY 179	X	X	
" Epoxide 7	X	X	
" Epoxide 8	X	X	

for each material. Preliminary analysis of the spectra showed no unexpected features. More detailed studies of these systems will be made only as required by the Program.

We have previously described a proton NMR method for quantitative determination of the resin-to-curing-agent ratio in TGMDA/DDS epoxy resin systems (5). An opportunity to assess the accuracy of the method arose in this year's Polymer Characterization Techniques Meeting, held with Air Force encouragement, at Rockwell International Center, Thousand Oaks, CA, 8-10 March, 1977. A round-robin analysis was carried out on a set of specially formulated TGMDA/DDS samples of undisclosed composition prepared by C. May of Lockheed. Our results are given in Table 2. The NMR method showed good precision, and readily detected the "off" formulation (# 3). In this regard, results of the NMR method equalled or were superior to the those obtained using accepted techniques such as infrared, differential scanning calorimetry or liquid chromatography. The origin of the systematic error of -1.5 phr in the NMR method is being investigated.

Table 2

Proton NMR Determination of DDS in Specially Formulated TGMDA/DDS Systems

Sample	Actual DDS (phr)	Found DDS (phr)
1	40	38.5
2	40	37.5
3	45	43.5
4	40	37.9

Future Work

Tasks to be carried out include:

1. Complete quality control parametric study and develop quality control factors for C_{10} Diamide and other selected resin systems.

2. Prepare detailed quality control procedures for monitoring the QC factors.

3. Determine utility of liquid chromatography for analysis of C_{10} Diamide and other resin systems.

4. Screen new commercial systems of interest.

REFERENCES

1. W. B. Moniz, C. F. Poranski, Jr., and S. A. Sojka, "Carbon-13 Fourier Transform NMR - An Important New Analysis Tool", Rept. NRL Progress, Aug., 1975, p. 1.

2. C. F. Poranski, Jr., W. B. Moniz, D. L. Birkle, J. T. Kopfle, and S. A. Sojka, "Carbon-13 and Proton NMR Spectra for Characterizing Thermosetting Polymer Systems. I: Epoxy Resins and Curing Agents", NRL Report 8092, June 20, 1977.

3. C. F. Poranski, Jr. and W. B. Moniz, "Characterization of Epoxy Resin Systems Using Carbon-13 Fourier Transform NMR", J. Coatings Tech., 49, No. 632, 57 (1977).

4. J. Hine and C. Y. Yeh, "Equilibrium in Formation and Conformational Isomerization of Imines Derived from Isobutyraldehyde and Saturated Aliphatic Primary Amines", J. Am. Chem. Soc., 89, 2669 (1967).

5. "High Performance Composites and Adhesives for V/STOL Aircraft, First Annual Report", (Willard D. Bascom and Luther B. Lockhart, Jr., Editors), Task C. Chemical Characterization, C. F. Poranski, Jr. and W. B. Moniz, NRL Memorandum Report 3433, pp. 35-53 (December 1976).

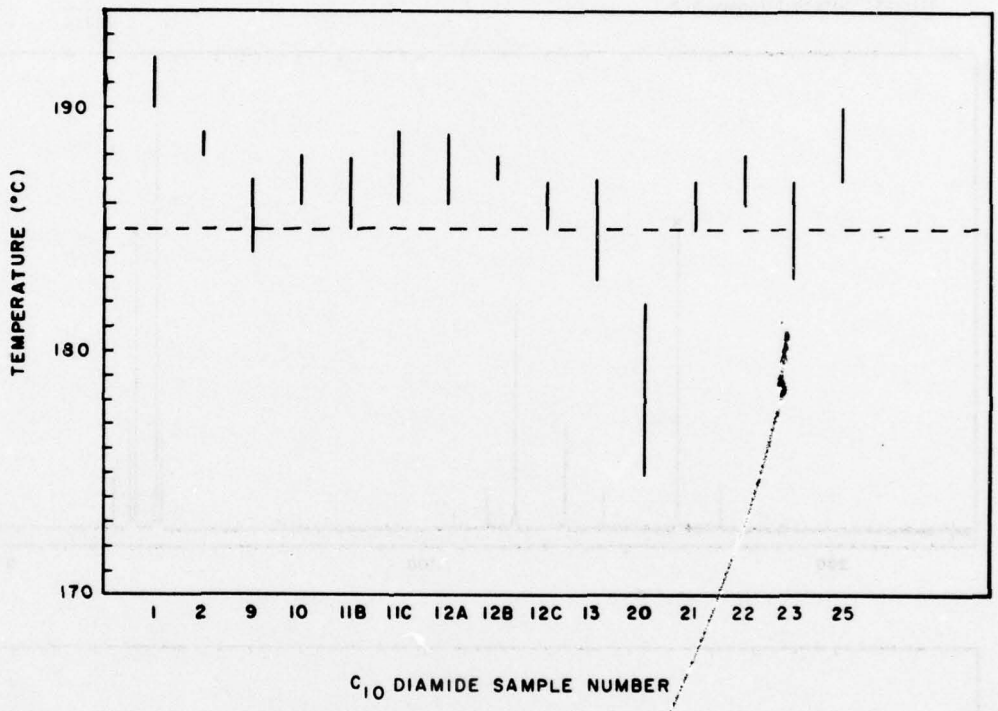

Fig. 1 — Melting points of C_{10} diamide samples received by the chemical characterization task. Samples 1 to 13 are NRL syntheses and samples 20-25 are Eastman products.

C_{10} Diamide

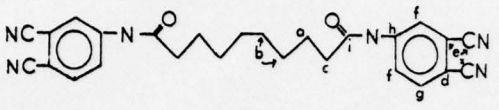

Source: NRL, Code 6120 (upper)
Eastman Kodak (lower)

Solvent: Dimethyl formamide ✖

Assignments:

a	25.6	g	135.4
b	29.8	h	144.7
c	37.6	i	173.3
d	108.5		
e	116.4		
f	123.4		

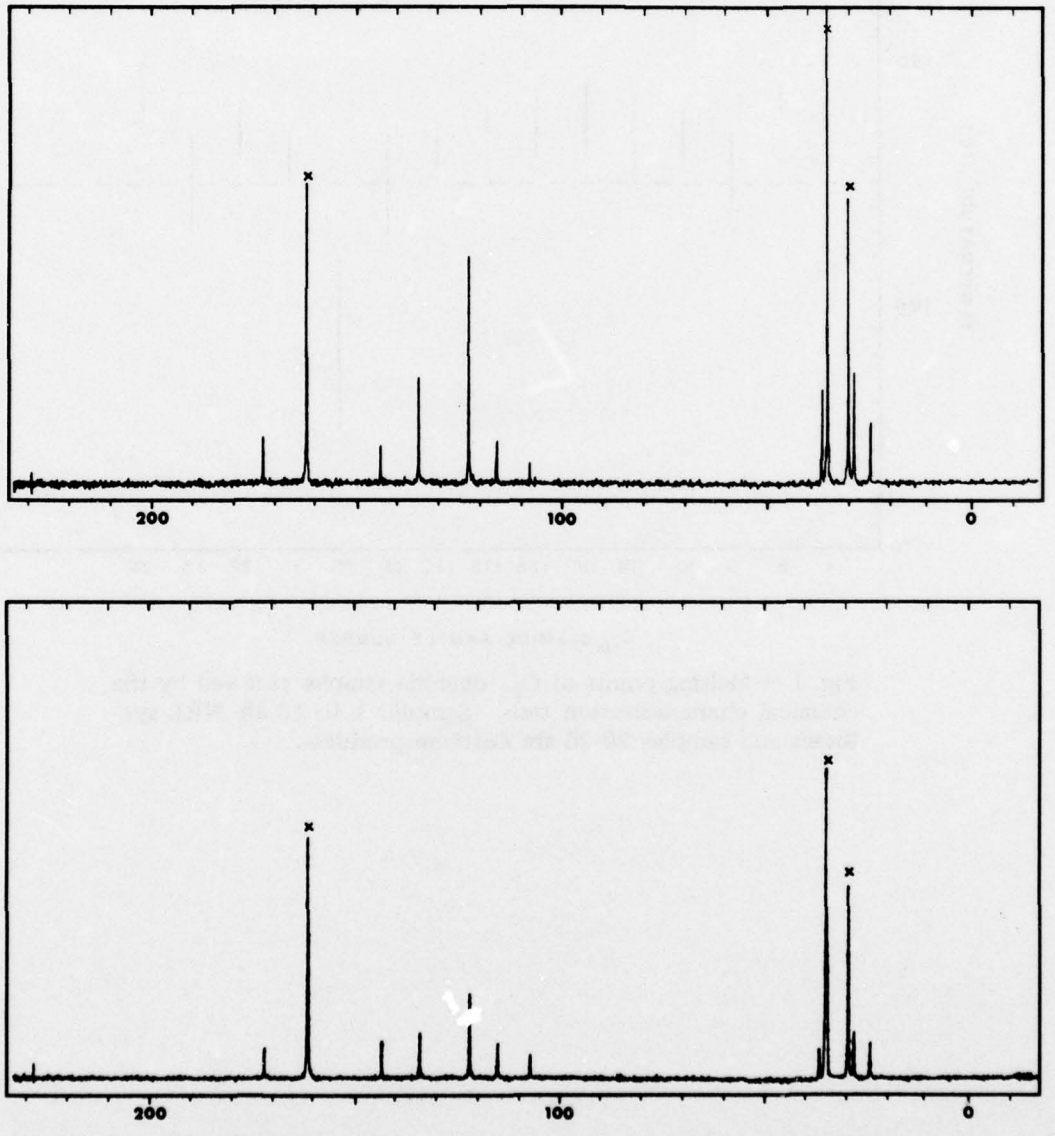

Fig. 2 — ^{13}C NMR spectra of two C_{10} diamide samples in dimethyl formamide

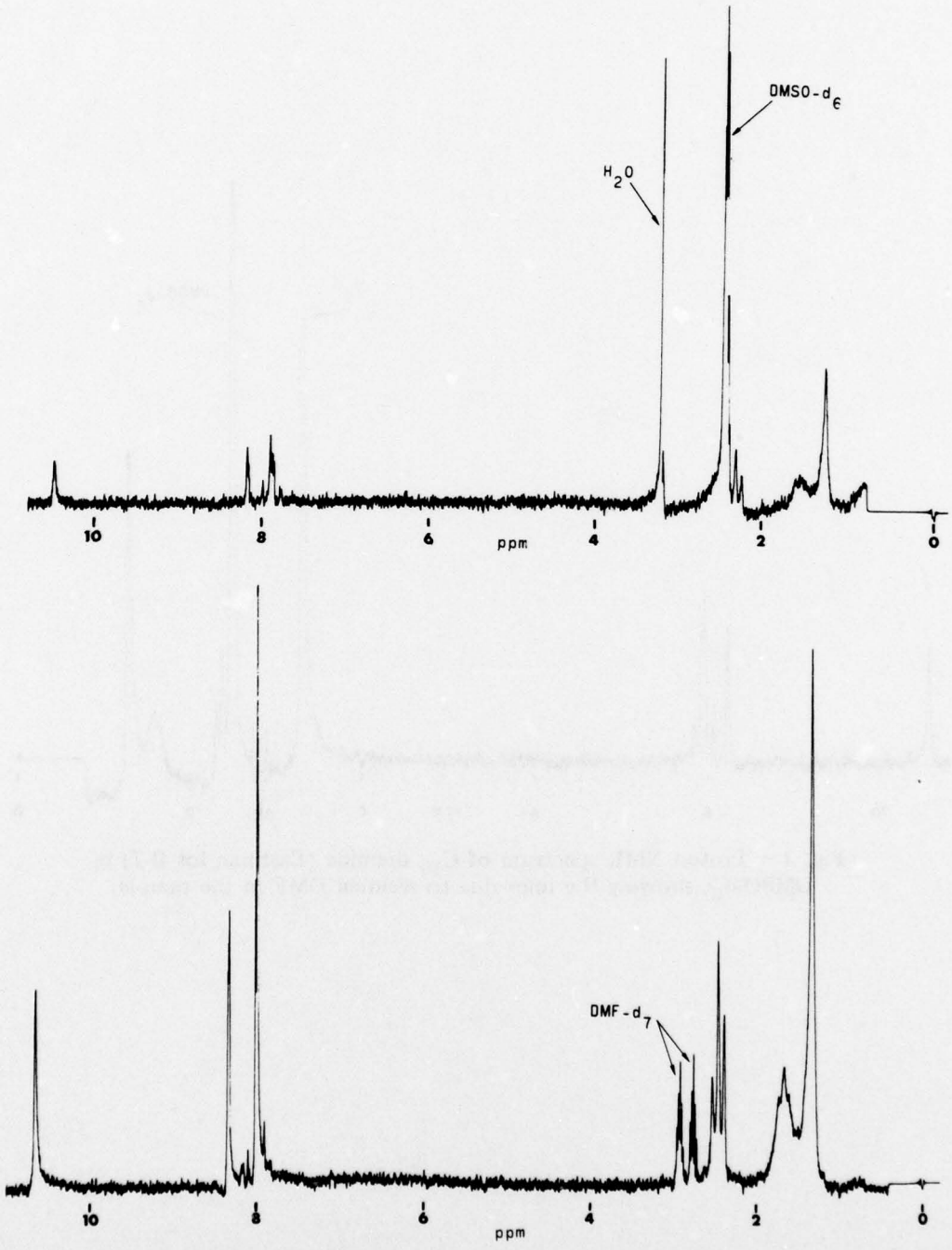

Fig. 3 — Proton NMR spectra of C_{10} diamide in dimethyl sulfoxide-d_6 (upper) and dimethyl formamide-d_7 (lower)

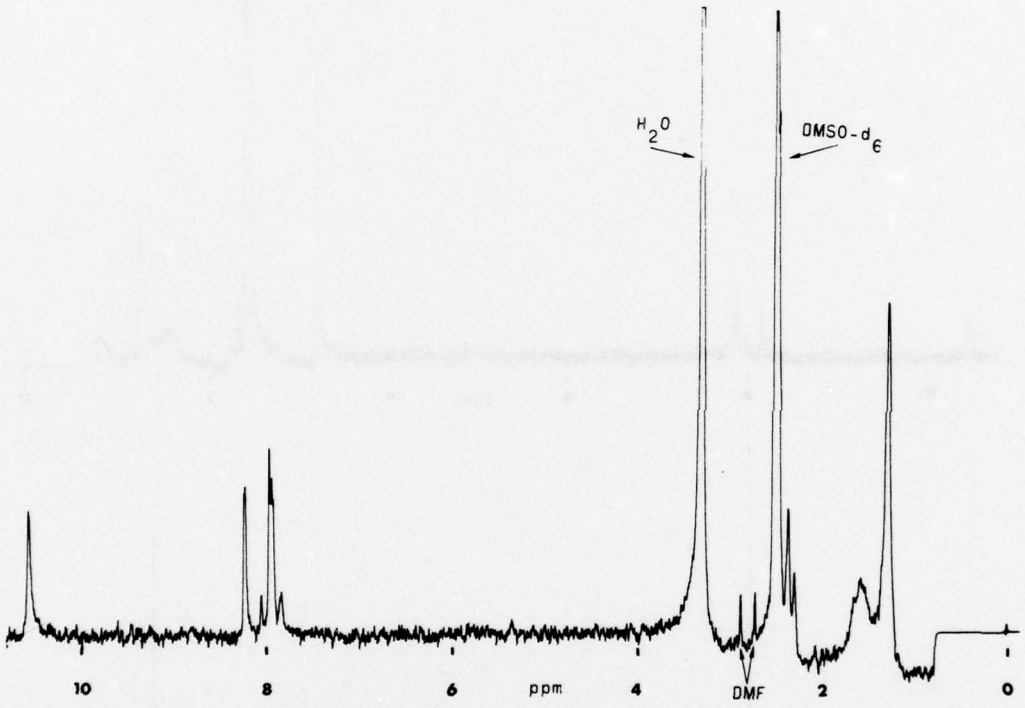

Fig. 4 — Proton NMR spectrum of C_{10} diamide (Eastman lot B-7) in DMSO-d_6, showing the lines due to residual DMF in the sample.

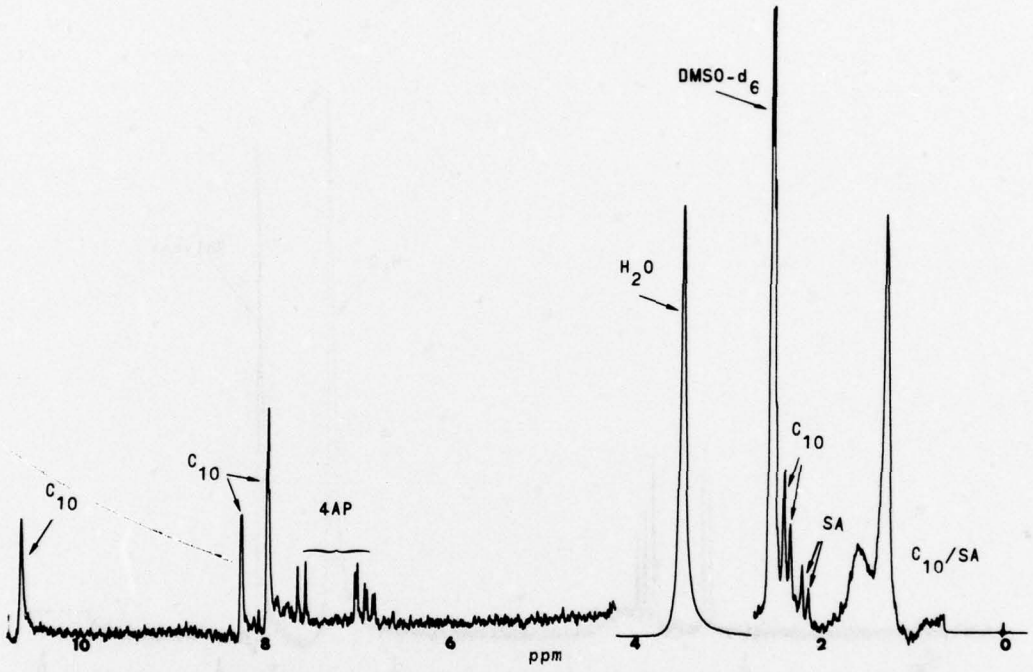

Fig. 5 — Proton NMR spectrum of material extracted with ethanol from a sample of C_{10} diamide which had a low melting point. (Sample # 20 in Fig. 1.) Besides lines due to C_{10} diamide (C_{10}) there are lines from 4-aminophthalonitrile (4AP) and sebacic acid (SA).

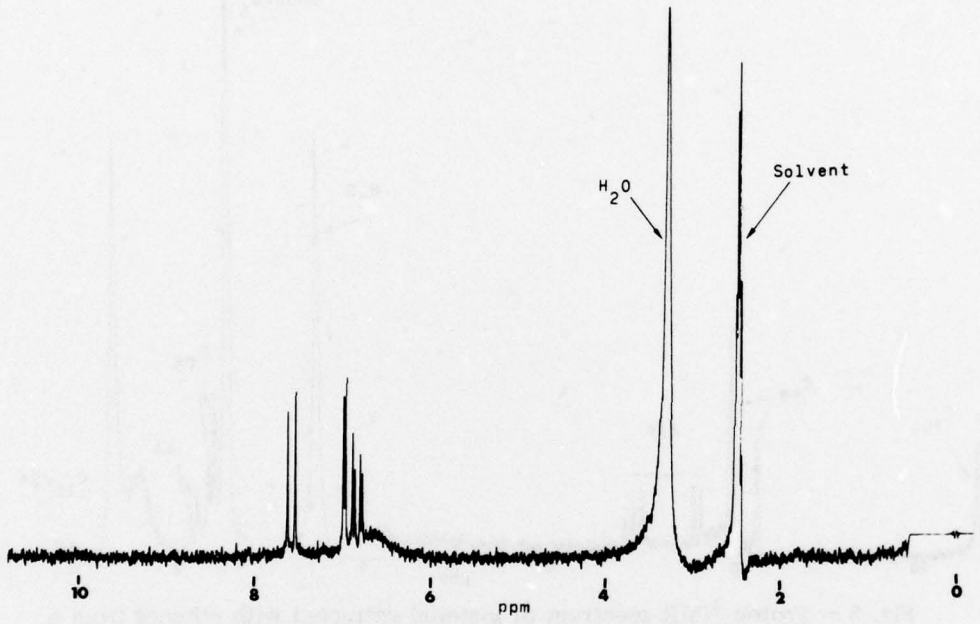

Fig. 6 — Proton NMR spectrum of 4-aminophthalonitrile in DMSO-d_6

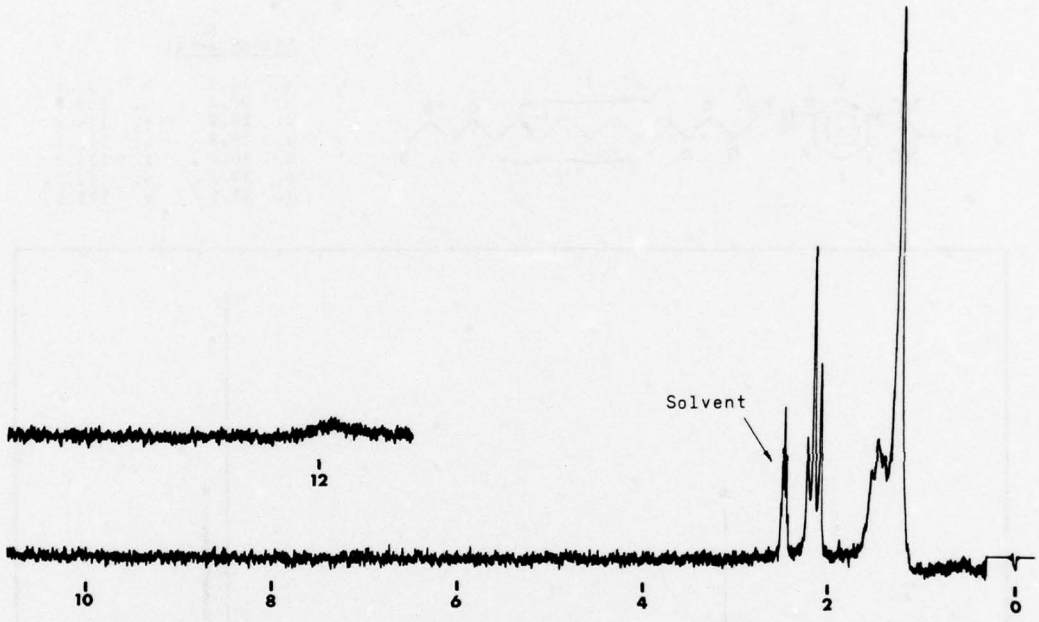

Fig. 7 — Proton NMR spectrum of sebacic acid in DMSO-d_6.
The broad peak at ~ 12 ppm is from the acid protons.

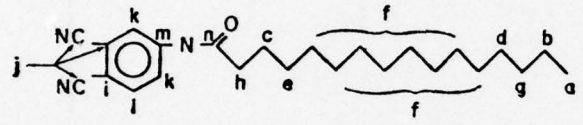

Assignments:

a.	14.4	h.	37.6
b.	23.2	i.	108.6
c.	25.8	j.	116.6
d.	29.8	k.	123.5
e.	30.0	l.	135.7
f.	30.3	m.	145.0
g.	32.5	n.	173.5

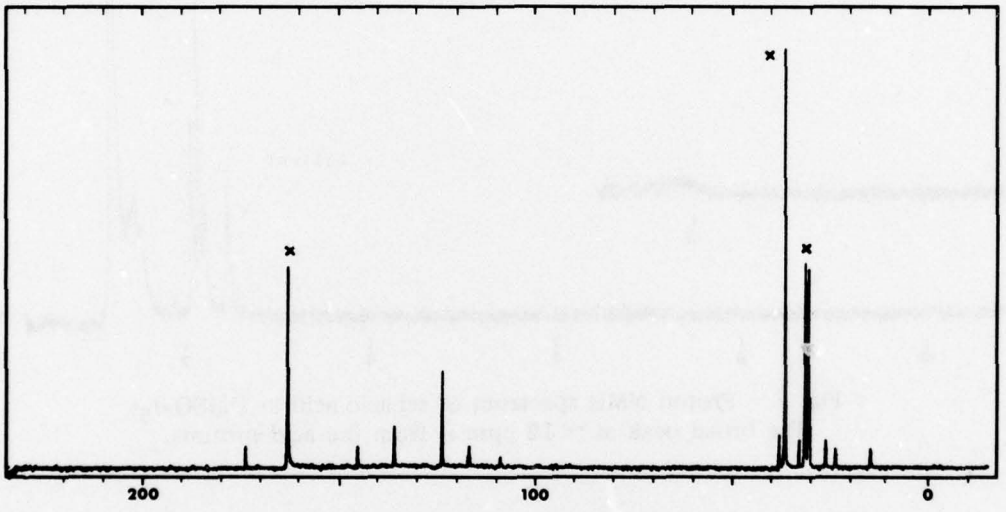

Fig. 8 — ^{13}C NMR spectrum of C_{16} monomide in DMF.
The three peaks marked X are due to the solvent.

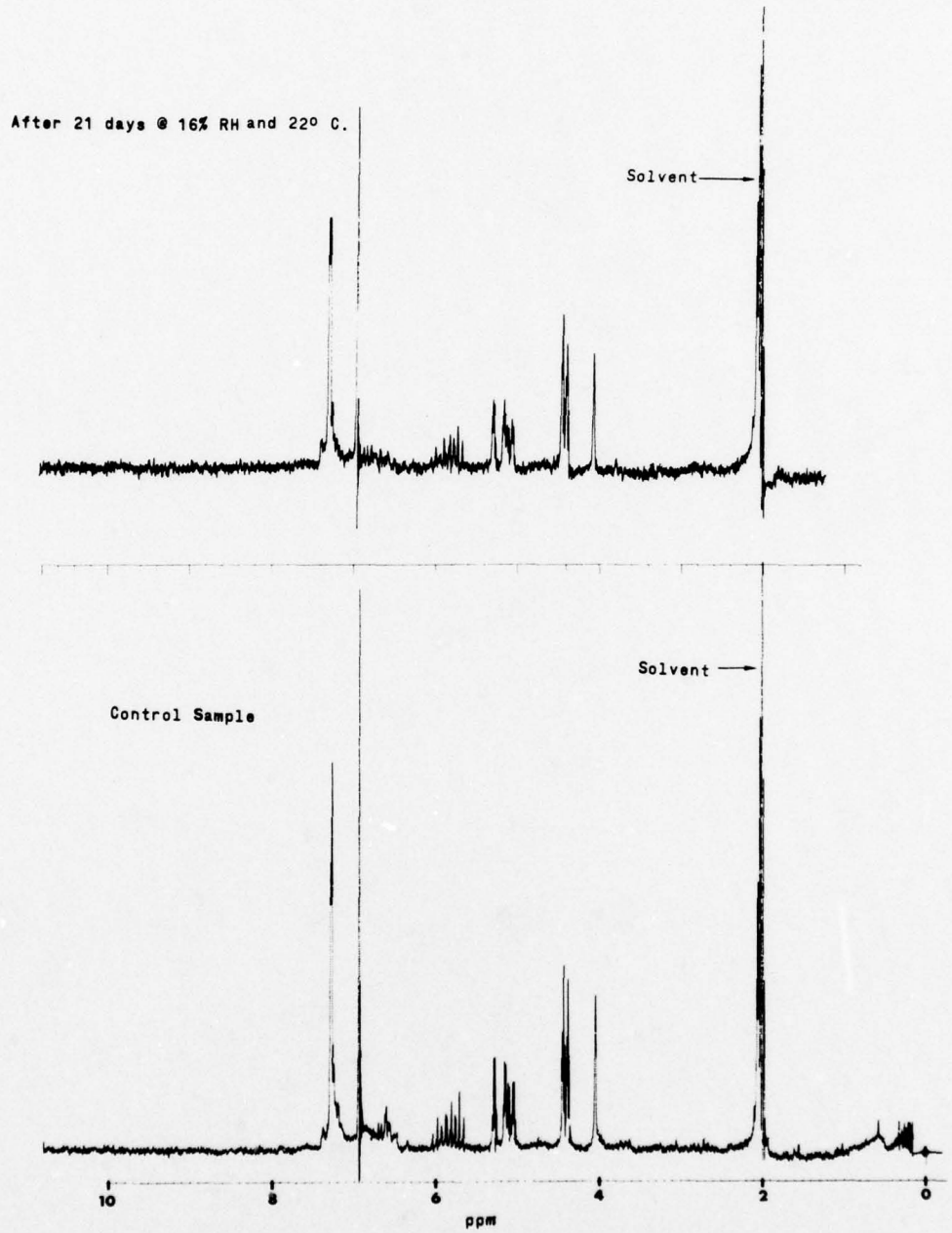

Fig. 9 — Proton NMR spectra of Hexcel F-178 resin extracted from fresh (lower) and aged (upper) F-178/T300 prepreg. The solvent is acetone-d_6.

RADIATION CURABLE RESINS

F. J. Campbell, W. Brenner*, L. M. Johnson and M. E. White
Radiation Effects Branch
Radiation Technology Division

INTRODUCTION

Radiation curing of adhesives and organic-matrix composites with a high energy electron beam offers many advantages over conventional heat curing processes. The electron beam cure is rapid, conserves energy, eliminates thermal distortion and stresses, and provides simplicity and versatility. Commercially available electron accelerators having magnetic beam-sweeping heads can be used for assembly line processing, and remote-controlled linac heads can be directed for localized processes such as spot-bonding, weld-bonding, applying repair patches and installing retrofit stiffeners. The objectives of this task are to develop radiation curable resins and to optimize the formulations for ease of processing and mechanical performance.

Radiation curing of commercially available resins has been previously demonstrated and data on adhesive shear strength versus dose and temperature during the irradiation were given (1). Other data illustrated the superiority of radiation curing over heat/peroxide curing for achieving high temperature strength (2). These resins were polyesters and vinyl ester-modified epoxies formulated with various reactive monomers. The current effort has concentrated on the development and characterization of other radiation curable resin systems having higher temperature stability than is normally achievable with polyesters or epoxies.

PROGRESS

Modified Polyimides

Several commercially available polyimide-type resins have exhibited good high temperature stability well above the service temperature of the best epoxy resins now being used for bonding aircraft structures. Thus, for supersonic aircraft and for some V/STOL designs where jet exhausts are deflected near the fuselage, these resins are being proposed for adhesives and composites.

*Division of Applied Sciences, New York University

The problem with these polyimides is that they are solids in the precured stage. Therefore, in order to fabricate structures by heat curing, the application of high temperature and pressure is required to get the necessary flow and surface contact for a bonded assembly. This must be followed by even higher temperatures and longer times at high pressure to complete the curing (or crosslinking reaction) that produces the high temperature stability. The resulting crosslinked polyimide resins have also been found to lack fracture toughness, an essential property for structural adhesives.

Our major effort has been directed toward developing polyimide formulations having fracture toughness and high temperature stability as well as the other qualities desired of radiation curable resins, namely: fluid resin for easy assembly, low dose required for curing, low shrinkage during cure, no postcure heating required.

Initial studies involved an evaluation of some formulation variables in which commercially available addition-type polyimide resins were modified by the addition of various proportions of materials categorized as reactive solvents, crosslinkers and toughеners. Three different polyimide resins were mixed with six different potential solvents that were known to have reactive groups that would crosslink with the resins when exposed to radiation. Initially it was found that only one of these, N-vinyl-2-pyrrolidone (VP), was a good solvent for the polyimide prepolymer, bismaleimide of methylene dianiline (BMDA), commercially available as Kerimid 601. This combination, in the proportion of 100 pts BMDA/50 pts VP, became the base resin for initial radiation curing studies. At a dose of 300 KGy (1 KGy=0.1 Mrad) it reacted to produce a hard, crosslinked resin, but it was too brittle to serve as a good adhesive.

Improving Fracture Toughness

Two improvements were obviously necessary. One was to reduce the dose required to reach maximum cure. This was approached by adding polyfunctional monomers that would increase the crosslinking rate. The other was to add a flexible resin or a rubber which would impart toughness to the cured composition by the formation of a particulate second phase in the basic crosslinked polyimide.

Experiments with four different crosslinkers and four different toughener additives in various proportions were evaluated by an initial screening test for heat distortion temperature, utilizing Thermomechanical Analysis (TMA) to determine the combination of additives and radiation dose that would produce the crosslinked polymeric structure with the highest temperature value. A DuPont Model 943 Thermomechanical Analyzer equipped with a normal penetration probe was used for these measurements. As illustrated in Fig. 1, the specimen is heated at a constantly increasing temperature while under a weighted quartz-rod probe, and a trace of the probe displacement

versus sample temperature is recorded. As the tip begins to penetrate, the movement is recorded by an electrical signal translated from the rod to the recorder by an LVDT (linear variable differential transformer). The temperature at which penetration begins, T_p, is determined by the point of intersection of the lines drawn tangent to the pre-T_p and post-T_p parts of the curve*.

specimens were cured with a 20 kGy dose using a 3-MeV electron beam. They were then aged at 232°C for periods up to 500 hours and tested at 232°C. The results, listed in Table 2, show that one commercial adhesive that is normally heat cured, Loctite LO-559, has good radiation cured strength and excellent thermal stability at 232°C. The Loctite 328-18, which is also normally heat cured, is rated by the manufacturer for 177°C, and the results show it has less heat stability than the others. Although the other three materials in this series have excellent thermal aging stability, the test results show that they are not as strong as the Loctite adhesives, probably due to their low toughness and thus low peel strength. Additional tests are in progress to determine the effects of long-time exposures to water and acetone on the bond strength of these adhesives.

size of the conveyor carts. For larger size components or complete assemblies it is technically feasible to construct larger facilities employing appropriate conveyors and multiple-head beam scanners. The maximum energy available from Dynamitron-type accelerators is 4 MeV, which will uniformly cure laminates with a density of 1.5 g/cm^3 and up to 10 mm thickness. Fig. 5 provides a curve of useful electron beam penetration versus electron energy for a material of unit density from which the actual thickness can be computed (3). Useful beam penetration is that thickness of material which receives an approximately equal dose on front and back surfaces.

The testing programs will proceed with evaluations of the high temperature aging stability and environmental resistance of the radiation cured resin systems that have been optimized for adhesive and composite applications.

References

1. F. J. Campbell, A. L. Cox and J. L. Godstone, "Studies of Electron Beam Curing of Polyesters for Adhesives," Technology in Transition, Volume 20, SAMPE Engineering Series, 1975.

2. F. J. Campbell, B. A. Rugg and W. Brenner, "Electron Beam Curing Improves High Temperature Strength of Vinyl Ester Adhesives," Diversity-Technology Explosion, Volume 22, SAMPLE Engineering Series, 1977.

3. E. H. Morganstern, "Processing With Radiation," Chemtech, October 1974.

4. [illegible]

Table 2

Aging of Electron Beam Cured Polyimide-Type Adhesives at 232°C

Adhesive	Single Lap Shear Strength, MPa (psi)		
	Initial at 20°C	Tested at 232°C after aging at 232°C	
		70 hrs.	500 hrs.
Loctite 328-18	10.1 (1460)	8.8 (1280)	5.8 (840)
Loctite LO-559	9.9 (1430)	9.7 (1405)	9.2 (1340)
Hexcel F-178	3.1 (450)	3.3 (480)	3.0 (430)
Modified Kerimid 601[a]	2.8 (410)	2.7 (385)	2.8 (410)
Modified Hexcel F-178[b]	3.0 (430)	3.2 (460)	2.9 (420)

[a] 100 pts Kerimid 601
40 pts diallyl phthalate
10 pts 4-aminophenyl ether

[b] 100 pts Hexcel F-178
40 pts diallyl phthalate
10 pts 4-aminophenyl ether

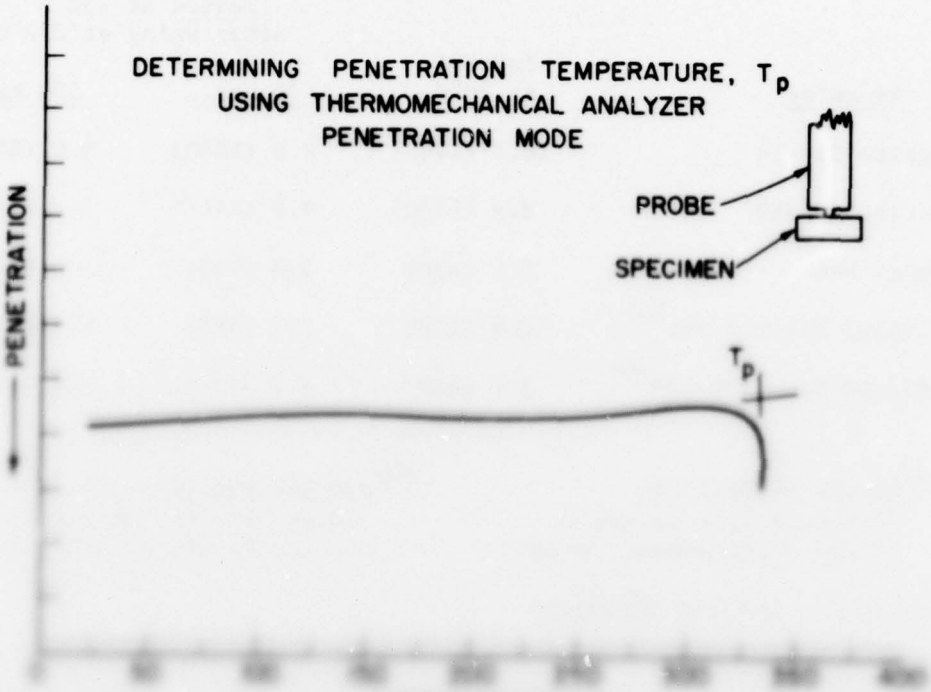
DETERMINING PENETRATION TEMPERATURE, T_p
USING THERMOMECHANICAL ANALYZER
PENETRATION MODE
PROBE
SPECIMEN
PENETRATION
T_p

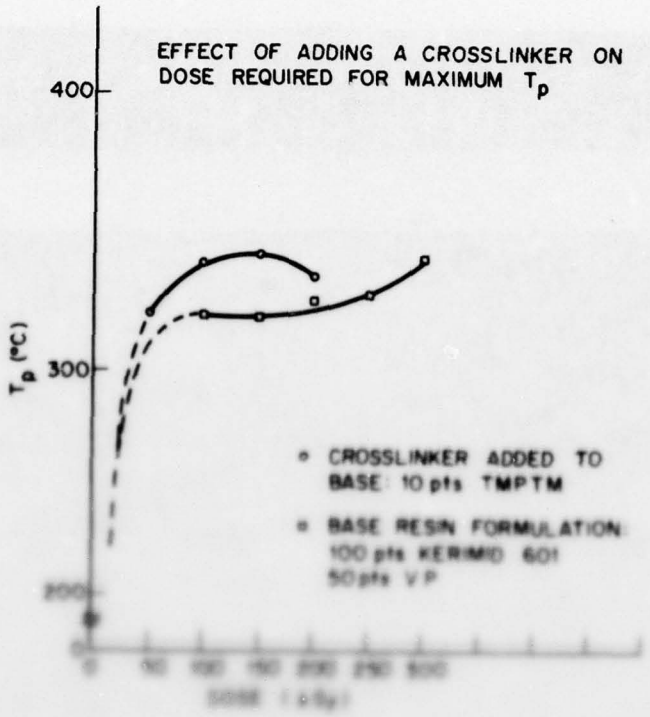
EFFECT OF ADDING A CROSSLINKER ON
DOSE REQUIRED FOR MAXIMUM T_p
400
300
200
T_p (°C)
• CROSSLINKER ADDED TO BASE: 10 pts TMPTM
• BASE RESIN FORMULATION:
100 pts KERIMID 601
50 pts V P

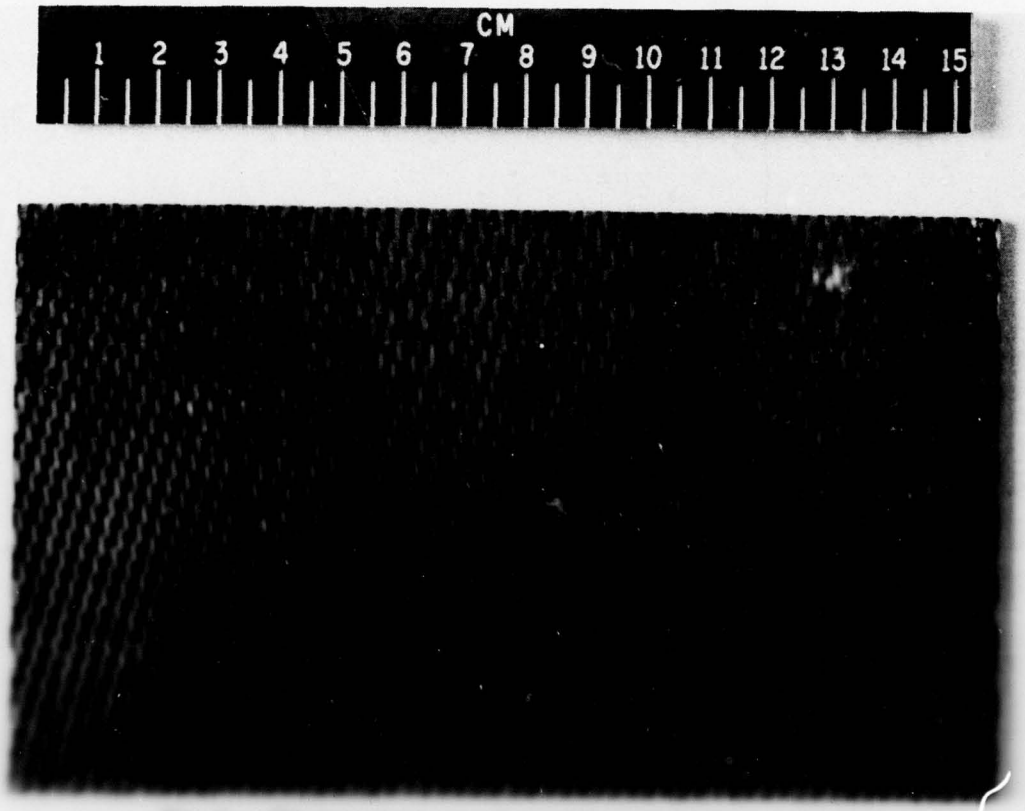

Fig. 1 — Electron beam cured graphite-polyimide composite

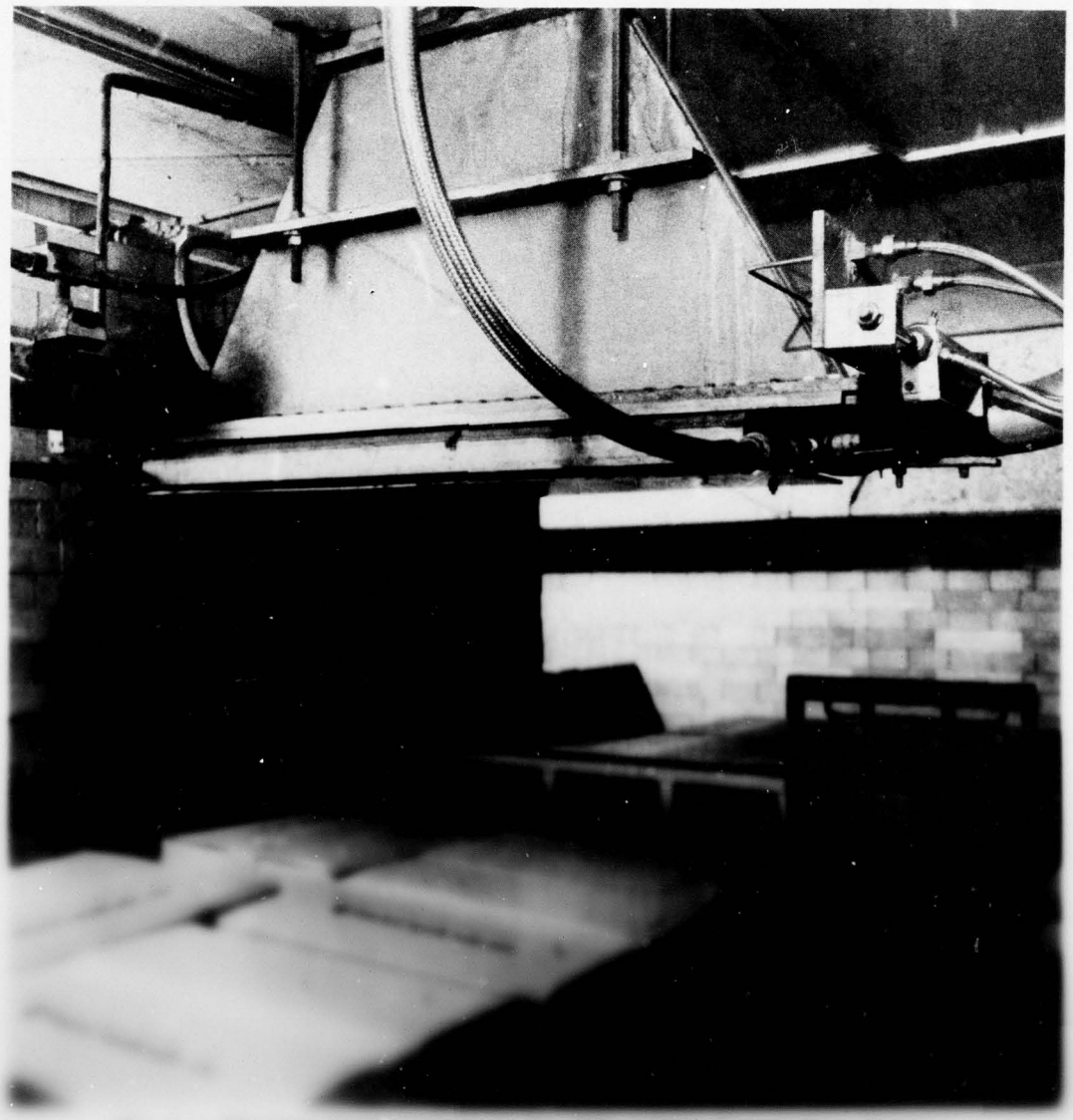

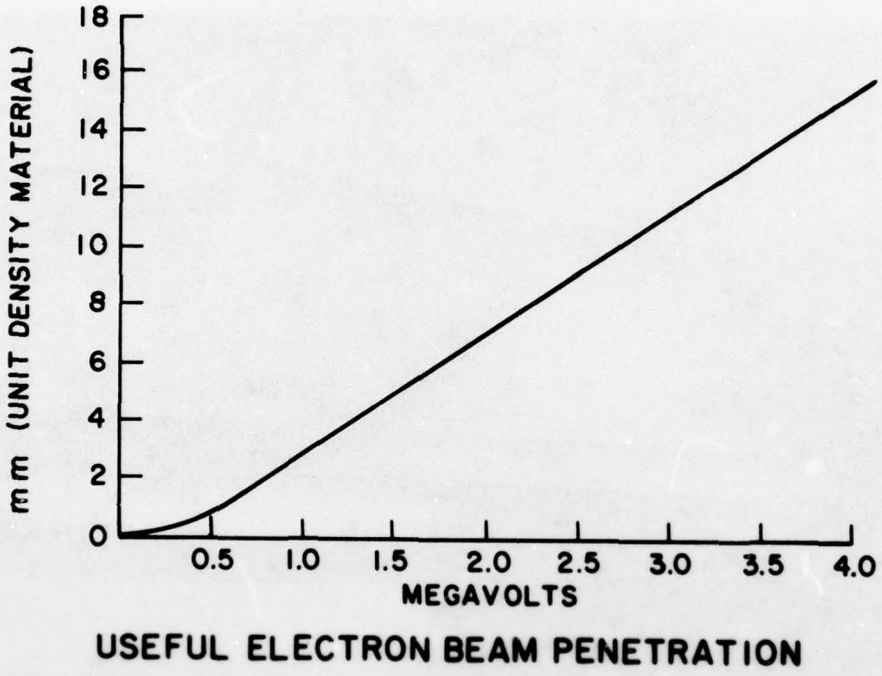

Fig. 5 — Useful electron beam penetration vs unit density material thickness (3)

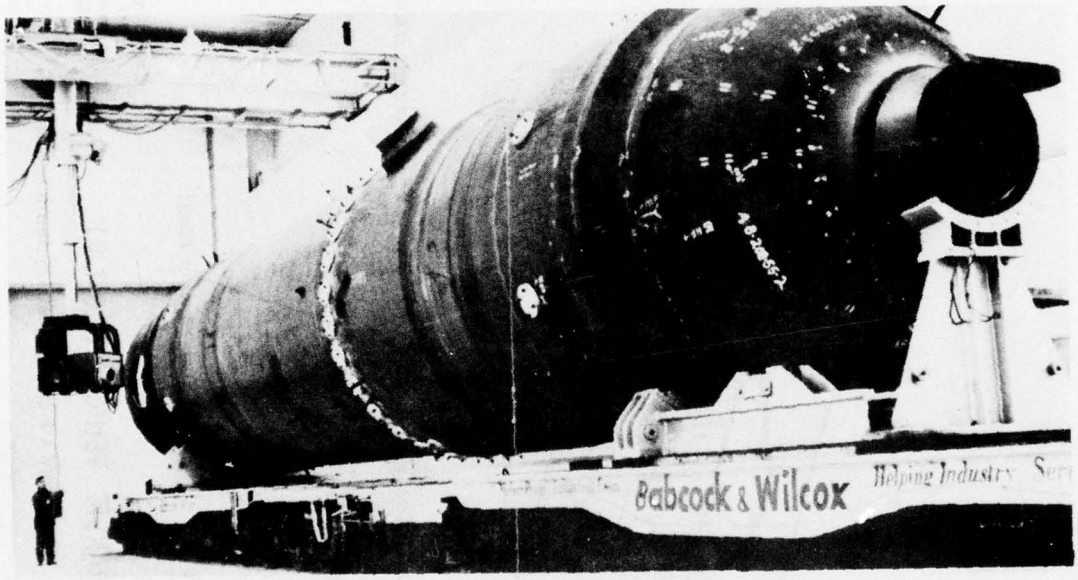

Fig. 6 — A portable linac being readied tor an x-ray radiographic inspection. (Courtesy of Varian Associates)

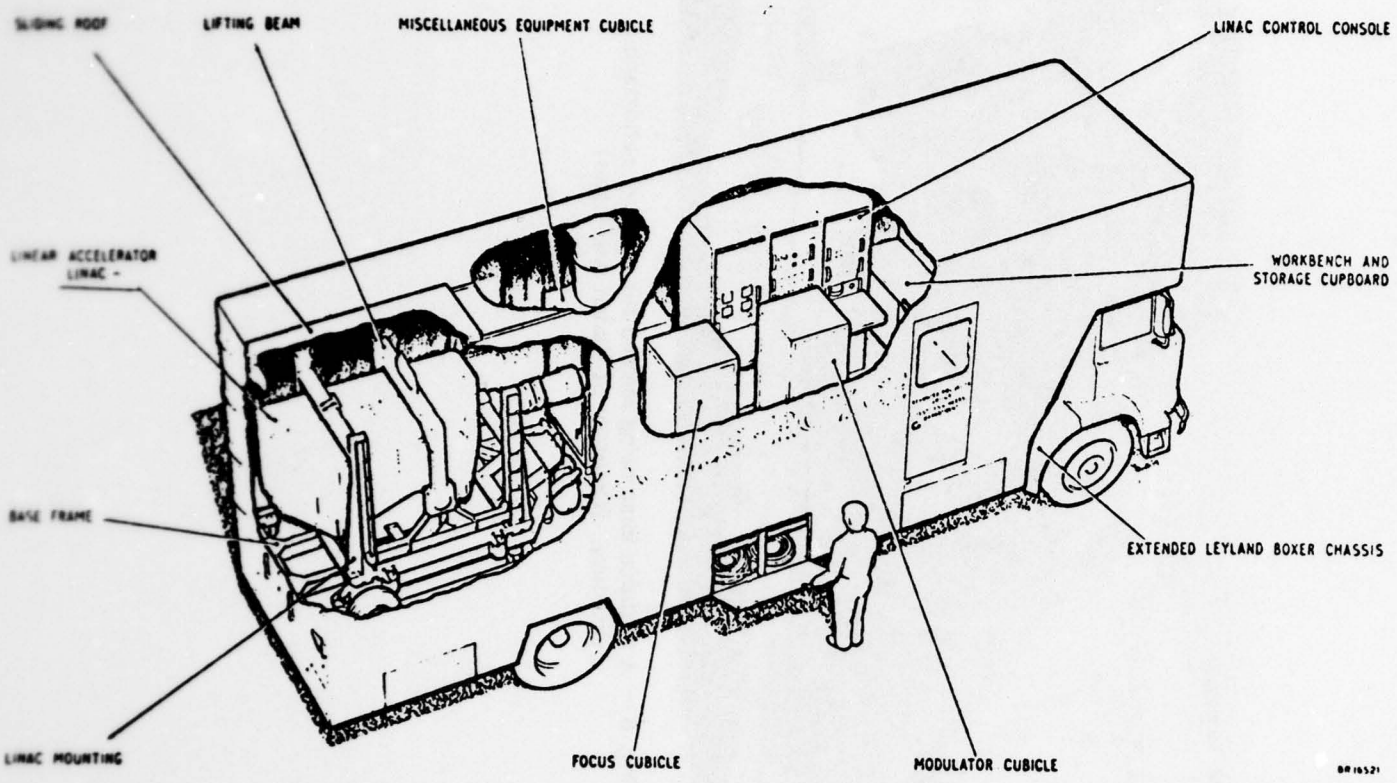

LINAC CONTROL AND TRANSIT VEHICLE (L.C.T.V.)

Fig. 7 — A van-transported linac unit. (Courtesy of Radiation Dynamics, Ltd.)

FABRICATION OF COMPOSITES

R. Y. Ting and H. C. Nash
Polymeric Materials Branch
Chemistry Division
Naval Research Laboratory
Washington, D. C. 20375

Introduction

The objective of this task is to develop fabrication conditions for the preparation of fiber-reinforced resin-matrix composites of interest to the V/STOL Program. Once the processing parameters are determined, laminates are fabricated, characterized and delivered for testing in the Design Optimization Task.

The fabrication of fiber-reinforced composites involves a complex combination of physical and chemical processes. Basically, it begins with the hand layup of a predetermined number of prepreg plies in proper sequence. The lay-up is then subjected to a properly designed curing cycle and a consolidation process. For curing the laminate, a time-temperature history is prescribed with given heating rates, dwell times, cure temperatures and cooling rates. As to the consolidation process, important considerations are given to the applied pressure, the type and amount of bleeder material and designs of dam and vacuum bag. Lastly, the laminate is post-cured for a given length of time at a fixed post-cure temperature.

Three composite systems are to be fabricated in this Task. While fixing the reinforcing fiber as Thornel 300 graphite fiber (T-300), three resin systems were selected for comparison: an epoxy system (Narmco 5208), a polyimide resin (Hexcel F-178) and the NRL-developed C-10 phthalocyanine resin. Because of the wide range of physical properties these resin systems represented, manufacturer's recommended cure cycles were always accepted as a reasonable starting point for the establishment of base-line fabrication cycles. Variations from these conditions were systematically made to adjust to the available processing equipment, to minimize laminate void content and to optimize laminate mechanical properties.

To ensure the quality of the laminates produced, physical and mechanical characterizations were carried out before the laminates were delivered for testing. Physical characterizations performed included determinations of laminate density and void/fiber/resin

volume fractions by both acid digestion and ultrasonic scanning methods. Tensile strength, tensile modulus and Poisson's ratios were also determined by using an Instron Rheometer. The details of these characterization techniques were described in an earlier report (Ref. 1).

Laminate Fabrication

For each fiber-matrix system, two types of laminates were prepared: 16-ply angle plies and 16-ply quasi-isotropic configurations. Fig. 1 shows the designs of these laminates. In each case, the 25.4 cm x 25.4 cm (10" x 10") laminates were symmetric with respect to a mid-plane. The angle plies consisted of six different orientations including 0^{o}, $\pm 15^{o}$, $\pm 22,5^{o}$, $\pm 30^{o}$, $\pm 37.5^{o}$ and $\pm 45^{o}$. The quasi-isotropic laminate had the configuration of $(90^{o}, \pm 45^{o}, 0^{o})$. These laminates, after physical and mechanical characterizations, will be evaluated in the in-plane loader and the box-beam 3-D testing machine both at room temperature and at high temperature, e.g. 204^{o}C (400^{o}F). To date the required Narmco 5208/T-300 and Hexcel F-178/T-300 laminates have been prepared. Tables I and II give the fabrication cycles for Narmco 5208/T-300 and Hexcel F-178/T-300 laminates, respectively.

C-10 Phthalocyanine/T-300 Graphite Fiber Prepreg

Because in-house equipment for producing large amounts of prepreg material is not available, procurement contracts were sought with commercial contractors to produce C-10 phthalocyanine/T-300 graphite fiber prepregs.* The C-10 phthalocyanine resin will be supplied to the contractors by NRL. The contracts included the following basic elements:

1. The resin should be applied by hot melt methods to obtain a resin content of 38-42%, such that the estimated prepreg production of each 10 lbs. of resin supply is 350-400 sq. ft.

2. The prepreg must be 12-inch wide tape and supplied in sheets of at least 24 inches in length.

3. The fiber must be Thornel 300, 3K filament, untwisted, UC-309 size.

4. The contractor will establish and provide the following data: (a) melt viscosity, (b) melt point depression, (c) percent flow, (d) density, (e) gel time, (f) thickness/ply (cured), and (g) recommended cure cycle.

*Multiple contract awards have been made to U. S. Polymeric Chemicals, Inc. and to the Composites Division of the Ferro Corporation.

AD-A054 637 NAVAL RESEARCH LAB WASHINGTON D C F/G 11/4
HIGH PERFORMANCE COMPOSITES AND ADHESIVES FOR V/STOL AIRCRAFT.(U)
FEB 78 W D BASCOM, L B LOCKHART

UNCLASSIFIED NRL-MR-3721 SBIE-AD-E000 155 NL

2 OF 2
AD
AD054637

END
DATE FILMED
6 -78
DDC

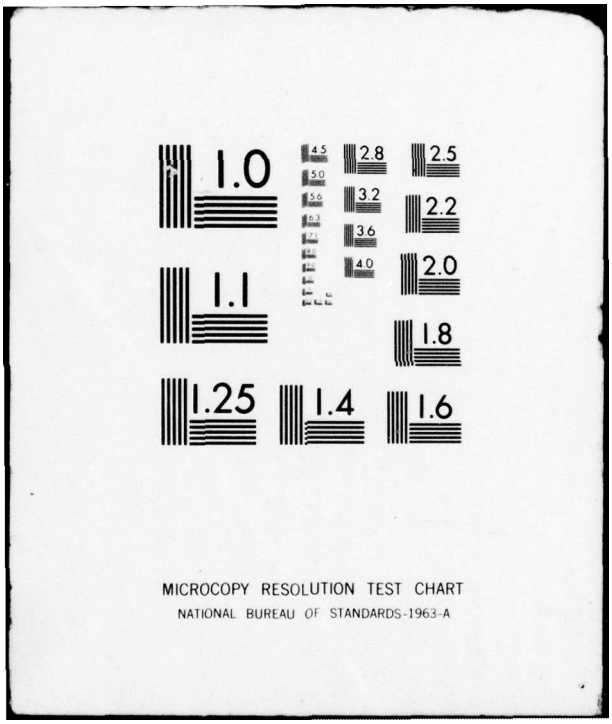
1.0
1.1
1.25
1.4
1.6
1.8
2.0
2.2
2.5
2.8
3.2
3.6
4.0
4.5
5.0
5.6
6.3
7.1
MICROCOPY RESOLUTION TEST CHART
NATIONAL BUREAU OF STANDARDS-1963-A

5. The contractor must be capable of large prepreg production for possible future Navy use.

Once this prepreg material is received, laminates will be fabricated and evaluated for comparison with the Narmco 5208/T-300 and Hexcel F-178/T-300 systems.

Prepreg Aging Study

A major difficulty in handling the epoxy or polyimide/graphite fiber prepreg, such as the Hexcel F-178/T-300 system, is that the material must be stored at very low temperatures (i.e. ~ -20°C). Before lay-up, the prepreg must be allowed to warm up to room temperature, a process during which much moisture could be adsorbed by the prepreg through condensation. The manufacturer's suggested shelf life for the Hexcel prepreg, for example, is only three weeks at room temperature, and only six months even at freezer temperatures. Presumably, excessive B-staging may take place at room temperature, and at the same time the resin system may degrade by absorbing moisture from the atmosphere.

A short-term prepreg aging test using the Hexcel F-178/T-300 material was carried out to examine the effect of temperature and humidity on the prepreg properties. Materials exposed to various humidity levels at room temperature were chemically analyzed by IR and proton NMR techniques, (see Chemical Characterization Task). Unidirectional 16-ply laminates, 15 cm x 15 cm (6" x 6") in size, were also fabricated using these exposed materials and their mechanical properties evaluated as a function of prepreg out-time.

Fresh prepreg materials were cut, packed in kits and stored at room temperature in three environmental chambers controlled at 16%, 50% and 95% relative humidity, respectively. The kits were essentially small aluminum shelves with 17 open slots. Each kit therefore contained seventeen pieces of prepreg, 15 cm x 15 cm in size with one piece in each slot. After a specified period of aging, a kit was removed from storage and a 16-ply laminate prepared on the same day. The extra sheet of aged prepreg from each kit was used for chemical analysis. Samples were cut from the laminates and post-cured at 249°C (480°F) for 10 hrs. Tests were then carried out to determine if any change occurred in their mechanical properties relative to composites prepared from unaged prepreg. The short-beam shear test was chosen to determine the interlaminar shear strength, a resin-dominated property. The flexure test was selected to measure the laminate flexural strength, a fiber-dominated property. The results are shown in Figs. 2 and 3 with the mechanical properties plotted as a function of prepreg out-time. It was clear that over the 21-day aging period no significant change had occurred in either interlaminar shear strength or flexural strength. Results of chemical analyses seemed to agree with this conclusion.

However, some physical changes did take place as aging proceeded. First of all, during the aging period the prepreg material clearly showed a steady loss of tackiness. In fact, near the end of the 21-day aging period the prepreg was so dry and brittle that it became extremely difficult during lay-up to keep all plies properly aligned and adhered together as one piece. Secondly, it was also observed that the bleeding during curing was greatly reduced for aged samples. Over the 15 cm x 15 cm area the fresh samples would completely wet and soak thoroughly through the bleeder plies, but for the aged samples the amount of flow seemed to have been decreased. As aging continued, the increase in unwetted portions on the bleeder plies was evident, particularly around the corners of the square plies. The implications of these observed physical changes on laminate performance is not yet clear. This aging test is presently being continued. The plan is to extend the aging period to at least six months. Similar tests will also be performed on C-10 phthalocyanine/T-300 prepreg as soon as the material arrives from the prepreg contractors.

Reference

1. NRL Memo Rept. 3433, "High Performance Composites and Adhesives for V/STOL Aircraft", ed. W. D. Bascom and L. B. Lockhart, Jr., Dec. 1976.

Table I

Fabrication Cycle for Narmco 5208/T300 Prepreg

1. Place lay-up in press.
2. Put spacer bars in place so that press may be closed without applying pressure to the sample.
3. Close press.
4. Apply full vacuum, hold 50 minutes.
5. Heat platens to 135°C (275°F) at 7°C/min.
6. Hold at 135°C for 1 hr.
7. Remove spacer bars and apply 6.9×10^5 Pa (100 psi) pressure to the laminate and release vacuum.
8. Heat to 177°C (350°F) at 7°C (12°F)/min.
9. Hold at 177°C for 2 hrs.
10. Slow cool under pressure to < 100°C.
11. Post cure for 4 hrs. at 204°C (400°F).

Table II

Fabrication Cycle for Hexcel F178/T300 Prepreg

1. Place lay-up in press.
2. Put spacer bars in place so that press may be closed without applying pressure to the sample.
3. Close press.
4. Apply full vacuum and hold for 2 hrs.
5. Heat platens to 121°C (250°F) at 7°C/min.
6. Hold at 121°C for 1 hr.
7. Remove spacer bars and apply 6.9×10^5 Pa (100 psi) pressure to the sample and release vacuum.
8. Heat to 177°C (350°F) at 7°C/min.
9. Hold at 177°C for 2 hrs.
10. Slow cool under pressure to 60°C (140°F).
11. Post cure for 10 hrs. at 249°C (480°F).

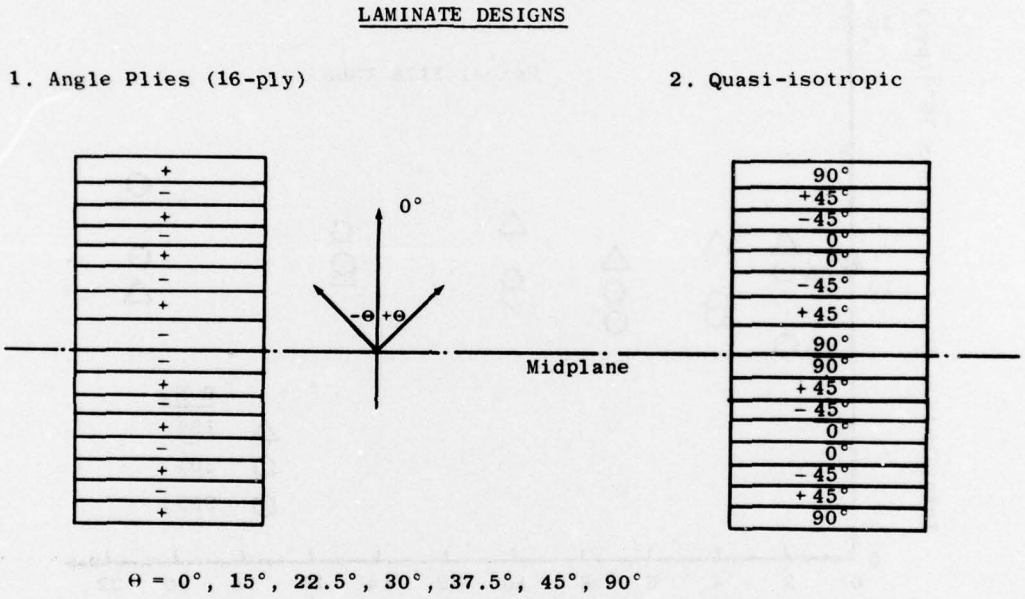

Fig. 1 — Laminate designs for angle ply and quasi-isotropic configuration plates

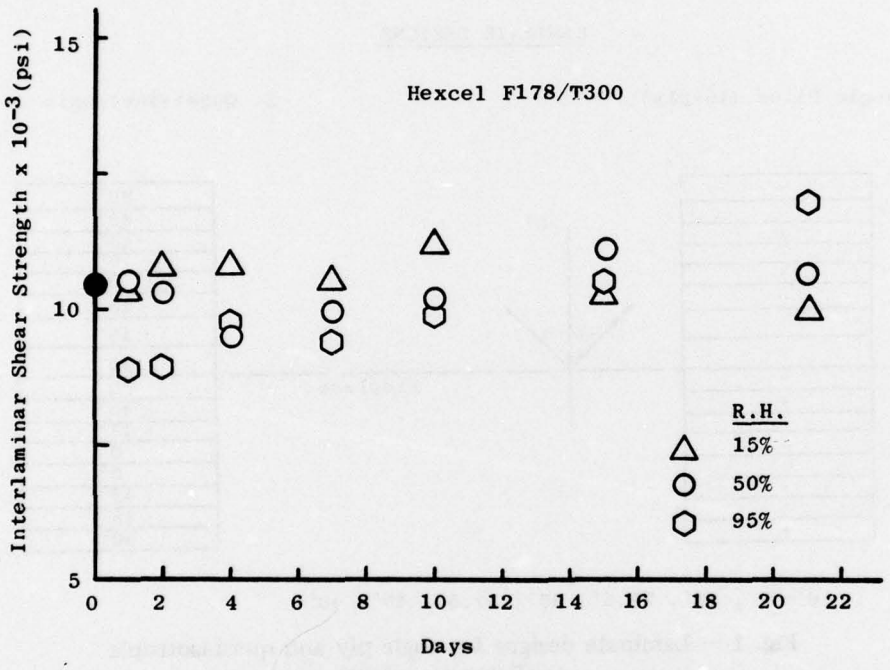

Fig. 2 — Interlaminar shear strength of Hexcel F-178/T300 laminates as a function of prepreg out-time

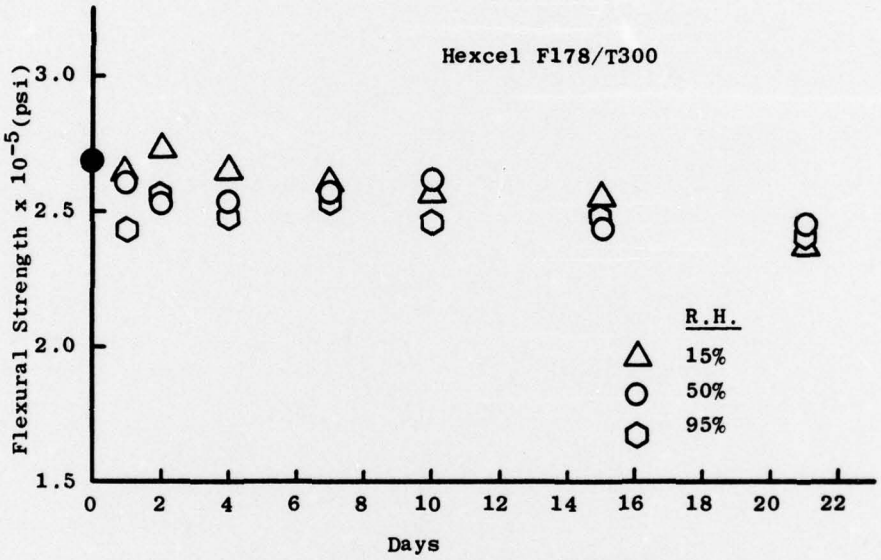

Fig. 3 — Flexural strength of Hexcel F-178/T300 laminates as a function of prepreg out-time

FAILURE CRITERIA FOR COMPOSITE STRUCTURES

L. A. Beaubien, M. F. Clifford, P. W. Mast, D. R. Mulville,
S. A. Sutton, R. W. Thomas, J. Tirosh and I. Wolock
Mechanics of Materials Branch
Ocean Technology Division

and

D. L. Hunston
Polymeric Materials Branch
Chemistry Division
Naval Research Laboratory

Part I. Failure Criteria for Composites

Part II. Failure Criteria for Adhesive Joints

PART I. FAILURE CRITERIA FOR COMPOSITES

INTRODUCTION

A technique was developed for predicting the initiation of failure under in-plane loading in a general structure of a composite material from failure data obtained on test coupons under in-plane loading. The technique is based on the concept that if the strain field within the region under consideration in the general structure is similar to a strain field previously observed in a test coupon of the same material, then the same loading conditions which caused failure in the test coupon will cause failure in the structural prototype. An in-plane loader was used to develop failure data on test coupons, as described in the previous annual report [1]. Typical failure surfaces are shown in Figure 1 for a series of Thornel 300/5208 graphite/epoxy composites in which the included angle of the reinforcement is varied.

BOX BEAM STUDIES

A box beam was selected to demonstrate the procedure for utilizing data obtained on small composite test coupons in the in-plane loader to predict the fracture behavior of a structural component. The complex loads could be developed in this component which would be typical of those that the composite material would be subjected to in a general structural application. Figure 2 is a general schematic of the box beam. A box beam constructed entirely of graphite/epoxy composite would be quite expensive. Therefore, aluminum was used for the sides and faces. Aluminum face sheets 12 in. x 18 in. x 0.125 in. (305 mm x 457 mm x 3.2 mm) were bolted to 1.5 in. (38 mm) deep aluminum channels. There was a circular cut-out in the face into which was bolted the composite material to be tested. Thus the graphite/epoxy test material would be subjected to loadings similar to those applied in the in-plane loader

tests and the aluminum box beam would be usable for many tests merely by replacing the graphite/epoxy disk for each test. The composite disk was 4.5 in. (114 mm) in diameter and 0.1 in. (2 mm) thick and contained a notch 2.75 in. (70 mm) long. The notch had the same geometry as that used in the test coupon and was formed using a 25 mil (0.6 mm) thick diamond-tipped cut-off wheel. The length of the unbroken ligament at each end of the notch was at least as long as that in the test coupon so that the same finite element grid would apply. On the other hand, the unbroken ligament in the disk could not be made too long or else the box beam might fail in the aluminum rather than in the composite disk. To permit the development of a wide range of complex loads in the box beam, two multi-holed loading plates were bolted to the ends. Pinning clevises through various combinations of the top and bottom holes allowed a range of loadings, consisting of combinations of tension, shear and in-plane bending, to be applied to the box beam, using a single actuator universal testing machine (see Fig. 3). The box beam tests were conducted by loading the specimen at approximately 1000 lb. (4,448 N) increments and maintaining the load while examining the area surrounding the ends of the notch for signs of failure initiation, using a microscope. In the in-plane loader tests, the point of failure initiation had been determined using a dissipated energy criterion [1]. The dissipated energy is the non-recoverable strain energy absorbed by the fracture process. This procedure is more objective and more accurate than that used in the box beam tests. However, the point at which cracks were first observed visually in the latter tests was usually agreed upon by several observers. Several tests were conducted using the box beam, and the results are reported later. Since there are seven holes each in the top and the bottom loading plates of the box beam, there were 49 possible loading combinations. To graphically represent the combination for a particular test, the coordinates of the upper and the lower loading holes were specified by the distance from the respective center holes. The x and y coordinates represent the upper and lower holes, respectively, and the vertical axis represents the load at the initiation of failure (Figure 4). In Figure 3, the upper pin is located in the third hole which is nine inches (229 mm) to the left of the center hole, so that the x-coordinate = 9. The lower pin is located in the second hole which is six inches (152 mm) to the right of the center hole, so that the y-coordinate is -6. This is shown in Figure 4. For symmetric loading, only one prediction of failure conditions was required for both ends of the notch, whereas for unsymmetric loading, it was necessary to make independent predictions for each end of the notch since the stress states were different.

PROCEDURE FOR PREDICTING INITIATION OF FAILURE IN BOX BEAM

A procedure was developed to translate the failure surface obtained for the test coupons into a predictive failure surface for the box beam. The stress analysis required for this procedure was accomplished using a newly developed interactive finite element parametric simulative system, TOTAL [2]. First, a small subregion is delineated about the notch tip in the test coupon. This region is shown in Figure 5a, outlined on the finite element grid used in the coupon stress analysis. Then an identical region is delineated about each end of the notch on the box beam test disk. In order to conduct a structural analysis of the box beam, three levels of substructuring were used to model the notch tip region (Fig. 5c). The zone of failure in both the box beam and the test coupon have identical grid geometries. The strains are determined in these subregions for each loading case, using TOTAL. There are three loading cases each for the coupon and for the box beam, as shown in Fig. 6. The results of the stress analyses for the six cases are presented in graphical form in Figs. 7-12.* The strain fields depicted are for the full coupon geometry for the test coupon and for the box beam disk. However, the actual strain fields represented by $\left({}^{C}\underline{Q}_{B}^{H}\right)$, $\left({}^{C}\underline{Q}_{B}^{V}\right)$, $\left({}^{C}\underline{Q}_{B}^{R}\right)$ for the coupon and $\left({}^{K}\underline{Q}_{B}^{H}\right)$, $\left({}^{K}\underline{Q}_{B}^{V}\right)$, $\left({}^{K}\underline{Q}_{B}^{R}\right)$ for the box beam are only those within the failure zone subregions about the notch tips. The strain response of the structures is assumed to be linear and therefore the strain field for a particular displacement $\| \left({}^{C}H_{B}, {}^{C}V_{B}, {}^{C}R_{B}\right)$ of the coupon is expressible as a linear combination of the strain fields $\left({}^{C}\underline{Q}_{B}^{H}\right)$, $\left({}^{C}\underline{Q}_{B}^{V}\right)$, $\left({}^{C}\underline{Q}_{B}^{R}\right)$. That is:

$$ {}^{C}_{C}\underline{D} = \left({}^{C}H_{B}\right)\left({}^{C}\underline{Q}_{B}^{H}\right) + \left({}^{C}V_{B}\right)\left({}^{C}\underline{Q}_{B}^{V}\right) + \left({}^{C}R_{B}\right)\left({}^{C}\underline{Q}_{B}^{R}\right) \qquad (1) $$

---

* The numerical modeling of the stress and displacement field in the vicinity of the notch obtained with the TOTAL program was verified by an experimental stress analysis, using a photoelastic coating bonded to the composite disk. A satisfactory correlation was obtained for various combinations of in-plane loads.

Similarly the strain field ${}^{K}_{K}\underline{L}$ for a particular loading, $\left({}^{K}H_{B}, {}^{K}V_{B}, {}^{K}R_{B}\right)$ of the box beam is expressible as a linear combination of the strain fields $\left({}^{K}_{Q}\underline{H}_{B}\right)\left({}^{K}_{Q}\underline{V}_{B}\right)\left({}^{K}_{Q}\underline{R}_{B}\right)$ or

$$ {}^{K}_{K}\underline{D} = \left({}^{K}H_{B}\right)\left({}^{K}_{Q}\underline{H}_{B}\right) + \left({}^{K}V_{B}\right)\left({}^{K}_{Q}\underline{V}_{B}\right) + \left({}^{K}R_{B}\right)\left({}^{K}_{Q}\underline{H}_{B}\right) \qquad (2) $$

The use of equations 1 and 2 greatly reduces the number of stress analyses needed and therefore the computing time necessary to determine strain fields ${}^{C}_{C}\underline{D}$ and ${}^{K}_{K}\underline{D}$. In developing the failure surface for the box beam, fifteen loading cases are used for the coupon and forty-nine cases for the box beam. Without the use of equations 1 and 2, 64 stress analyses (one for each of these loading cases) are needed. With the use of equations 1 and 2, only six stress analyses are needed, one for each of the basis strain field vectors in the test coupon and in the box beam.

An equivalence relationship is now imposed between the failure of the material in the coupon in the zone of failure subregion and the failure of the same material in the box beam in similar subregions about the notch tips. If the strain fields ${}^{C}_{C}\underline{D}$ and ${}^{K}_{K}\underline{D}$ are equal and if ${}^{C}_{C}\underline{D}$ is a failure condition in the coupon, then ${}^{K}_{K}\underline{D}$ is a failure condition in the box beam. The problem then is to determine what loading conditions in the box beam produce strain fields ${}^{K}_{K}\underline{D}$ that are similar to the strain fields ${}^{C}_{C}\underline{D}$. The technique used to compare strain fields (equivalent to a least squares fit) is that of normal projection of the strain fields ${}^{K}_{Q}\underline{H}_{B}$, ${}^{K}_{Q}\underline{V}_{B}$, ${}^{K}_{Q}\underline{R}_{B}$ into the subspace spanned by the strain fields $\left({}^{C}_{Q}\underline{H}_{B}\right)$, $\left({}^{C}_{Q}\underline{V}_{B}\right)$, $\left({}^{C}_{Q}\underline{R}_{B}\right)$. For the examples used here this method renders the following results.

$$ {}^{K}_{C}\underline{D}^{H} = 0.014\ {}^{C}_{Q}\underline{H}_{B} + 0.0\ {}^{C}_{Q}\underline{V}_{B} - 0.009\ {}^{C}_{Q}\underline{R}_{B} \qquad (3) $$

$$ {}^{K}_{C}\underline{D}^{V} = 0.049\ {}^{C}_{Q}\underline{H}_{B} + 0.120\ {}^{C}_{Q}\underline{V}_{B} - 0.180\ {}^{C}_{Q}\underline{R}_{B} \qquad (4) $$

$$ {}^{K}_{C}\underline{D}^{R} = 0.012\ {}^{C}\underline{Q}_{B}^{H} + 0.007\ {}^{C}\underline{Q}_{B}^{V} - 0.010\ {}^{C}\underline{Q}_{B}^{R} \tag{5} $$

Figure 13 graphically depicts ${}^{K}_{C}\underline{D}^{V}$, ${}^{K}_{K}\underline{D}^{V}$ for visual comparison. Since each of the vectors $\left({}^{K}\underline{Q}_{B}^{H}\right)$, $\left({}^{K}\underline{Q}_{B}^{V}\right)$, $\left({}^{K}\underline{Q}_{B}^{R}\right)$ for this example is 450-dimensional (i.e., 150 nodes in the subregion and 3 strain components in each node), it cannot be expected that in all cases the representation which is in a three-dimensional subspace will be an exact duplicate. Therefore a measure of error is desirable to determine the degree of approximation. Define the errors e^{H}, e^{V}, e^{R} to be:

$$ e^{H} = \frac{||{}^{K}_{C}\underline{D}^{H} - {}^{K}\underline{Q}_{B}^{H}||}{||{}^{K}\underline{Q}_{B}^{H}||} \times 100 \tag{6} $$

$$ e^{V} = \frac{||{}^{K}_{C}\underline{D}^{V} - {}^{K}\underline{Q}_{B}^{V}||}{||{}^{K}\underline{Q}_{B}^{V}||} \times 100 \tag{7} $$

$$ e^{R} = \frac{||{}^{K}_{C}\underline{D}^{R} - {}^{K}\underline{Q}_{B}^{R}||}{||{}^{K}\underline{Q}_{B}^{R}||} \times 100 \tag{8} $$

where $||V||$ means the length of the vector $\underline{V}$. For the loading case shown in Figure 13, the computed errors are:

$$ e^{H} = 8.6\% \tag{9} $$

$$ e^{V} = 8.7\% \tag{10} $$

$$ e^{R} = 2.1\% \tag{11} $$

To establish a relation between the loading on the box beam and that for the coupon, such that the respective strain fields produced in the subregion about their notch tips are equal, it is necessary to relate the forces on the box beam, ${}^{K}\underline{t}_{B}$, to the forces on the coupon, ${}^{C}\underline{t}_{B}$. The displacement-force relationships of the box beam and the coupon, i.e., the stiffness or compliance, can be computed from the forces and displacements on the respective loading bondaries. When these relationships are combined with the transformations (3), (4) and (5), the desired relations between the coupon and the box beam are established. This procedure is illustrated in Fig. 14.

The relation between the load vectors can be expressed as

$$\left({}^{C}P\right)\left(\frac{{}^{C}\underline{t}_B}{{}^{C}P}\right) = \left[{}^{C}E\right]\left[{}^{K}_{C}D\right]\left[{}^{K}F\right]\ {}^{K}P\left(\frac{{}^{K}\underline{t}_B}{{}^{K}P}\right) \tag{12}$$

where $\left[{}^{C}E\right]$ = stiffness of the test coupon

$\left[{}^{K}_{C}D\right]$ = computed strain field in the box beam from that of the coupon based on least squares approximation

$\left[{}^{K}F\right]$ = compliance of the box beam

If $[L] = \left[{}^{C}E\right]\left[{}^{K}_{C}D\right]\left[{}^{K}F\right]$, then substituting in equation (12)

$$^{C}P\left(\frac{{}^{C}\underline{t}_B}{{}^{C}P}\right) = [L]\left({}^{K}P\right)\left(\frac{{}^{K}\underline{t}_B}{{}^{K}P}\right) \tag{13}$$

The magnitude of loading on the coupon can be expressed as

$$^{C}P = \sqrt{\left\{\left({}^{C}P\right)\left(\frac{{}^{C}\underline{t}_B}{{}^{C}P}\right)\right\}^{T}\left\{\left({}^{C}P\right)\left(\frac{{}^{C}\underline{t}_B}{{}^{C}P}\right)\right\}} \tag{14}$$

From equation (13),

$$^{C}P = \sqrt{\left\{[L]\ \left({}^{K}P\right)\left(\frac{{}^{K}\underline{t}_B}{{}^{K}P}\right)\right\}^{T}\left\{[L]\ \left({}^{K}P\right)\left(\frac{{}^{K}\underline{t}_B}{{}^{K}P}\right)\right\}} \tag{15}$$

or

$$^{C}P = {}^{K}P\sqrt{\left(\frac{{}^{K}\underline{t}_B}{{}^{K}P}\right)^{T}\left[L^{T}\right][L]\left(\frac{{}^{K}\underline{t}_B}{{}^{K}P}\right)} \tag{16}$$

Solving for the loading on the box beam in terms of the loading on the test coupon,

$$K_P = \frac{C_P}{\sqrt{\left(\frac{K_{t_B}}{K_P}\right)^T \left[L^T\right] [L] \left(\frac{K_{t_B}}{K_P}\right)}} \qquad (17)$$

To allow a simple analytic representation of the load failure surface, it is approximated by a flat surface of $C_P = 2000$. This is a good approximation as can be observed from Fig. 15, when it is considered that the actual points of comparison for the particular loadings used in the box beam tests described in the next section lie along the far edge where $\theta_2 = -45$.

Substituting in Equation (17)

$$K_P = \frac{2000}{\sqrt{\left(\frac{K_{t_B}}{K_P}\right)^T \left[L^T\right] [L] \left(\frac{K_{t_B}}{K_P}\right)}} \qquad (18)$$

The resulting values of K_P define the failure surfaces for the box beam. As stated previously, there is a failure surface for each end of the notch.

The procedure for transforming the coupon failure surface into a predicted structural component failure surface does not require the approximation of a flat failure surface for the test coupons. Instead, for each particular loading condition of interest, one can obtain the actual value for the failure load from the test coupon failure surface and substitute that value in Equation (17) to calculate the predicted load for the structure under that specific loading condition.

BOX BEAM EXPERIMENTAL FAILURE SURFACE COMPARISON WITH THE PREDICTED FAILURE SURFACE

In comparing the predicted box-beam failure surface with the experimentally observed one, several points must be kept in mind. One, failure initiation is not only predicted for a particular load, but also for the left or right end of the notch, or both. Two, the predicted failure surface, based on in-plane loader failure data, probably has greater accuracy than the experimentally observed failure points for the box beam specimens, as indicated earlier, due to the methods used for determining initiation of failure.

The combined failure surfaces for the left and right notch ends are depicted in figures 16 and 17 and are presented in tabular form below.

LOAD AT FAILURE

EXPERIMENT	TYPE OF LOADING	LEFT END		RIGHT END	
		PREDICTED	OBSERVED	PREDICTED	OBSERVED
1	Tension	9,015	10,600	9,015	10,600
2	Tension Bending	6,900	6,240	no failure	no failure
3	Tension Shear	10,600	8,320	" "	" "
4	Tension Shear Bending	8,500	8,700	" "	" "

Thus the technique described provides a valid method for predicting the conditions for the initiation of failure in a fiber-reinforced composite structure under complex in-plane loading. At present, the method is valid only for a structural defect having the same geometry as that in the test coupon. A technique is now being developed for the purpose of extrapolating test coupon results to defects with different geometries.

NOMENCLATURE

Forces:

S = shear force
T = tensile force
M = bending moment

$\underline{t} = \begin{Bmatrix} S \\ T \\ M \end{Bmatrix}$ = force vector applied to structure (test coupon or box beam)

Displacements:

H = horizontal displacement
V = vertical displacement
R = rotation (in-plane)

$\underline{d} = \begin{Bmatrix} H \\ V \\ R \end{Bmatrix}$ = displacement vector applied to structure

Reference frame:

B = reference frame located at midpoint of boundary
N = reference frame located at notch tip

Structure:

$\alpha_i \begin{cases} C = \text{test coupon} \\ K = \text{test component (box beam)} \end{cases}$

$i = 1,2$

Q = basis strain field vector in failure zone

$^{\alpha_1}_{\alpha_2}D$ = computed strain field in failure zone for structure α_1 as linear combination of strain fields Q in structure α_2

P = magnitude of loading applied to structure

L = matrix based on structural properties of box beam and coupon used to relate forces on the two structures

E = stiffness of the structure

F = compliance of the structure

Subscripts and superscripts are for purposes of identification and are not utilized in the mathematical procedures.

EXAMPLES

$^{C}H_{B}$ = Horizontal displacement at boundary (B) of test coupons (C)

$^{K}\underline{Q}^{V}_{B}$ = Basis strain field vector in failure zone of box beam (K) due to vertical displacement (V) at mid-point of boundary (B)

$^{K}_{C}\underline{D}$ = Computed strain field in failure zone of box beam (K) from strain field in test coupon (C)

$^{K}_{C}\underline{D}^{R}$ = Computed strain field, due to in-plane rotation, in failure zone of box beam (K) from strain field in test coupon (C)

REFERENCES

1. L. A. Beaubien et al, "Task F Design Optimization," in High Performance Composites and Adhesives for V/STOL Aircraft (W. D. Bascom and L. B. Lockhart, Jr, ed.) First Annual Report, NRL Memorandum Report 3433, December 1976, p. 101.

2. L. A. Beaubien, "TOTAL: Interactive Graphics System for the Two-Dimensional Analysis of Linear Elastic Solids," in Structural Mechanics Software Series (N. Perrone and W. Pilkey, ed.) Vol. I, University Press of Virginia, 1977, p. 275.

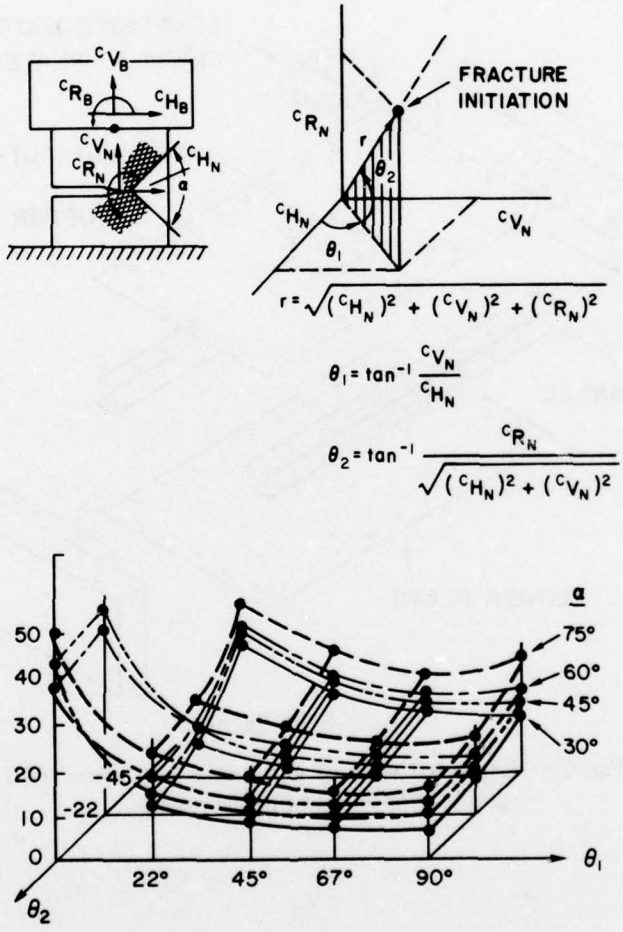

Fig. 1 — Graphite epoxy composite failure surfaces

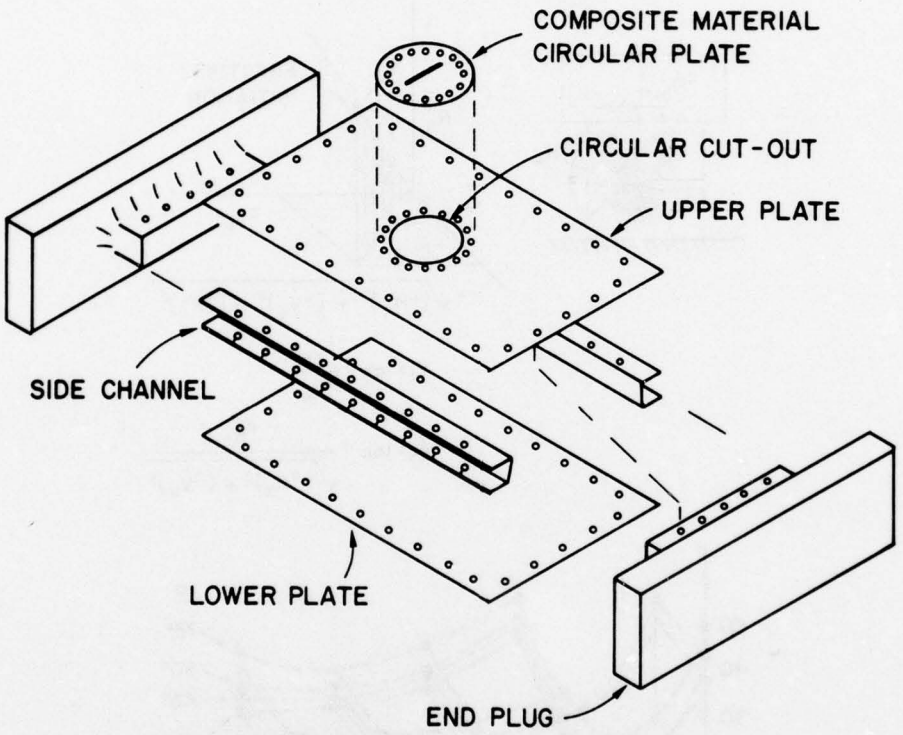

Fig. 2 — Exploded view of aluminum box beam with graphite/epoxy composite insert

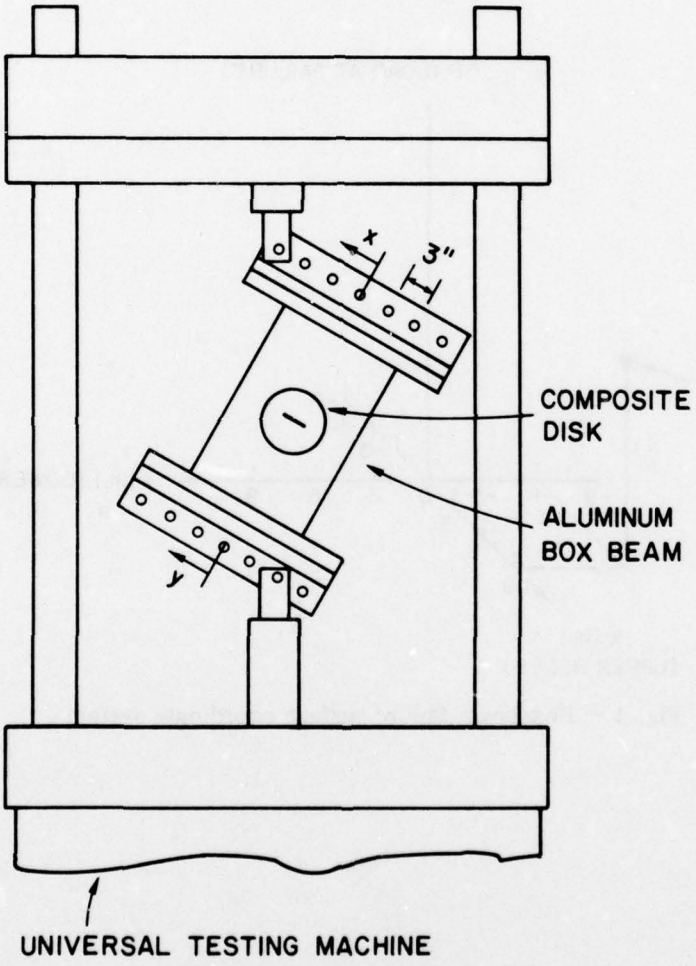

Fig. 3 — Box beam loading system

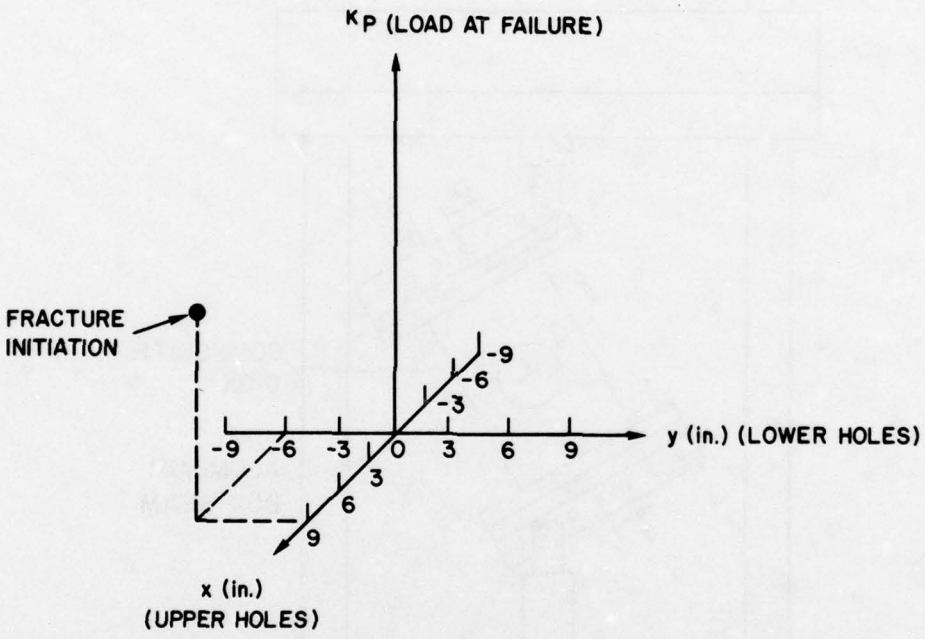

Fig. 4 — Box beam failure surface coordinate system

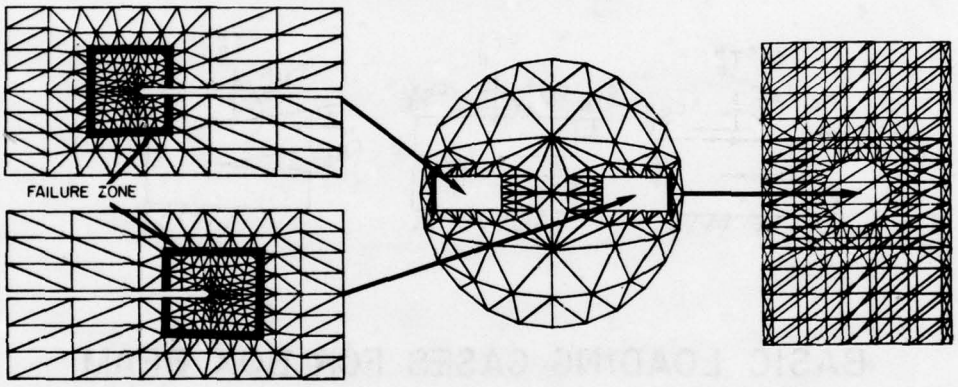

Fig. 5 — Substructuring technique for simulating failure zone in box beam

BASIC LOADING CASES FOR COUPON

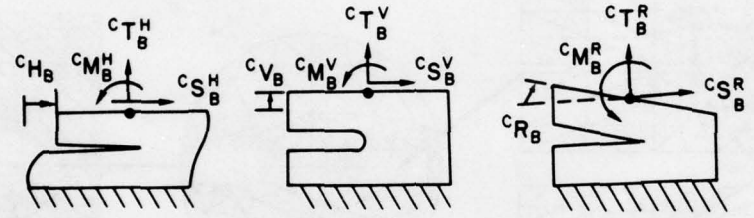

BASIC LOADING CASES FOR BOX BEAM

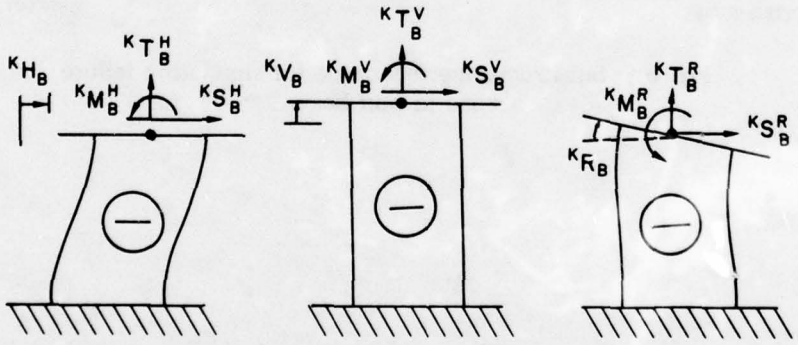

Fig. 6 — Basic loading cases for test coupon and for box beam

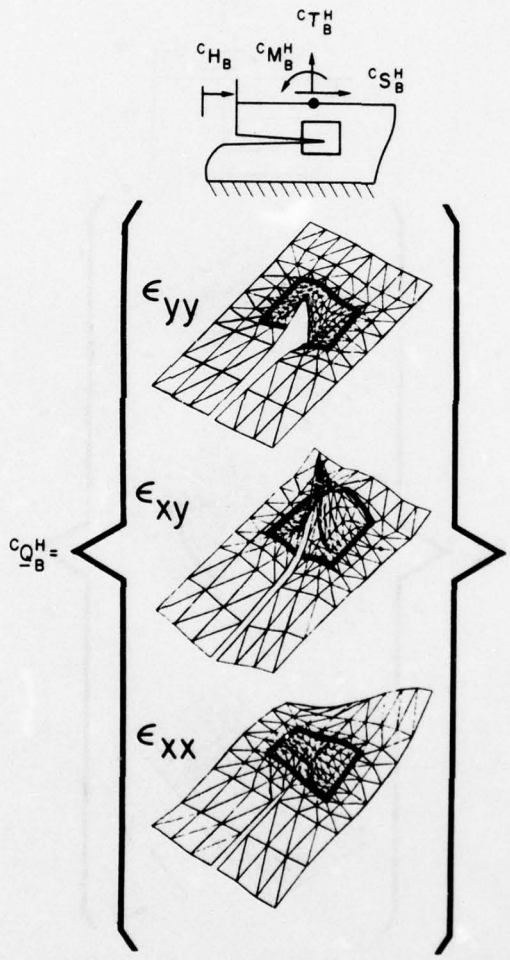

Fig. 7 — Strain field $^{C}\underline{Q}_{B}^{H}$, due to horizontal displacement, $^{C}H_{B}$, of coupon

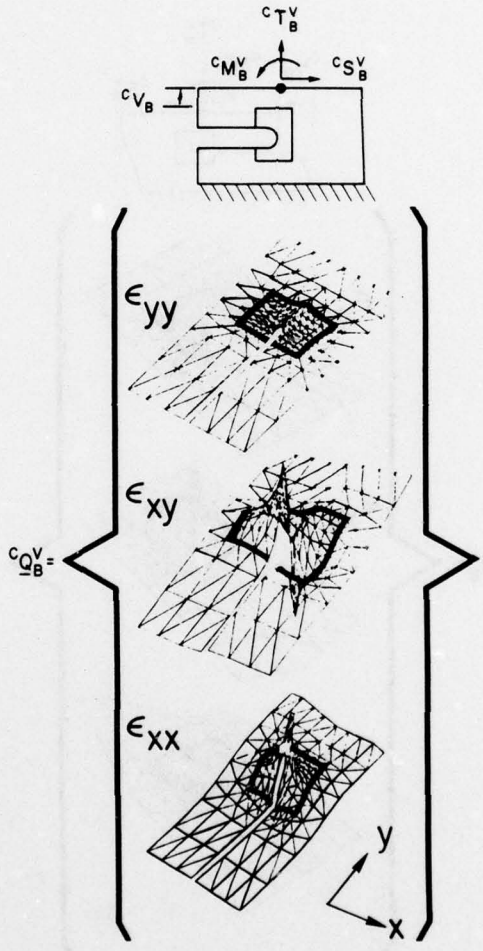

Fig. 8 — Strain field $^{c}\underline{Q}_{B}^{V}$, due to vertical displacement, $^{c}V_{B}$, of coupon

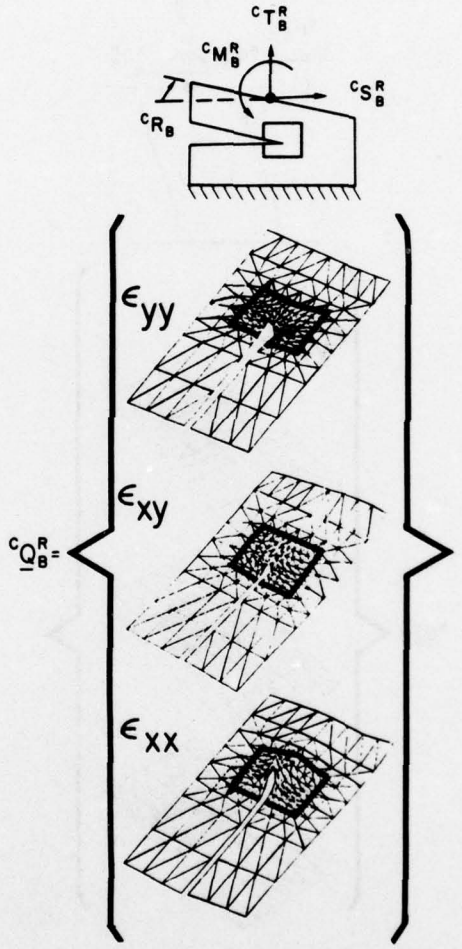

Fig. 9 — Strain field $^{C}\underline{Q}_{B}^{R}$, due to rotation, $^{C}R_{B}$, of coupon

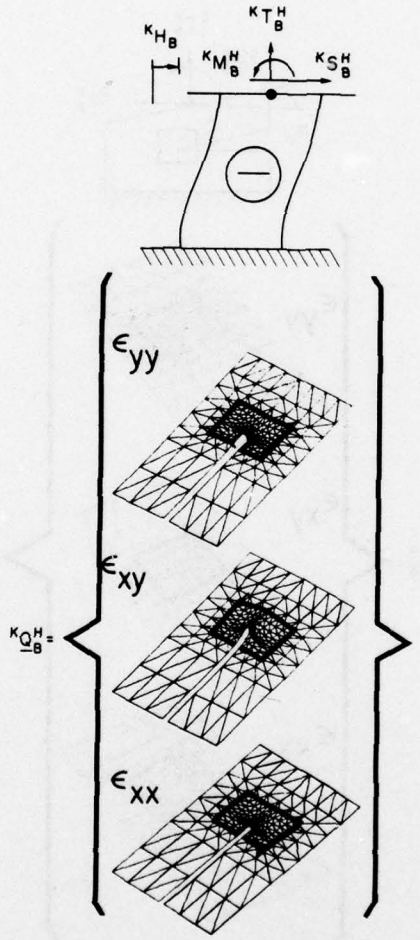

Fig. 10 — Strain field $^{K}\underline{Q}_{B}^{H}$, due to horizontal displacement, $^{K}H_{B}$, of box beam

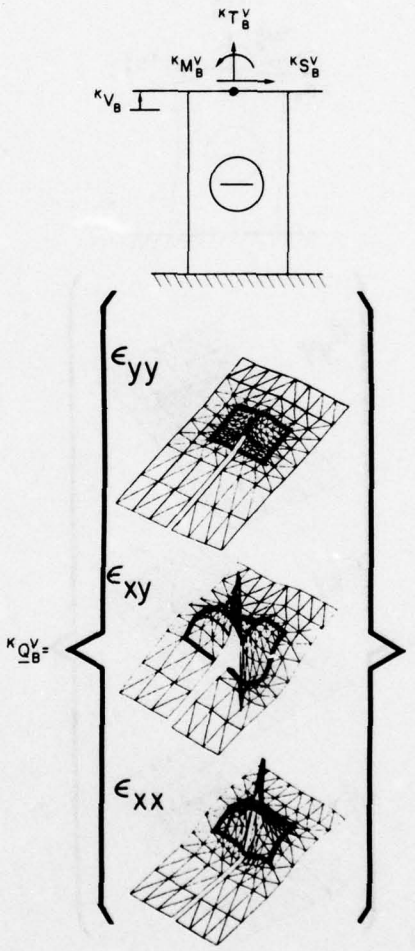

Fig. 11 — Strain field, $^{K}\underline{Q}_{B}^{V}$, due to vertical displacement, $^{K}V_{B}$, of box beam

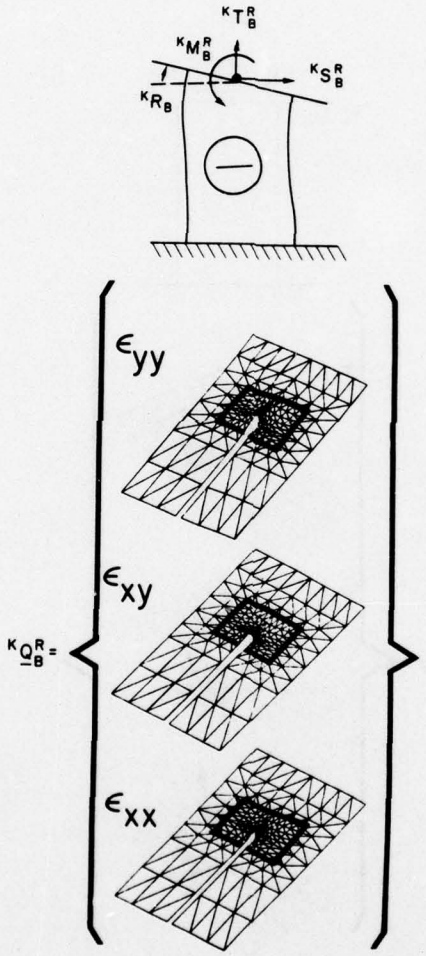

Fig. 12 — Strain field, $^{K}\underline{Q}_{B}^{R}$, due to rotation, $^{K}R_{B}$, of box beam

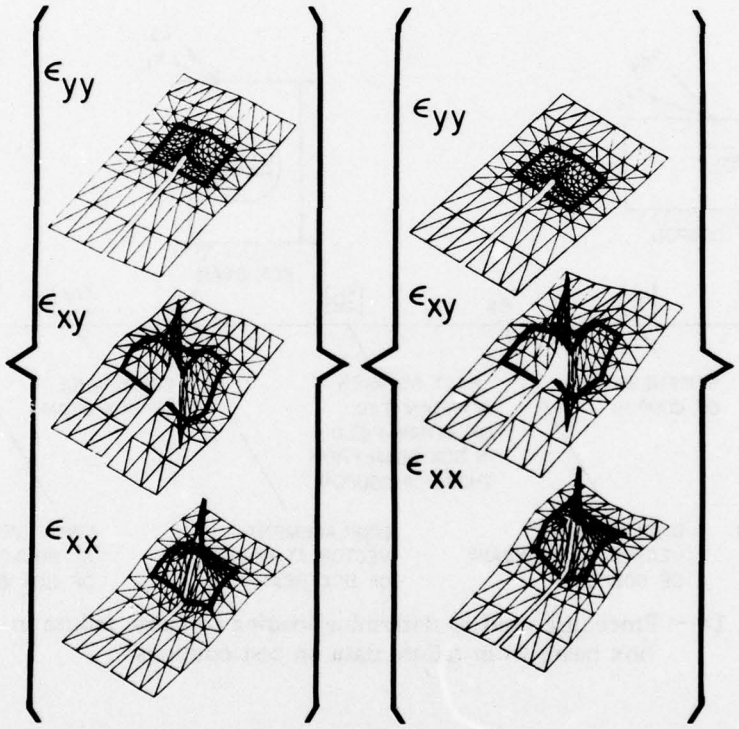

BOX BEAM STRAIN FIELD VECTOR, ${}^{K}\underline{Q}_{B}^{V}$

APPROXIMATION TO BOX BEAM STRAIN FIELD VECTOR, ${}^{K}\underline{Q}_{B}^{V}$ BY

$$ {}^{K}_{C}\underline{D}^{V} = 0.049\ {}^{C}\underline{Q}_{B}^{H} + 0.120\ {}^{C}\underline{Q}_{B}^{V} - 0.180\ {}^{C}\underline{Q}_{B}^{R} \quad (4) $$

Fig. 13 — Box beam strain field vector and its approximation as a linear sum of the coupon strain field vectors

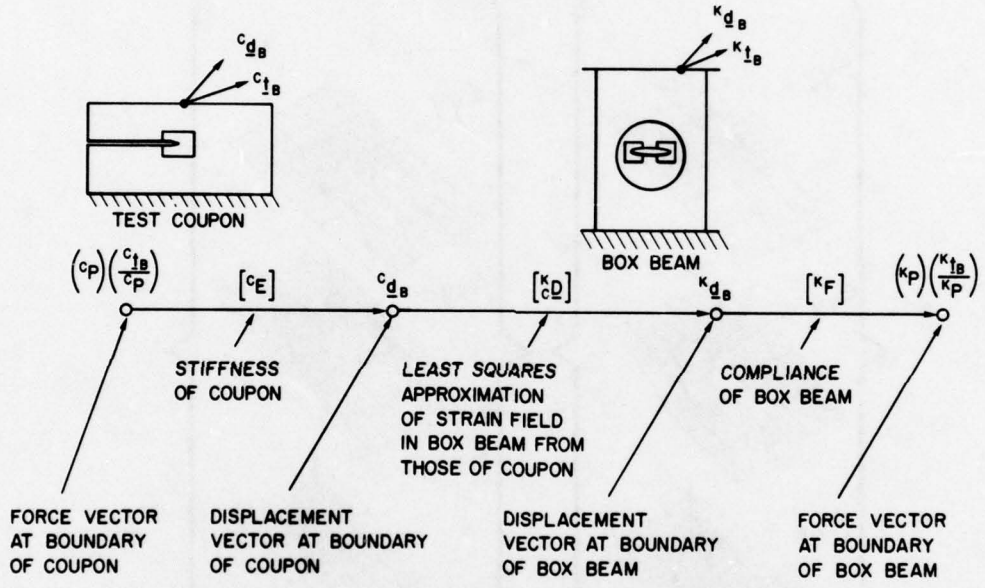

Fig. 14 — Procedure used to determine loading to cause failure in box beam from failure data on test coupons

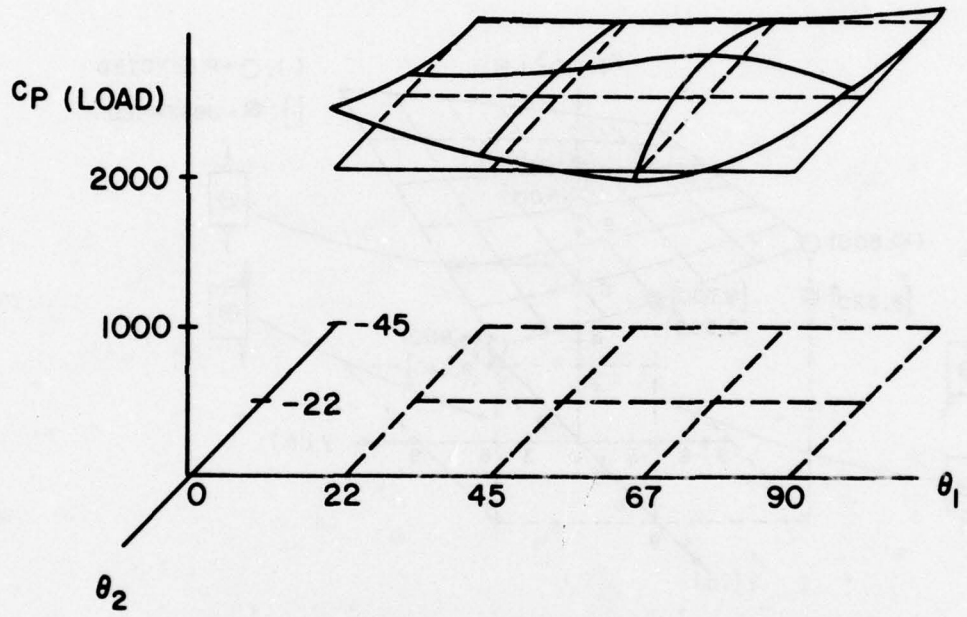

Fig. 15 — Failure surface for test coupons of graphite/epoxy crossply laminate (30° included angle) and approximation by a flat surface

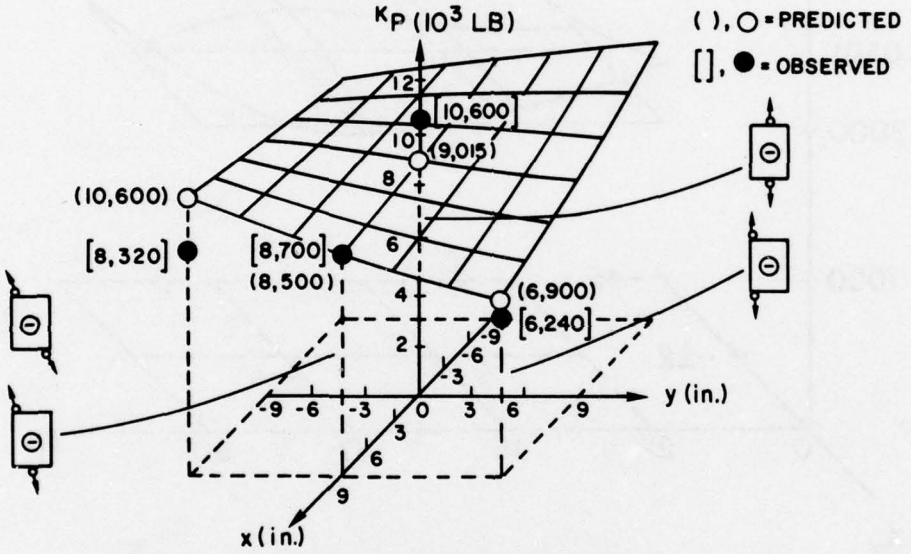

Fig. 16 — Box beam failure surface, for left end of notch

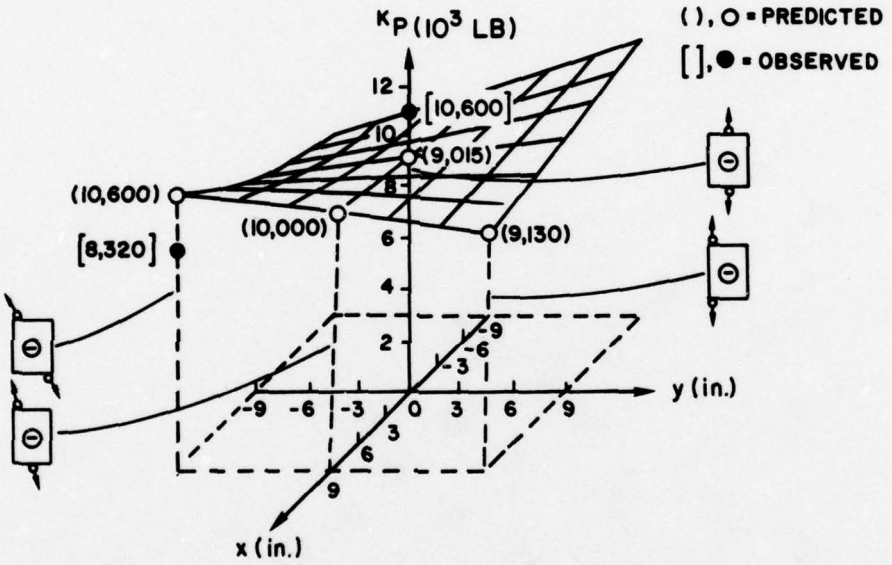

Fig. 17 — Box beam failure surface, for right end of notch

PART II. FAILURE CRITERIA FOR ADHESIVE JOINTS

INTRODUCTION

The present study concentrated on failures arising from precracks placed along the interface in a specimen geometry consisting of bulk epoxy samples bonded to aluminum plates. These specimens were subjected to a wide range of in-plane loads using a unique multi-axial loading facility [1]. Failure criteria were established for the bonded specimens based on onset of non-linearity due to crack growth or plastic deformation. Results of these studies were compared with failure criteria obtained using a larger scale specimen based on a formulation for the strain energy release rate.

EXPERIMENTAL PROCEDURE

Materials

The particular adhesive system chosen for this study was a bisphenol A diglycidyl ether (DGEBA) epoxy modified by adding 15% of an elastomeric material, carboxy-terminated butadiene acrylonitrile, (CTBN). When cured this sytem produces small particles of elastomer dispersed in a rigid epoxy matrix. Such a material provides an excellent model for commercial structural adhesive systems which generally consist of a rigid matrix, used to obtain a high modulus, and various types of additives, designed to improve toughness.

Laboratory coupons fabricated for failure studies were single-edge-notch type specimens of the geometry shown in Figure 1. The specimen configuration was a plate of bulk adhesive cast and cured against a similar plate of aluminum. Specimens were made using 6061-T6 aluminum, whose surface had been glass-peened and treated with acid chromate etching prior to bonding. Aluminum plates were placed in a Teflon mold, epoxy was cast in place and the specimens were cured for 16 hours at 120°C. Details of the

epoxy composition and properties are presented elsewhere by Bascom et al [2]. Specimens were then removed from the mold, machined to thickness and inspected to insure that no voids or bubbles were present along the bond. A notch was then machined along the interface and a small cut was made at the tip of the notch with a razor to produce a precrack. In addition, a specimen, as shown in Figure 2, was fabricated with an inclined edge crack at the interface between the bulk adhesive and the aluminum. This specimen was made using the same materials and techniques described above for the smaller specimens. An initial crack was inserted into this specimen so that it grew along the bond line. The purpose of the larger specimen study was to determine if strain energy release rate values computed for the small specimens could be related to results obtained on a larger specimen.

Loading Systems

The in-plane loader referred to in Part I was also used in these studies to apply the types of displacements shown in Figure 3 to the test specimens shown in Figure 1. The larger specimen shown in Figure 2 was loaded uniaxially in a universal testing machine under a constant displacement rate of 0.21 mm/sec (0.5 inches/min). As the magnitude of the applied load was increased, the initial crack grew along the interface between the bulk adhesive and the aluminum. This mode of failure corresponded to that observed for particular loading cases for the single-edge-notch specimens as described in Table 1.

DATA ANALYSIS

The point of failure initiation was determined in the in-plane loader tests using a dissipated energy criterion. The dissipated energy is the non-recoverable strain energy absorbed by the fracture process, and this calculated value increased rather sharply as the displacement increased. Values of shear, tension and bending loading at this point were used as a failure criterion for this specific combined load state. Similar results were obtained for other loading states with the exception of those specimens which did not exhibit brittle behavior. For specimens which failed in a ductile manner, the point of non-linear deformation which exceeded that normally observed in the brittle specimen was used as a failure criterion.

Visual observations of the specimens during testing provided a means of detecting crack growth. Indication of crack initiation was in good agreement with the occurrence of initial increases in the dissipated energy. Plastic

deformation of the bulk adhesive along the interface was observed for specimens in which crack growth did not occur. Consequently, it was possible to distinguish visually between brittle and ductile, i.e., crack growth and plastic deformation, behavior of the laboratory coupons. These failure mechanisms were readily confirmed by examination of the specimens following testing. Specimens which exhibited large plastic deformation showed little or no debonding, while those which failed by crack growth showed a small amount of plastic deformation prior to fracture.

Fracture Mechanics Analysis

A fracture mechanics representation for failure initiation can be obtained using stress-intensity factors based on analytic solutions of stress distributions for elastic half-spaces by Erdogan [3,4], and Rice and Sih [5]. These methods, or those proposed by Wu and Thomas [6], Anderson et al [7], and Mulville et al [8] for strain energy release rates for interfacial crack growth, are applicable only for linear elastic materials behavior and are restricted to self-similar crack growth. Consequently, these techniques can only be applied when these conditions are satisfied. Stress-intensity factors for two semi-infinite cracks between dissimilar media have been formulated by Sih [9] using stress analysis presented by Erdogan [3]. Based on the loading and geometry shown in Figure 4, the expressions for k_1 and k_2 are

$$k_1 = \frac{e^{\pi\varepsilon}}{\pi\sqrt{a}} \left[P\cos(\varepsilon \ln 2a) + Q \sin(\varepsilon \ln 2a)\right] \qquad (1)$$

and

$$k_2 = \frac{e^{\pi\varepsilon}}{\pi\sqrt{a}} \left[Q\cos(\varepsilon \ln 2a) - P\sin(\varepsilon \ln 2a)\right] \qquad (2)$$

where $\varepsilon = (1/2\pi)\ln\alpha$ and α is defined as the bi-elastic constant, $\alpha = (\mu_2 K_1 + \mu_1)/(\mu_2 K_2 + \mu_2)$. The values of μ_1, μ_2 correspond to the respective shear moduli for each half-space, K_1 and K_2 are defined as follows, $K_i = 3-4\nu_i$ for plane strain or $K_i = (3-\nu_i)/(1 + \nu_i)$ for plane stress, where ν_i is Poisson's ratio and $i = 1,2$. As shown in Figure 4, P and Q are normal and shear loads respectively and a is one-half of the total bonded length. The strain energy release rate can be formulated from (1) and (2) using the expression presented by Molyshev and Salganik [10] and Erdogan and Gupta [11] for interfacial cracks.

$$\mathcal{G} = \frac{\pi}{2\mu_1\mu_2} \frac{(\mu_1 + K_1\mu_2)(\mu_2 + K_2\mu_1)}{[(1 + K_1)\mu_2 + (1 + K_2)\mu_1]} (K_1^2 + K_2^2) \qquad (3)$$

The resulting formulation for $\mathcal{G}$ is then

$$\mathcal{G} = \frac{(P^2 + Q^2)}{2\pi a} \frac{e^{2\pi\varepsilon}}{\mu_1\mu_2} \frac{(\mu_1 + K_1\mu 2)(\mu_2 + K_2\mu_1)}{[(1 + K_1)\mu_2 + (1 + K_2)\mu_1]} \qquad (4)$$

where μ_1, μ_2, K_1 and K_2 are as defined above.

An alternate representation for strain energy release rate also based on Erdogan's [3] analysis was presented by Anderson et al [7] in the following form

$$\mathcal{G} = \frac{(P^2 + Q^2)}{32\pi a} (\beta_1 e^{-\pi\gamma} + \beta_2 e^{\pi\gamma}) \qquad (5)$$

where

$$\beta_1 = - \frac{(1 + K_1)(1 + \alpha)}{2\mu_1} \qquad (6)$$

and

$$\beta_2 = - \frac{(1 + K_2)(1 + 1/\alpha)}{2\mu_2}$$

In these expressions α is the bi-elastic constant and $\gamma = (1/2\pi)\ln\alpha$, which is ε in the formulations (1) and (2). The functional form of (4) and (5) is identical except for differences in the coefficients which describe the materials constants. One distinction between these analyses is that the crack area assumed in formulating (5) included both upper and lower crack surfaces, whereas in (4) only the plane crack surface is used. Consequently, strain energy release rate values computed using (5) will be approximately one half of the value obtained using (4).

A formulation for the strain energy release rate for interfacial cracks between dissimilar media subjected to in-plane moments can be expressed in a similar manner. Using the stress analysis presented by Erdogan [3] for bonded elastic half-spaces loaded by in-plane moments, M, as shown in Figure 4, the stress intensity factors are

$$k_1 = \frac{2e^{\pi\varepsilon}}{\pi(1 + 4\varepsilon^2)} \frac{M}{a^{3/2}} [\cos(\varepsilon\ln 2a) + 2\varepsilon\sin(\varepsilon\ln 2a)] \qquad (8)$$

and

$$k_2 = \frac{2e^{\pi\varepsilon}}{\pi(1 + 4\varepsilon^2)} \frac{M}{a^{3/2}} [2\varepsilon\cos(\varepsilon\ln 2a) - \sin(\varepsilon\ln 2a)] \quad (9)$$

The strain energy release rate for interfacial crack growth due to an applied moment can be obtained from (8), (9) and (3) as follows

$$\mathcal{G} = \frac{4M^2 e^{2\pi\varepsilon}}{\pi^2(1+4\varepsilon^2)a^3} \frac{(\mu_1 + K_1\mu_2)(\mu_2 + K_2\mu_1)}{\mu_1\mu_2[(1 + K_1)\mu_2 + (1 + K_2)\mu_1]} \quad (10)$$

For combined shear, tension and bending loading expressions for the stress intensity factors are determined by summing (1) and (8) to obtain k_1

$$k_1 = \frac{e^{\pi\varepsilon}}{\pi\sqrt{a}} \left[P\cos(\varepsilon\ln 2a) + Q\sin(\varepsilon\ln 2a) + \frac{2M}{(1 + 4\varepsilon^2)a} \left\{\cos(\varepsilon\ln 2a) + 2\varepsilon\sin(\varepsilon\ln 2a)\right\}\right] \quad (11)$$

and (2) and (9) to obtain k_2

$$k_2 = \frac{e^{\pi\varepsilon}}{\pi\sqrt{a}} \left[Q\cos(\varepsilon\ln 2a) - P\sin(\varepsilon\ln 2a) + \frac{2M}{(1 + 4\varepsilon^2)a} \left\{2\varepsilon\cos(\varepsilon\ln 2a) - \sin(\varepsilon\ln 2a)\right\}\right] \quad (12)$$

The stress intensity factors in (11) and (12) can then be combined using (3) to derive an expression for the strain energy release rate

$$\mathcal{G} = \left[P^2 + Q^2 + \frac{4M(Pa + 2\varepsilon Qa + M)}{(1 + 4\varepsilon^2)a^2}\right] \frac{e^{2\pi\varepsilon}}{\pi^2 a} \left\{\frac{(\mu_1 + K_1\mu_2)(\mu_2 + K_2\mu_1)}{\mu_1\mu_2[(1 + K_1)\mu_2 + (1 + K_2)\mu_1]}\right\} \quad (13)$$

This formulation for $\mathcal{G}$, (13), can be used to analyze debonding between two dissimilar materials subjected to in-plane shear, tension and bending loads. Its use is restricted to elastic materials response and to self-similar crack growth; i.e., a crack initially at the bond line, which continues to propagate along the bond.

Application of this analysis, (13), to experimental data was restricted to specimens which exhibited interfacial crack growth. Distinctions between debonding failure mode vs crack growth away from the bondline into the adhesive or large scale plastic deformation were made by visual observations both during and after testing.

RESULTS AND DISCUSSION

Results of the failure analysis for single-edge-notch and inclined crack bonded specimens are presented in Table 1, where θ_1 is related to the ratio of tension to shear displacements, θ_2 is related to the ratio of in-plane bending to the magnitude of the shear and tension displacements, r and T are the magnitude of the displacement and loading at failure respectively.

The fracture mechanics analysis developed for interfacial crack growth, Equation (13), was used to calculate a value of $\mathcal{G}_c$ for the specimen loaded at $\theta_1 = 45°$ and $\theta_2 = 0$. Results of this calculation are shown in Table 1 along with $\mathcal{G}_c$ values calculated for other loading cases, in which the mode of failure was interfacial accompanied by a small amount of plastic deformation. Although based on a limited amount of data, the results for the single-edge-notch at $\theta_1 = 45°$, $\theta_2 = 0$ and for the inclined crack specimen under the same loading are in relatively good agreement. These results indicate that at least for this loading condition, comparable values of $\mathcal{G}_c$ can be obtained on larger scale specimens. Results of the interfacial fracture analysis also indicate that as the amount of in-plane bending increases, i.e., $\theta_1 = 67°$, $\theta_2 = 22°$, and $\theta_1 = 67°$, $\theta_2 = 45°$ that the value of $\mathcal{G}_c$ increases slightly.

The values of $\mathcal{G}_c$ reported here for interfacial failure are less than the values obtained by Bascom et al [2] for the bulk adhesive material. Values of $\mathcal{G}_c$ for the bulk epoxy modified with CTBN were approximately 3500 J/m^2 compared with interfacial values of 1320 to 2960 J/m^2. Similar results have been reported by Mostovoy et al [12]. They also observed little correlation between bulk and adhesive values for $\mathcal{G}_c$. Bascom et al [2] theorize that the constraint of the adherends in adhesive joints prevent full development of a plastic zone near the crack tip. This constraint restricts the deformation of the adhesive prior to failure and results in reduced values of $\mathcal{G}_c$.

Based on this hypothesis, a similar behavior would be expected for the bonded specimens considered in this study. The reduction in $\mathcal{G}_c$ should be less than for an adhesive joint, since a single adherend imposes less constraint on the deformation of the adhesive than two adherends in a joint configuration.

In all cases of crack growth along the interface, the crack propagated in the adhesive near bonded interface and replicated the surface features of the aluminum adherend. This observations agrees with previous studies by Bascom et al [13] and Mulville and Vaishnav [14] on interfacial failure.

CONCLUSION

Failure studies of modified epoxy-aluminum bonded specimens are presented for a wide range of in-plane loads. A failure surface representation for crack initiation or onset of large plastic deformation was plotted in terms of shear, tension and in-plane bending loading components. This representation provided a convenient method of visualizing the point of failure initiation for various loading states. The experimental studies demonstrated that the mode of failure for the bonded specimens was dependent on the relative magnitudes of the shear, tension and bending loading components. Combinations of tension and bending, for example, produced a different failure mode than tension alone. The failure modes observed ranged from crack growth into the bulk adhesive to crack growth near or along the interface, and finally, to large scale plastic deformation of the adhesive.

A fracture mechanics formulation was developed to describe interfacial failure in bonded specimens under combined in-plane loading. Values of $\mathcal{G}_c$ were computed for specimens which failed by crack propagation along the bond. Comparisons made with values reported for the bulk modified adhesive showed that interfacial values were up to 50% less depending on the mode of loading. These results can be interpreted in terms of the constraining influence of the adherend, which restricts development of a plastic zone near the crack tip and thus reduces the fracture toughness.

The method of evaluating bonded materials described herein has application in many areas of interfacial failure. This technique may be extended to determining the effects of surface preparations and coatings, residual stresses and adhesive modifications on fracture and stress corrosion cracking. Correlation between various failure modes and

in-plane loading conditions may lead toward an understanding of failure mechanisms associated with adhesive joints.

REFERENCES

1. Mast, P., Thomas, R., Beaubien, L., Sutton, S., Mulville, D., Tirosh, J. and Wolock, I., "A Semi-Automatic In-Plane Loader for Testing Composite Materials," Manuscript in preparation.

2. Bascom, W. D., Cottington, R. L., Jones, R. L. and Peyser, P., "The Fracture of Epoxy- and Elastomer-Modified Epoxy Polymers in Bulk and as Adhesives," J. Appl. Poly.Sci. Vol. 19, pp. 2545-2562 (1975).

3. Erdogan, F., "Stress Distribution in a Nonhomogeneous Elastic Plane with Cracks," ASME J. of Applied Mechanics, Vol. 30, No. 2, pp. 232-236, 1963.

4. Erdogan, F., "Stress Distribution in Bonded Dissimilar Materials With Cracks," ASME J. of Applied Mechanics, Vol. 32, No. 2, pp. 403-410, 1965.

5. Rice, J. R. and Sih, G. C., "Plane Problem of Cracks in Dissimilar Media," ASME J. of Applied Mechanics, Vol. 32, No. 2, pp. 418-423, 1965.

6. Wu, E. M. and Thomas, R. L., "Interfacial Fracture Phenomena," Proceedings of the Fifth International Congress on Rheology, Vol 1, edited by Shigeharu Onogi, University of Tokyo Press and University Park Press, Baltimore, Maryland, pp. 575-587, 1969.

7. Anderson, G. P., Devries, K. L. and Williams, M. L., "Finite Element in Adhesion Analyses," Int. J. of Fracture, Vol. 9, No. 4, pp. 421-435, 1973.

8. Mulville, D. R., Mast, P. W. and Vaishnav, R. N., "Strain Energy Release Rate for Interfacial Cracks Between Dissimilar Media," Engineering Fracture Mechanics, Vol. 8, pp. 555-565, 1976.

9. Sih, G. C., "Handbook of Stress-Intensity Factors," Institute of Fracture and Solid Mechanics, Lehigh University, Bethlehem, Pennsylvania, 1973.

10. Malyshev, B. M. and Salganik, R. L., "The Strength of Adhesive Joints Using the Theory of Cracks," Int. J. of Fracture Mechanics, Vol. 1, No. 2, pp. 114-128, 1965.

11. Erdogan, F. and Gupta, G., "The Stress Analysis of Multi-Layered Composites with a Flaw," Int. J. Solids and Structures, Vol. 7, No. 1, pp. 39-61, 1971.

12. Mostovoy, S., Ripling, E. J. and Bersch, C. F., "Fracture Toughness of Adhesive Joints," J. Adhesion, Vol. 3, pp. 125-144, 1971.

13. Bascom, W. D., Timmons, C. O. and Jones, R. L., "Apparent Interfacial Failure in Mixed Mode Adhesive Fracture," J. of Material Science, Vol. 10, pp. 1037-1048, 1975.

14. Mulville, D. R. and Vaishnav, R. N., "Interfacial Crack Propagation," J. Adhesion, Vol. 7, pp. 215-233, 1975.

TABLE I. FAILURE ANALYSIS OF BONDED SPECIMENS

Single-edge-notch Specimen-Number	θ_1	θ_2	r	T	$\mathcal{G}_c$ (13) in-lb/in^2	J/m^2	FAILURE MODE
886	90°	0°	28.6	1780			Crack growth into adhesive
887	90°	22°	29.6	1480			Crack growth into adhesive near bondline
888	90°	45°	28.4	1170			Crack growth in adhesive near bondline
896	67°	0°	24.5	1170			Crack growth in adhesive near bondline
897	67°	22°	25.1	1370	7.5	1320	Crack growth along bonded interface
898	67°	45°	20.1	1310	9.5	1680	Crack growth along bonded interface
899	67°	45°	23.8	1250	16.9	2960	Crack growth along bonded interface
889	45°	0°	23.6	1300	10.1	1770	Crack growth along bonded interface
890	45°	22°	28.3	1320			Large scale yielding prior to failure along bond line
891	45°	45°	24.0	1070			Large scale yielding prior to failure along bond line
893	22°	0°	38.0	1610			Large scale yielding prior to failure along bond line

TABLE I. FAILURE ANALYSIS OF BONDED SPECIMENS (Continued)

Single-edge-notch Specimen-Number	θ_1	θ_2	$\underline{r}$	$\underline{T}$	$\mathcal{G}_c(13)$ in-lb/in^2	J/m^2	FAILURE MODE
894	22°	22°	38.4	1750			Large scale yielding prior to failure along bondline
895	22°	45°	30.4	1910			Large scale yielding prior to failure along bondline
892	0°	0°	52.6	2770			Large scale yielding
Inclined-edge Crack-specimen	45°	0°			13.0	2280	Crack growth along bonded interface

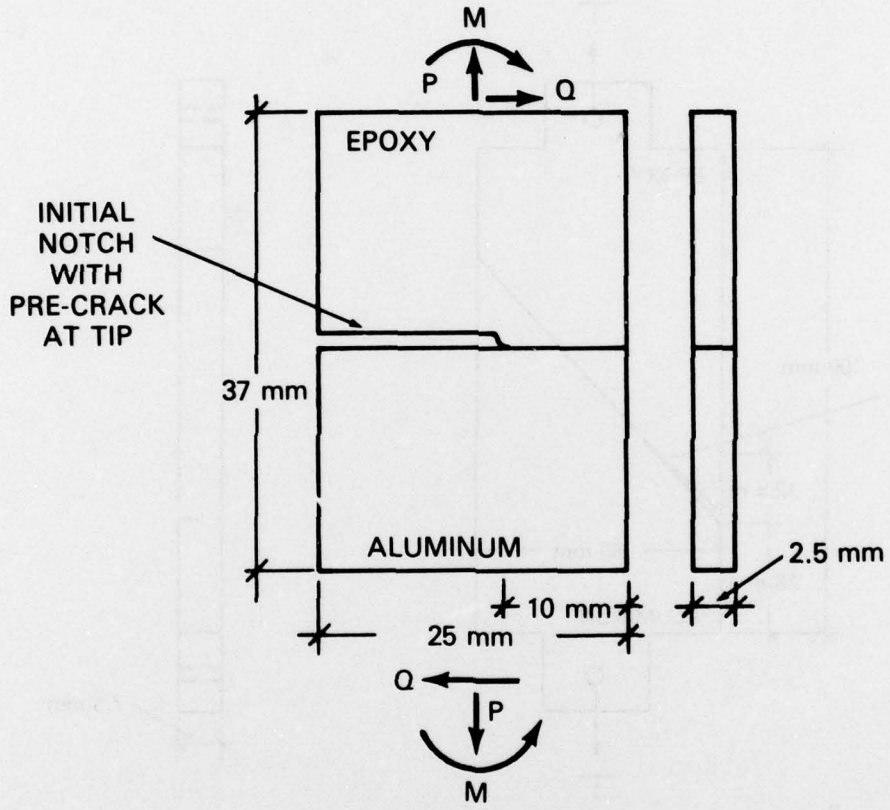

Fig. 1 — Single-edge-notch bonded specimen

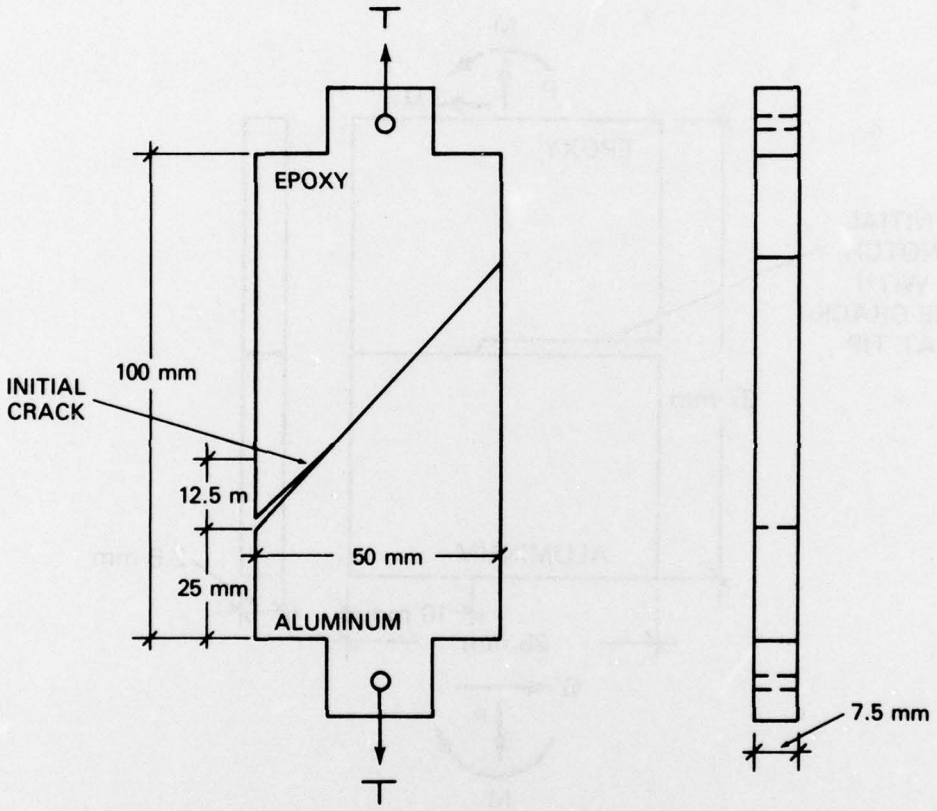

Fig. 2 — Inclined-edge-crack bonded specimen

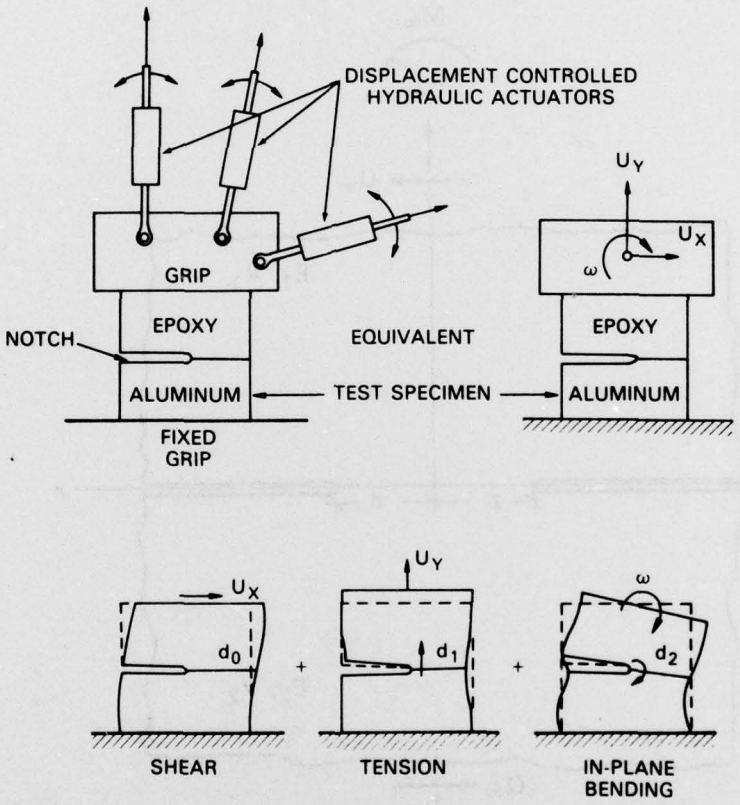

Fig. 3 — Single-edge-notch specimen subjected to tension, shear and rotational displacement

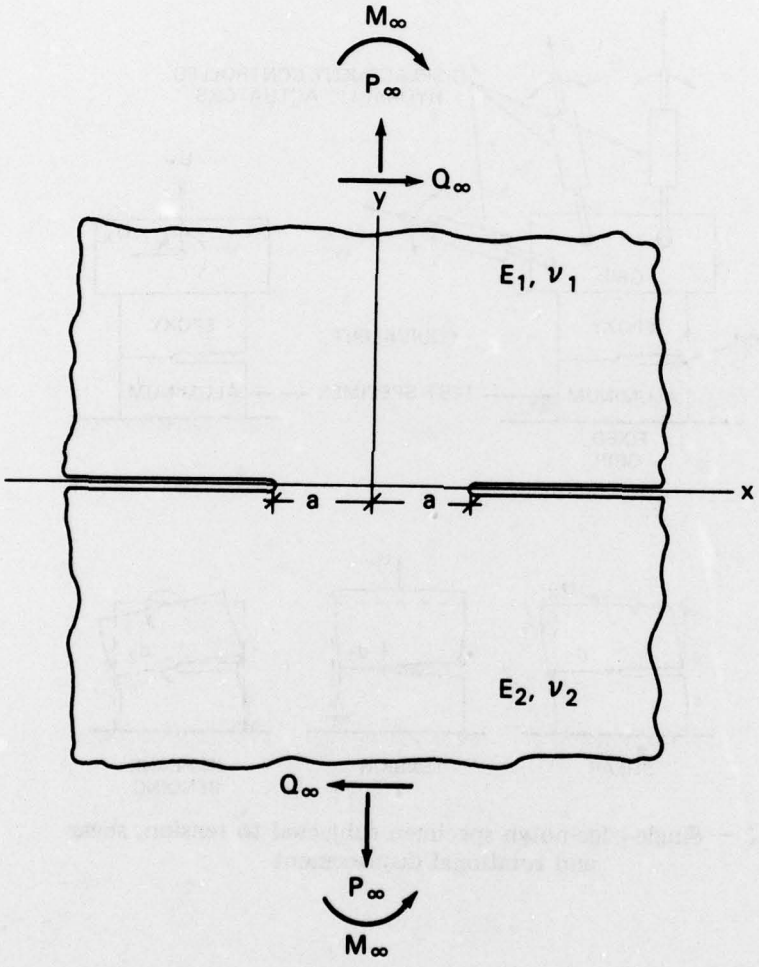

Fig. 4 — Bonded elastic half spaces under tension, shear and bending loading